STUDY OF RUBBING PHENOMENON DUE TO CONTACT BETWEEN ROTOR AND GUIDE IN ROTATING MACHINERY AND ITS MINIMIZATION

BY

Enaiyat Ghani Ovy

A thesis submitted to the Department of Mechanical & Chemical Engineering (MCE) in partial fulfillment of the requirement for the degree of

Master of Science in Mechanical Engineering

Department of Mechanical & Chemical Engineering (MCE)

ISLAMIC UNIVERSITY OF TECHNOLOGY (IUT)
ORGANIZATION OF ISLAMIC COOPERATION (OIC)

August, 2012

STUDY OF RUBBING PHENOMENON DUE TO CONTACT BETWEEN ROTOR AND GUIDE IN ROTATING MACHINERY AND ITS MINIMIZATION

A thesis submitted to the Department of Mechanical & Chemical Engineering (MCE) in partial fulfillment of the requirement for the degree of

Master of Science in Mechanical Engineering

BY

Enaiyat Ghani Ovy

Under the Guidance of

Dr. Md. Zahid Hossain

Department of Mechanical & Chemical Engineering (MCE)

ISLAMIC UNIVERSITY OF TECHNOLOGY (IUT)
ORGANIZATION OF ISLAMIC COOPERATION (OIC)

August, 2012

CANDIDATE'S DECLARATION

It is hereby declared that this thesis or any part of it has not been submitted elsewhere for the award of any degree or diploma.

(Signature of the Supervisor)

Dr. Md. Zahid Hossain
Associate Professor
Department of Mechanical and
Chemical Engineering
Islamic University of Technology (IUT)
Board Bazar, Gazipur: 1704, Bangladesh

(Signature of the Candidate)

Enaiyat Ghani Ovy
Student No: 091603
Department of Mechanical and
Chemical Engineering
Islamic University of Technology (IUT)
Board Bazar, Gazipur: 1704, Bangladesh

RECOMMENDATION OF THE BOARD OF EXAMINERS

The thesis titled "Study of Rubbing Phenomenon due to Contact between Rotor and Guide in Rotating Machinery and its Minimization", submitted by Enaiyat Ghani Ovy, Student Number. 091603 of the academic year 2011-2012 has been found as satisfactory and accepted on 02.08.2012 as partial fulfillment of the requirement for the degree of Master of Science in Mechanical Engineering.

1. _____ Chairman (Supervisor)
   Dr. Md. Zahid Hossain
   Associate Professor
   Department of Mechanical and Chemical Engineering
   Islamic University of Technology (IUT)
   Board Bazar, Gazipur: 1704, Bangladesh.

2. _____ Member (Ex-Officio)
   Prof. Dr. Md. Abdur Razzaq Akhanda
   Head
   Department of Mechanical & Chemical Engineering
   Islamic University of Technology (IUT)
   Board Bazar, Gazipur-1704, Bangladesh.

3. _____ Member
   Dr. Md. Nurul Absar Chowdhury
   Professor
   Department of Mechanical and Chemical Engineering
   Islamic University of Technology (IUT)
   Board Bazar, Gazipur: 1704, Bangladesh.

4. _____ Member (External)
   Dr. Md. Abdus Salam Akanda
   Associate Professor
   Department of Mechanical Engineering
   Bangladesh University of Engineering and Technology (BUET)
   Dhaka, Bangladesh.

ACKNOWLEDGEMENT

At first, I would like to show my deepest gratitude to Dr. Md. Zahid Hossain, my supervisor, for providing me with supports and guidance throughout my pursuit of master's degree. His thoughts and precious suggestions motivated me to find out in depth scenarios of this research work. This thesis would never have been accomplished without Dr. Zahid's guidance and encouragement.

My cordial thanks also go to Prof. Dr. Md. Abdur Razzaq Akhanda, Head, department of Mechanical and Chemical Engineering, IUT for providing me every facility to complete this thesis. I am also grateful to Prof. Dr. Md. Nurul Absar Chowdhury for giving me numerous precious suggestions for the experimental work. My sincere gratitude also goes to Dr. Yukio Ishida of Nagoya University, Japan whose extensive works and valuable suggestions helped me analyzing different sections of this thesis.

I would also like to thank Dr. Mir Md. Maruf Morshed and Dr Mohammad Ahsan Habib for sharing their valuable ideas and opinions regarding my research work. Thanks to all the members of IUT Machine Shop and Applied Mechanics Laboratory for helping me in setting up the experimental test rig and collecting data. I am also grateful to Dr. Md. Abdus Salam Akanda for managing time to review my thesis in his very busy time.

Last but not least, gratitude goes to my parents, Md. Abdul Ghani, and Mrs. Lubna Ghani, for their selfless love, encouragement, and supports throughout my progress and academic pursuit.

Abstract

In an industry, rotor-to-stator or rotor-to-guide rubbing is a very common problem. The contact (rub and impact) between rotor and guide creates excessive vibration which may even lead to the permanent damage of a mechanical system. Therefore, considering this extremely important scenario, this research work identifies the characteristic of rubbing phenomena in rotating machineries by simulation and experiment. To minimize rubbing, both the circular and lemon type backup bearing have been considered in this work. First the mathematical models for both these types of bearings are analyzed. Then the models are simulated in MATLAB SIMULINK. Simulation results are discussed elaborately for different clearances between the shaft and the backup bearing and initial conditions. These results are then validated by the experimental results. Although it is obvious from this research that circular backup bearing is efficient in minimizing the excessive vibration, but the rubbing between rotor and guide is still present which eventually damages the system. So, this work gives the priority to implement the lemon type backup bearing as the results show that lemon type backup bearing works certainly better in minimizing the rubbing between rotor and guide than the circular backup bearing.

NOMENCLATURE

x , y	the coordinate of the shaft displacement
r	the amplitude of shaft displacement
m	the rotor mass
M	the geometric center of the rotor
G	the gravitational center of the rotor
ω	the rotational speed of the rotor
ω_n	the natural frequency of the shaft system
k_e	the equivalent spring constant of the contact model at the backup bearing
c_e	the equivalent damping coefficient of the contact model at the backup bearing
e	the eccentricity
e_r	the coefficient of restitution
θ	the inclination of the rotor
F_k	the contact force component due to the equivalent spring constant k_e
F_c	the contact force component due to the equivalent damping coefficient c_e
F_f	the friction force due to contact
F_{kx}	the transferred value of F_k in the x direction
F_{ky}	the transferred value of F_k in the y direction
F_{cx}	the transferred value of F_c in the x direction

F_{cy}	the transferred value of F_c in the y direction
μ	the friction coefficient
F_{fx}	the transferred value of F_f in the x direction
F_{fy}	the transferred value of F_f in the y direction
δ'	the gap between the shaft and the backup bearing
R_s	the shaft radius
V_t	the tangential velocity of the rotor
t	time
k	the spring constant of the shaft
c	the damping coefficient of the shaft
x'	the non dimensional parameter for x
y'	the non dimensional parameter for y
δ	the non dimensional parameter for δ'
r'	the non dimensional parameter for r
e'	the non dimensional parameter for e
t'	the non dimensional parameter for t
ω'	the non dimensional parameter for ω
c'	the non dimensional parameter for c
F_k'	the non dimensional parameter for F_k
F_c'	the non dimensional parameter for F_c
F_f'	the non dimensional parameter for F_f
D_s	the shaft diameter
k_e'	the non dimensional parameter for k_e

c_e'	the non dimensional parameter for c_e
R'	the non dimensional parameter for R_s
β	the phase angle

TABLE OF CONTENTS

List of Tables

List of Figures

Chapter 1

Introduction

1.1 Introduction

In all the industries, rotating machines are mostly used because rotation offers an excellent way to transfer power from one point to another, or convert motion to different planes through gears, belts, shafts etc. Therefore, reliability as well as stability of rotating machines operating often at high speeds is very significant in industry. Generally the components of a rotating machine include a rotor, bearings and a support structure. Among all these components, there are some vital relations. Each component of the system has an effect on the overall dynamic behavior of the machine. To keep a stable motion of the rotor machinery is an important motivating factor in looking into the dynamic characteristic of the rotating system [1].

In the rotating machinery, rotor-to-stator or rotor-to-guide contact damages a rotor-shaft system and may cause severe hazards. The contact happens between a rotor and a stator due to manufacturing error, excessive imbalance, misalignment, bearing wear, smaller radial clearance between rotating shaft and casing, bad assembly and so on. This problem has been found in industry and also demonstrated in several literatures. Contact (rubs and impact) occurs in rotor casing, seals, unlubricated journal bearings, rotor loose guide attached to restrict a large deflection [2]. The rotor-to-stator rub phenomena can be classified as forward rub, backward rub and impact. Contact in rotating machinery can produce forward rub, backward rub and impact. A forward rubbing is a forced oscillation; however, a backward rubbing is a self-excited oscillation. In the forward rubbing whose whirling angular speed is the same as the rotational speed of the shaft, the stress at an arbitrary point inside the shaft does not change. In this case, the shaft rotation is opposite to the direction of friction force whereas the direction of rotational speed and whirling speed is same. On the other hand, in the backward rubbing, the whirling angular speed is not the same as the rotational speed of the shaft. Moreover the direction of the rotational speed and whirling speed is not same in this case. And the angular speed of the shaft and friction force works in the same direction. Therefore, in the backward rubbing, the stress inside the shaft varies and changes between the tension and the compression. So, the backward rubbing is far more dangerous with respect to fatigue fracture. Fig. 1.1 depicts and explains the phenomenon of forward and backward rubbing.

Fig. 1.1(a) describes the scenario of forward rubbing. Here, ω is the rotational speed of the rotor, Ω is the whirling speed of the rotor, M is the geometric center of the rotor and μN is the friction force produced due to contact between rotor and the guide. In the first case, the rotational speed and friction force direction is opposite which is also known as forward rub. And the direction of the whirling speed and rotational speed of the rotor is same. But in Fig. 1.1(b) as the rotor contacts with guide the rotational speed of rotor and the friction force act in the same direction and this phenomenon is considered as backward rub. In the backward rubbing condition, the direction of rotational speed and whirling speed is not same which is highlighted in the Fig. 1.1(b).

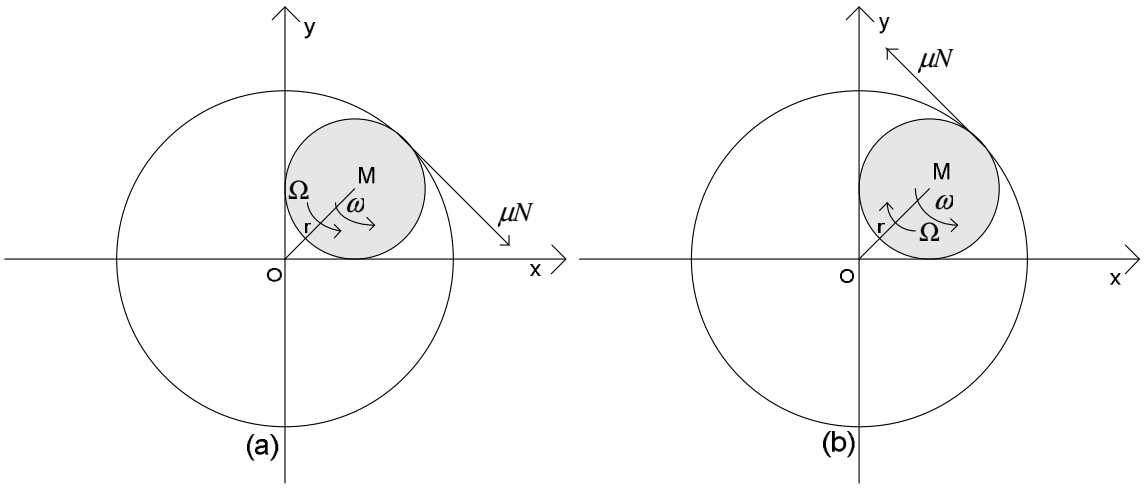

Fig. 1.1: Rubbing types: (a) Forward rub, (b) Backward rub

In general, the rubbing phenomenon is divided into two types, full annular rub and partial rub. Partial rub is the intermittent contact between the rotor and stator whereas full annular rub is defined by continuous contact during the entire whirling motion [3]. In the operation of a rotating machine, rotor-to-stator rub is a serious malfunction which can seriously affect on the machine performance and can even lead to a complete failure of the machine.

In this present work, the rubbing phenomenon between rotor and guide is identified by simulation as well as experiment. For the minimization of rubbing between rotor and guide two different mechanical ways have been implemented such as implementation of circular and lemon type guide. Further a simple Jeffcott rotor model is simulated for the investigation of rubbing between rotor and guide. The numerical model is developed by MATLAB SIMULINK. For different conditions, the rubbing phenomenon is observed. Finally a comparison between experimental and simulation work is carried out to validate the overall scenario of this research work.

1.2 Objectives of this Study

There are two main objectives of this research work.

- To study the phenomenon of rubbing during rotor-guide contact.

This provides the opportunity to observe forward rub or backward rub under different initial conditions. The behavior of rubbing is observed both experimentally and numerically.

- To minimize the rubbing by mechanical ways during rotor-guide contact.

This is the significant objective of this research work. The objective is explained elaborately by the typical resonance curve shown in Fig. 1.2. The symbol (o) denotes the resonance curves while there is no guide, i.e. no contact motion, and the symbol (●) denotes the resonance curves upon contact while the guide exists. From Fig. 1.2, it is clear that if the back up bearing is used then there will be two stable lines after the resonance depending on the initial conditions. One stable line has the higher amplitude and the other stable line has the lower value. In the higher amplitude line, the rubbing occurs between rotor and guide which is not good for the rotating machinery. Although the excessive vibration is minimized during resonance when the backup bearing is used, but the rubbing might even cause the system failure. Therefore, the prime goal of this research work is to create some disturbances to shift the upper line to the lower line (lower amplitude) after resonance. In this way, it is possible to minimize the rubbing.

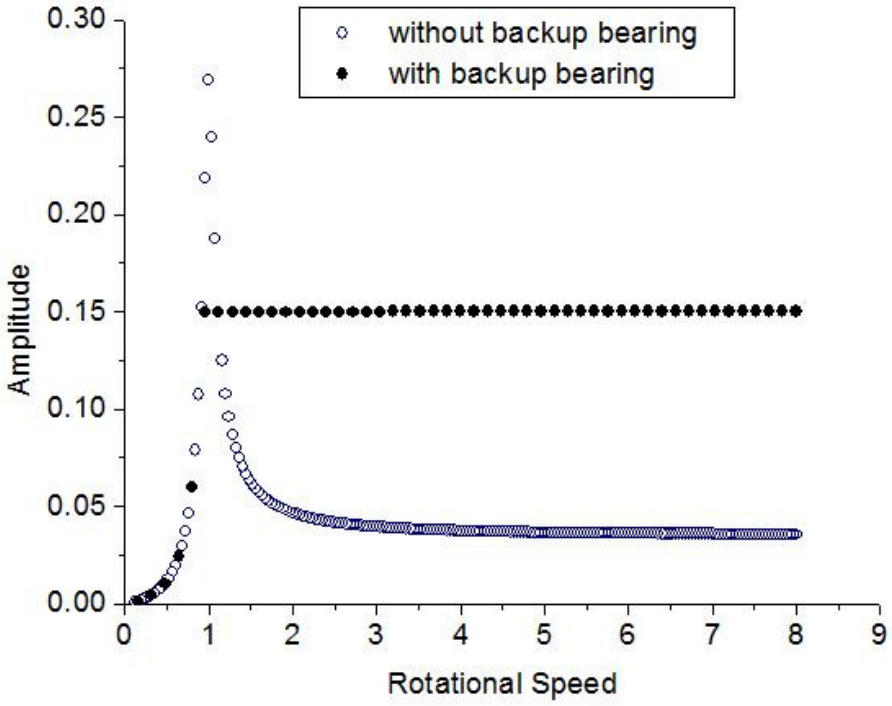

Fig. 1.2: Resonance Curve.

Chapter 2

Literature Survey

2.1. Historical Perspective [43]

Rotordynamics research has at least a 140 year history which actually started with Rankine's paper on whirling motions of a rotor in 1869. The advancement happened tremendously at the end of the nineteenth century with contributions by de Laval and others. De Laval invented a one stage steam turbine and achieved success in its operation. He showed that it was possible to operate above the critical speed by first using a rigid rotor and then a flexible rotor. (Stodora, 1924) [4].

In the early days, the crucial thing in designing rotating machinery was to avoid resonance and for that reason, it was the major concern for researchers and designers to predict the critical speed. Dunkerley (1894) [5] derived an experimental formula which gave the lowest critical speed for a multirotor system in 1894. The term *critical speed* was first used by him for the resonance rotational speed. Holzer (1921) [6] proposed an approximate method to calculate the natural frequencies as well as mode shapes of torsional vibrations.

Jeffcott was the first who developed the fundamental theory of rotordynamics in 1919. Jeffcott's great contributions can be appreciated if it is recalled that a shaft with a disk at the mid span is called the *Jeffcott rotor*, especially among researchers in the United States. This simplified fundamental rotor system is also called the *Laval rotor,* named after de Laval.

The progresses made in rotordynamics up to the beginning of the twentieth century are elaborated in the masterpiece written by Stodola (1924) [4]. This excellent book explains nearly the entire field related to steam turbines. Among other things, this book includes the dynamics of elastic shafts with disks, the dynamics of continuous rotors without considering the gyroscopic moment, the balancing of rigid rotors, and methods for determining approximate values of critical speeds of rotors with variable cross sections.

Rotordynamics then expanded to consider various other effects. Self excited vibrations became a serious problem when the rotational speed increased above the first critical speed. In the 1920s, Newkirk (1924) [7] and Kimball (1924) [8] first observed that internal friction of shaft materials could cause an unstable whirling motion. Newkirk and Taylor (1925) [9] investigated an unstable vibration called *oil whip,* which was due to an oil film in the journal bearings. Thereafter self-excited vibration attracted the attention of many researchers of the world.

After a decade, research on asymmetrical shaft system as well as asymmetrical rotor systems started. The former are systems with a directional difference in shaft stiffness, and the latter are those with a directional difference in rotor inertia. The examples of such systems are two pole generator rotors and propeller rotors. Terms with time varying coefficients appear in the governing equations as these directional differences rotate with the shaft. So these systems fall into the category of *parametrically excited systems*. The most important property of asymmetrical systems is the appearance of unstable vibrations in some rotational speed ranges. The vibrations of rotors with continuously distributed mass were also studied. The simplest

continuous rotor model corresponding to the Euler beam was first studied in the book by Stodola (1924) [4]. In the 1950s and 1960s, Bishop (1959) [10], Bishop and Gladwell (1959) [11], and Bishop and Parkinson (1965) [12] reported a series of papers on the unbalance response and the balancing of a continuous rotor. Eshleman and Eubanks (1969) [13] derived more general equations of motion considering the effects of rotary inertia, shear deformation, and gyroscopic moment, and investigated these effects. The most important and fundamental procedure to damp unfavorable vibrations is to eliminate geometric imbalance in the rotor. The balancing technique for a rigid rotor was established relatively early. A practical balancing machine based on this technique was invented in 1907 (Miwa and Shimomura, 1976 [14]). The arrival of high speed rotating machines made it necessary to develop a balancing technique for flexible rotors.

As rotors became lighter and rotational speeds higher, the occurrence of nonlinear resonances such as subharmonic resonances became a serious problem. Yamamoto (1955 [15], 1957 [16]) studied various kinds of nonlinear resonances after he reported on subharmonic resonances due to ball bearing in 1955. He discussed systems with weak nonlinearity that can be expressed by a power series of low order. In the 1960s, cracks were found in rotors of some steam turbines. To prevent serious accidents and to develop a vibration diagnosis system detecting cracks, research on vibrations of cracked shafts began. In the 1970s, Gasch (1976) [17] and Henry and Okah-Avae (1976) [18] investigated vibrations giving consideration to nonlinearity in stiffness due to open-close mechanisms. They showed that an unstable region appeared or disappeared at the major critical speed, depending on the direction of the unbalance.

The latest topic in rotordynamics is a study of magnetic bearings, which support a rotor without contacting it, and active dampers. This study has received considerable attention.

2.2 Investigation and Prevention of the Rubbing

Many significant researches have been found regarding the investigation of contact phenomena between rotor-to-stator and rotor-to-guide and also the suppression techniques of the vibration for the safe and reliable design of rotating machinery. For the investigation of the rubbing between the rotor and stator, Black (1968) [19] can be mentioned as a significant contributor to this problem. He tried to explain the scenario of rub elaborately using polar receptance of the rotor and stator on a radial symmetric rotor. He considered the rotor and stator both as linear multi-degree-of-freedom (d.f) systems including damping and dry friction at the clearance space. Interactions with dry friction counterwhirling were also considered. Some experimental results on counterwhirl within a ball bearing were given in his work and qualitatively compared with the theory. Ehrich (1966) [20] adopted a four degree of freedom model where the stator is replaced by a ring supported by spring and damper. This paper discussed the stability condition of backward rub with a simple model of inertia, stiffness and damping without considering friction and an unbalance of the system. Muszynska (1984) [21] made a comprehensive study on the

rubbing problem. He tried numerical simulations as well as experiments for various cases. Recently Choi (2002) [3] conducted experiments for various rubbing phenomena where he considered the whirling motion of full annular rotor rub. Numerical simulations were also done for the investigation of the physics of full annular rub. This research work reveals the effects of the friction co-efficient and the eccentricity of the rotor which explain the beginning of backward rolling and backward slipping as the rotor speed increases or decreases. Ishida et al. (2003) [2] performed the probability of the occurrence of forward rub, backward rub and impact by theoretical investigations and simulations. Ishida et al. (2009) [22] observed the vibration characteristics in turbo machinery with radial clearance between a bearing outer ring and a casing. This paper mainly focuses the nonlinear resonances and self excited oscillation investigations by numerical simulations. A model of a flexible rotor is presented there where the bearing collides with the casing due to the clearance and its equation of motions is derived.

Excellent works have also been found out on the light and short arc rubs in rotating machines. Pennacchi et al. (2009) [23] had worked on the effect of short arc rub typical of light contact on seals. An experimental study and a mathematical model aimed to analyze the effects of rotor-to-stator rub on seals were presented. For the fault diagnostics of rotating machinery, Chu and Lu (2005) [24] did extensive work on an experimental setup to simulate the nonlinear behavior of the rub impact of the rotor system. To simulate the condition of the full rub, a special structure of stator was designed. Experiments with different conditions, including one and two rotor with single and multi-disks, were performed. Muszynska and Goldman (1995) [25] concentrated on the periodic and chaotic patterns of rotor responses. Their research revealed the dynamic behavior of the rotor/bearing/stator systems with loose stationary joints. Feng and Zhang (2002) [26] discussed the vibration phenomena of a rotor rubbing with a stator caused by an initial perturbation. Their work showed that when friction was present the full rubbing behaved as backward whirling and when there was no friction on the contact surface between the rotor and the stator, the full rubbing behaved as forward whirling. Chu and Zhang (1997) [27] investigated the vibration characteristics of a rub impact rotor system supported on oil film bearings. Wenhui et al. (2008) [28] showed that the Lyapunov exponent was a valid method in identifying the bifurcation and chaos characteristics for rotor bearing system. They analyzed the bifurcation and chaos characteristics of a flexible rotor system with two unbalanced disks using the maximum Lyapunov exponent. Lu et al. (2003) [29] considered the existence of rub-impact periodic motions in an eccentric rotor system. Al-Wedyan et al. (2008) [30] performed the dynamic analysis of a rigid rotor system with a base of fluid film bearings subjected to vibrations. Li and Paidoussis (1994) [31] investigated analytically and numerically the dynamics of a shaver rotor/casing system with clearance and mass imbalance. Their results demonstrated the existence of both rubbing and impacting behavior.

From the recent literature survey, it has been found that misalignment causes significant rubbing phenomenon in turbo machinery [32]. Misalignment may be present because of improper machine assembly, thermal distortion and asymmetry in the applied load. Patel and Darpe (2009)

[6] explained the dynamics of misaligned rotors and attempted to improve the reliability of the misalignment fault diagnosis. In recent years, it has been found that higher efficiency requirements often lead to the reduction of clearances in seals. This leads to the problem of thermally induced vibrations [33]. Bachschmid et al. (2007) [33] analyzed the dynamical behavior of the machine considering thermally induced vibrations.

In industrial rotating machinery, rotor-to-stator rub can occur in different sections of the machine and can have different degrees of severity. The rotating machinery can cross some critical speeds during the run-ups and the run-downs and can interfere with the seals in case of incorrect design, excessive imbalance, misalignment, bad assembly or other causes. Fig. 2.1 shows the effect of rub on a seal which depicts that the threads are practically destroyed and the functionality of the seal are greatly damaged. From previous literature, it has been found that rub which occurs between parts have different stiffness, in particular when the rotor is stiffer than the stator or, more precisely, than the parts where the contact happens [23]. Rubbing phenomenon is also severe in electrical machines. Fig. 2.2 shows rubbing between rotor and stator in a motor.

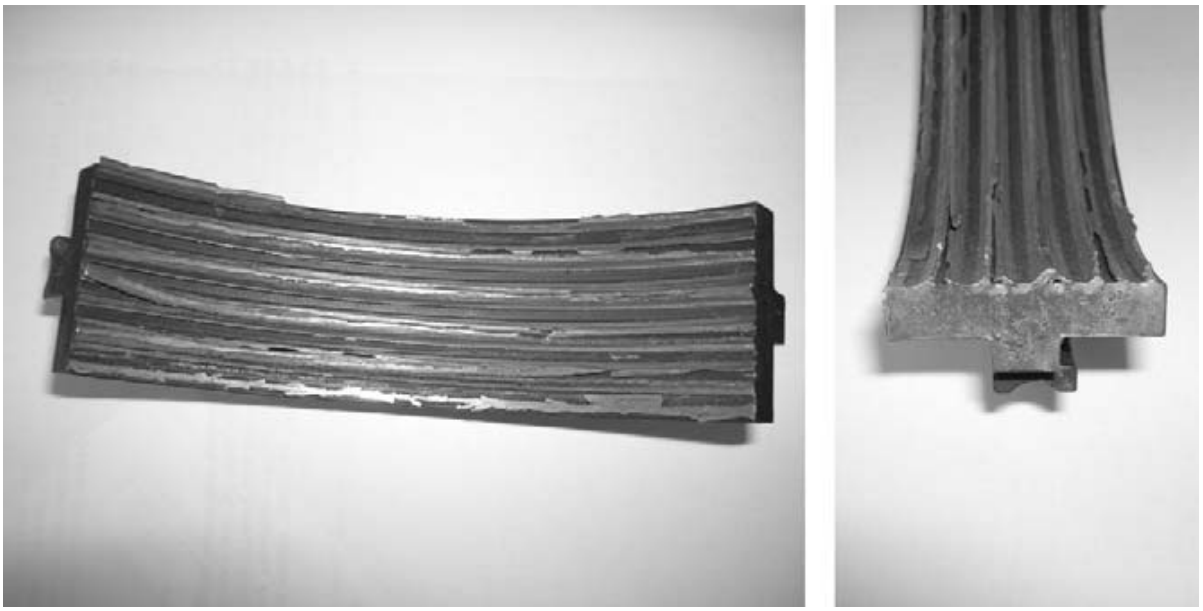

Fig. 2.1: Effect of the rub on a labyrinth seal [23].

Fig. 2.2: Rubbing of the rotor of a motor.

Researchers have also shown experimental evidence of heavy rub in rotating machines. Curami et al. (1986) [34] presented the experimental evidence of heavy rub in a 320 MW steam turbine. Stegemann et al. (1993) [35] analyzed significant tests on a 100 MW steam turbine with about 500 cases of rub.

Researches have also been carried out to suppress the vibration between the rotor-stator contacts. Various methods, including feedback control of the driving torque and changes to the system stiffness, etc., have been proposed to suppress the large vibrations of rotors during accelerating and decelerating past the critical speed (Nagaya et al., 1983; Suherman and Plaut, 1997) [36-37]. Changes to the system stiffness can be implemented by installment of the support springs made of memory metals (Nagaya et al., 1983), disk-type electrorheological damper (Yao and Meng, 1999), or magnetorheological fluid damper (Wang and Meng, 2001) [36,38-39]. Ding Q. (2004) [40] considered a flexible Jeffcott rotor mounted at the ends by identical squeeze film dampers (SFDs). His work revealed the effectiveness of application of a flexible internal support, which could be activated or deactivated at a certain position along the rotor to avoid the occurrence of diverging backward whirl. Jiang et al. (2006) [41] developed an optimal controller and a PD-controller to effectively reduce the rubbing severity. Although the backward rub or the partial impact vibrations are dangerous, they can be avoided by effectively lubricating the contact surface in order to decrease the friction [42]. Inoue et al. [42] proposed the suppression method of the forward rub by introducing the directional difference in the support stiffness of the guide or the backup bearing. This is certain that all these methods can be applied to avoid severe rubs between rotor and casing and to allow the rotor to pass through the critical speed safely. And investigations of these applications are really worthwhile.

2.3 Scope of the Present Study

In this present work, the rubbing phenomenon between rotor and guide is identified by simulation and experiment. For the minimization of rubbing between rotor and guide, circular and lemon shaped bearing have been implemented. From the literature review, it has been found that the mathematical model for the circular back up bearing has already been established. But no significant work has been identified on the development of the mathematical model for lemon type back up bearing. So the novelty of this research work is the mathematical model analysis for the lemon type backup bearing as well as implementation of this new type of bearing. Fig. 2.3 depicts different types of non circular bearings. In this research work, Fig. 2.3(a) is considered. Further a simple Jeffcott rotor model is simulated for the investigation of rubbing between rotor and guide for considering both the circular type backup bearing as well as lemon type backup bearing. The numerical model is developed with the help of MATLAB SIMULINK software. For different initial conditions, the rubbing phenomena are observed. In simulation, the clearance between shaft and inner surface of the backup bearing is varied. And for different clearances and initial conditions, the results are observed. The critical analysis is performed by comparing both the experimental and simulation results of the circular and lemon type backup bearing to implement the suitable bearing for minimizing the rubbing. Finally a comparison between experimental and numerical work are carried out to validate the overall scenario of this research work.

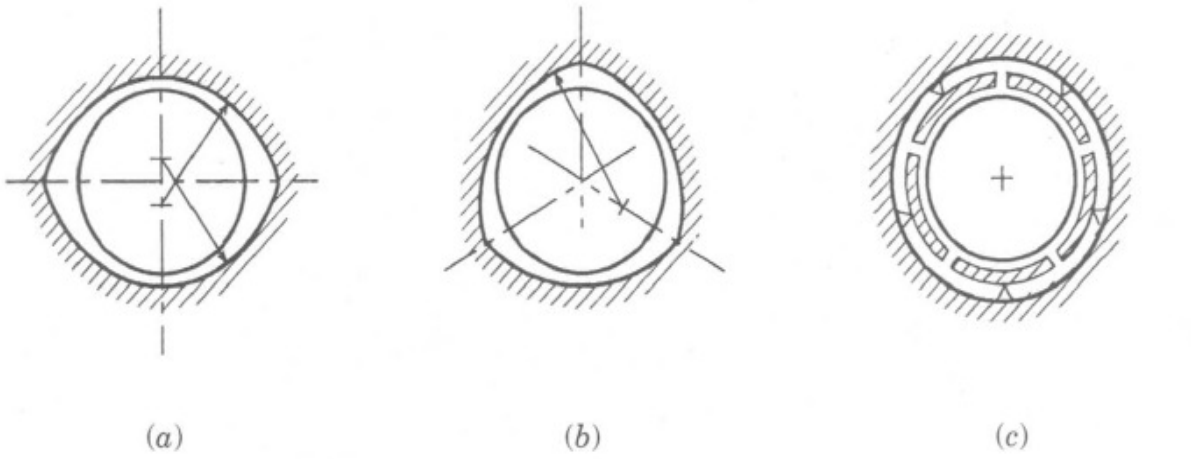

Fig. 2.3: Non circular bearings: (a) two lobe bearing with a lemon shape; (b) three lobe bearing; (c) tilting-pad bearing [43].

Chapter 3

Experimental Setup

3.1 Overview and Description of the Experimental Setup

The experimental setup in this study was manufactured by Bangladesh Machine Tools Factory (BMTF) Ltd. and Machine Shop of Islamic University of Technology (IUT). The photograph of the experimental setup is shown below in Fig. 3.1.

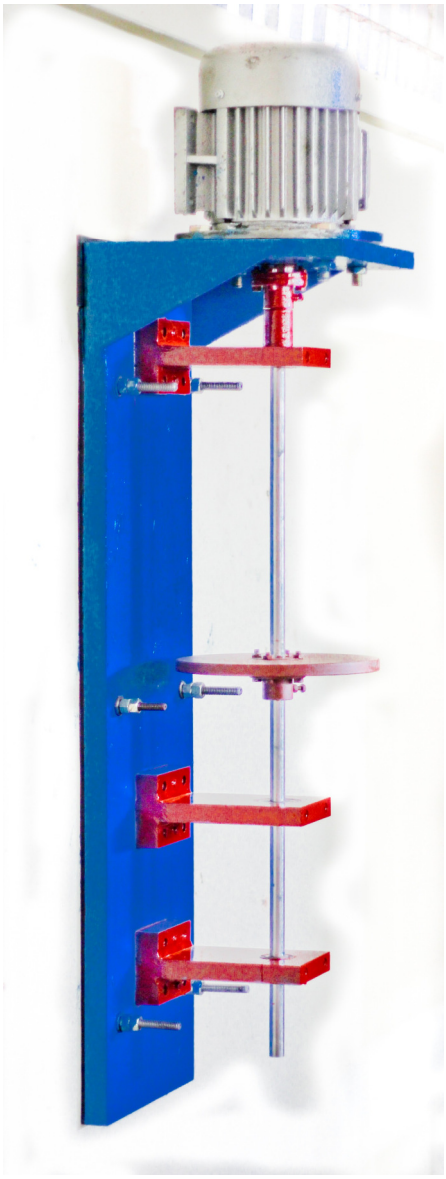

Fig. 3.1: Photograph of the experimental Setup.

Fig. 3.2 illustrates the design and major dimensions of the experimental test rig.

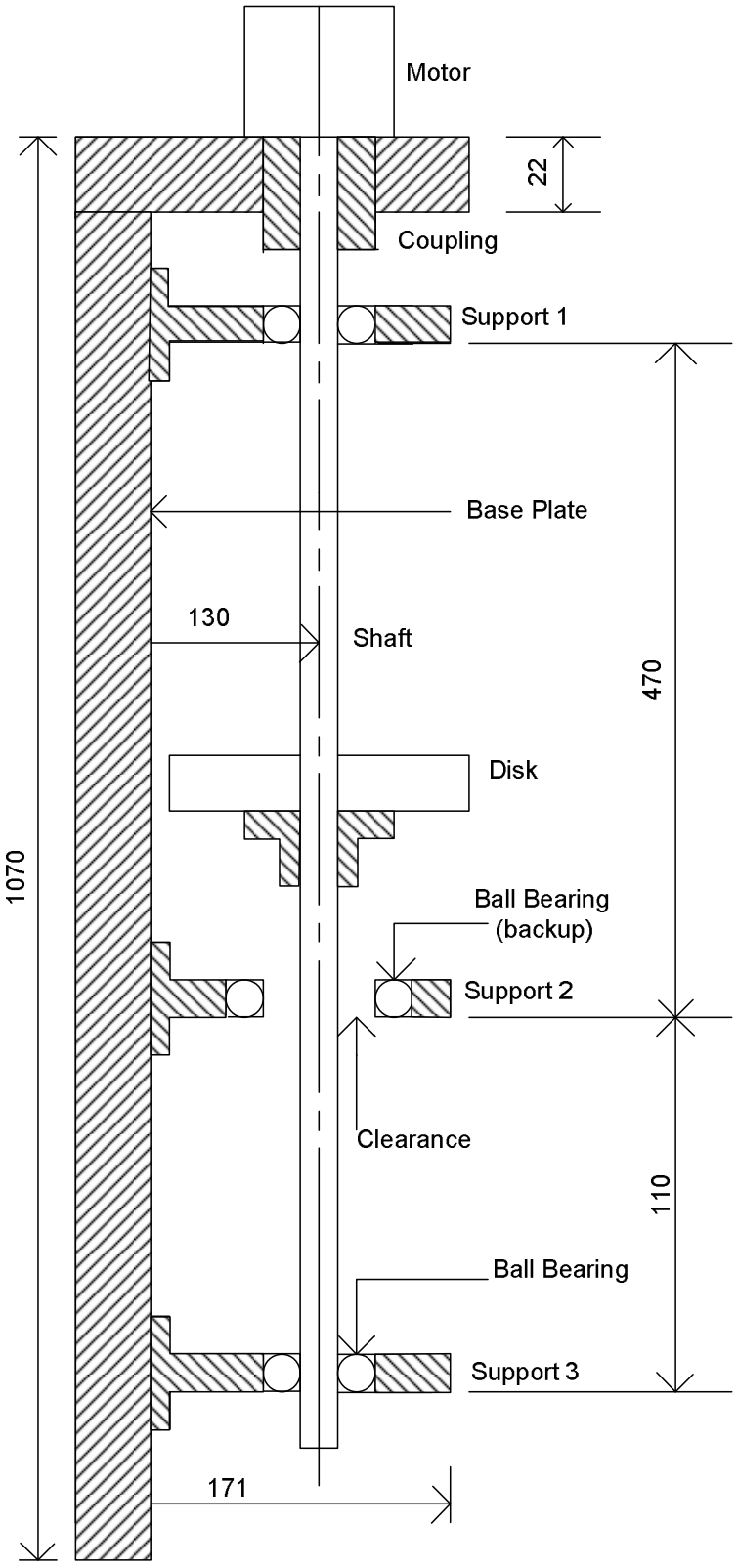

Fig. 3.2: Schematic of the setup enlightens the major dimensions (in mm) and part names.

An elastic shaft with the radius of 8 mm and the length of 970 mm is supported vertically by the ball bearings at both ends. Fig. 3.3 shows the bearing support at one end of the shaft. The inside diameter, outside diameter and the thickness of the upper and lower bearing are 16 mm, 35 mm and 11 mm, respectively. A disk (rotor) with the radius of 100 mm is attached at just the middle position of the shaft. The disk is supported by a bush which is then attached to the shaft with the help of pin. In this experiment, three types of disks were used. In all the cases the diameter of the disks was 200 mm but the thickness of the disks were 5 mm, 10 mm and 15 mm. Fig. 3.4 depicts the disk of 15 mm thickness of the experiment. The disk displacements in x and y directions were measured by the eddy current sensor (Lion Precision, Driver: ECL202e-U12-SAM-3.0 and Probe: U12B (STD MCX, STD HSG, P, 3 M)). Fig. 3.5 shows the eddy current sensor system used in this experiment and Fig. 3.6 depicts the mounting of this sensor's probe in front of the target. The target of the eddy current sensor is aluminum. Therefore a very thin aluminum sheet was attached to a certain portion of the shaft as the material of the shaft was stainless steel. The calibration parameters of the eddy current sensor are given in Table 3.1. The backup bearing is set at the position of 50 mm below the disk position with gap of $\delta = 2mm$. The inside diameter, outside diameter and the thickness of the backup bearing are 24 mm, 47 mm and 12 mm, respectively. The total setup is attached to the wall. Below the experimental setup, a rubber material is intentionally placed for damping purpose. A cover is used which is made of celluloid over the experimental test rig in case of any danger.

The motor used in this study is 3 phase induction motor which runs from 0 to 3000 RPM. The power of this motor is 1 HP which is regulated by an inverter (1 HP, VFD-EL, DELTA ELECTRONICS, INC.) This motor provides the system with rotation torque that allows for a rotordynamic investigation. A flange type coupling connects the motor to the shaft. Fig. 3.7 depicts the coupling between motor and shaft.

Table 3.1: Calibration parameters of eddy current sensor

Calibration Parameters	
Near Gap	600 μm
Range	3500 μm
Target	1-6061 Aluminum
Output	0 to 10 VDC
Sensitivity	2.857 mV/μm
Bandwidth	15000 Hz

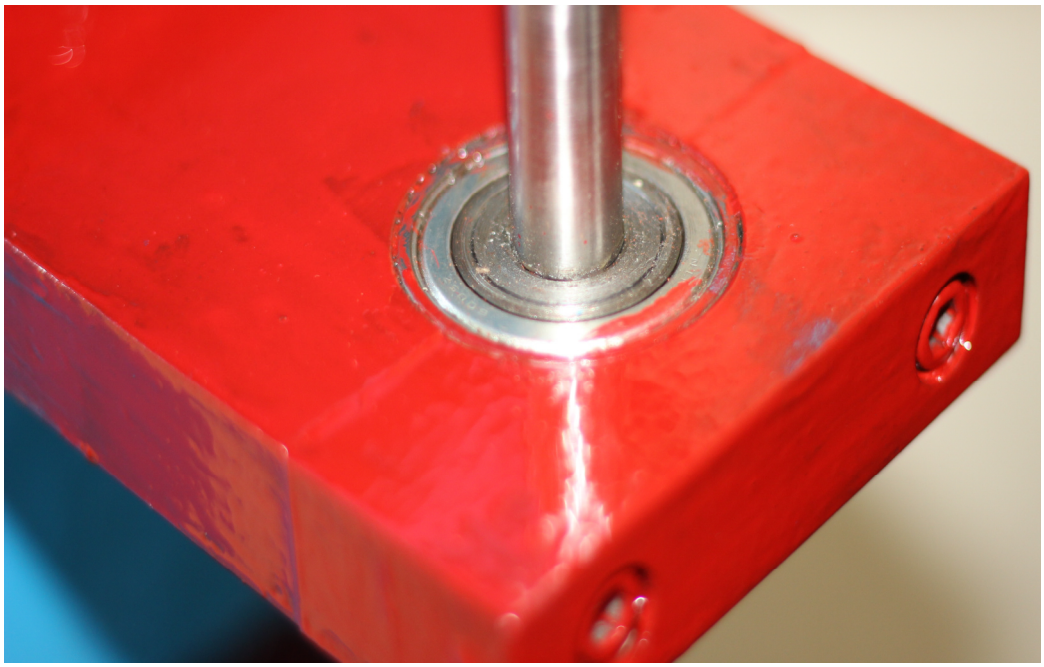

Fig. 3.3: Photograph of the bearing support at one of the ends.

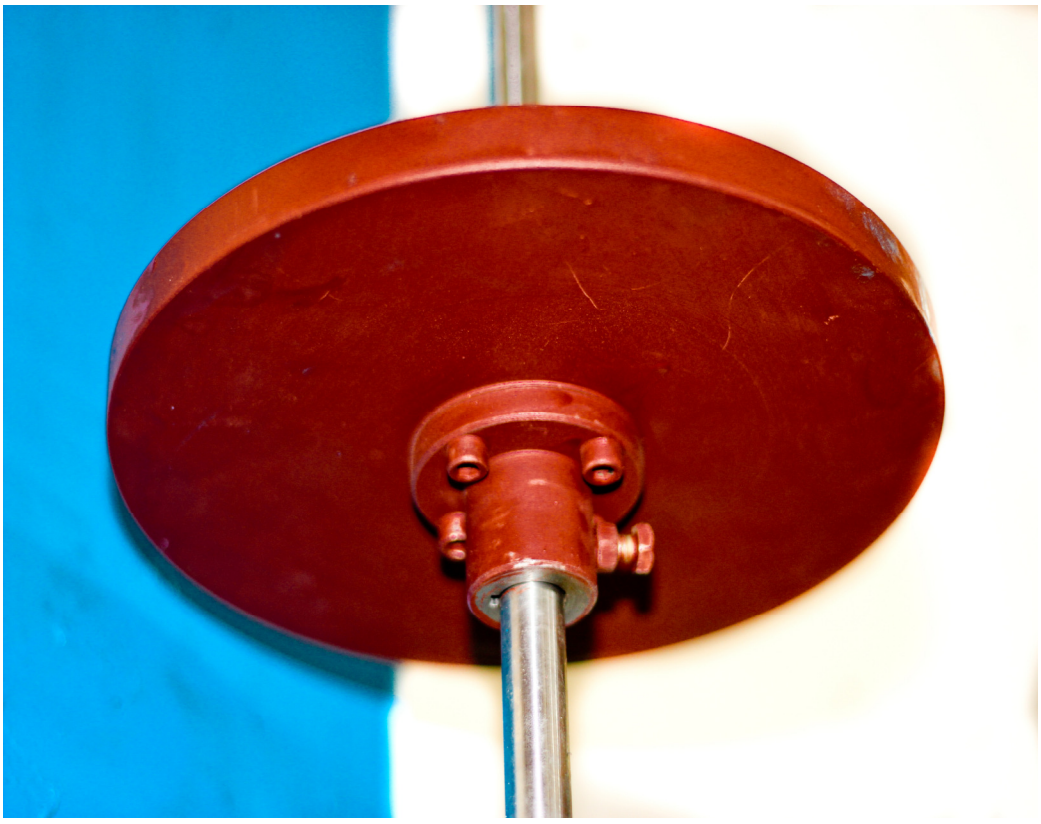

Fig. 3.4: Photograph of the disk (15 mm thickness).

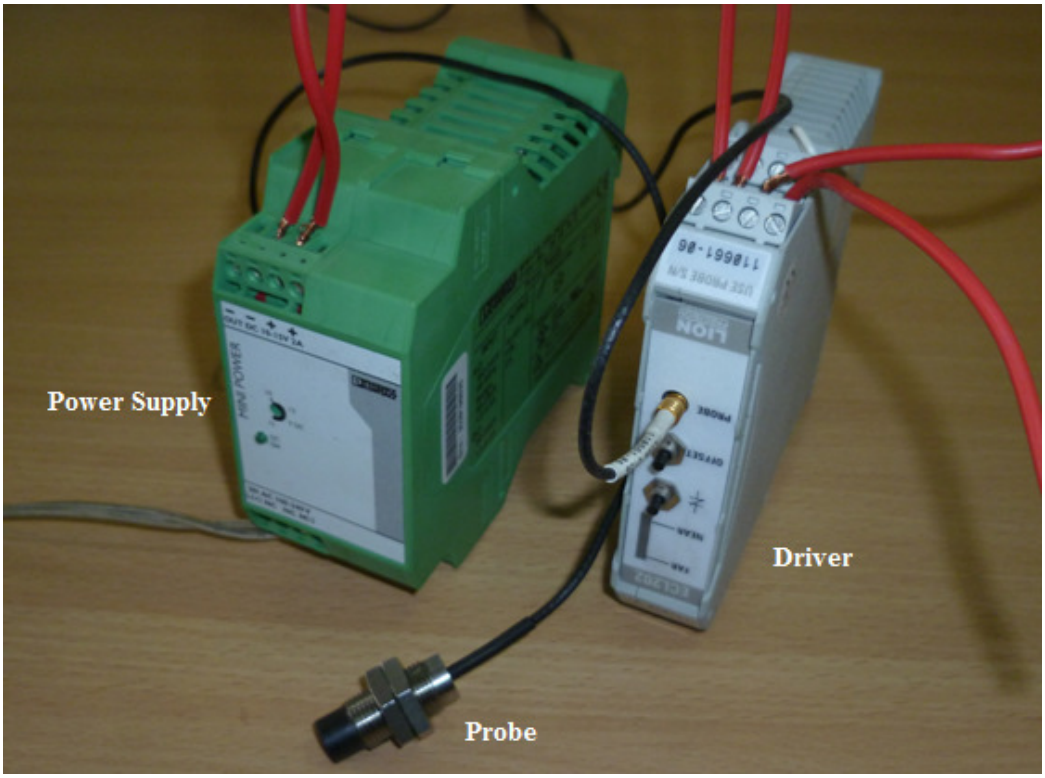

Fig. 3.5: Photograph of the eddy current sensor system.

Fig. 3.6: Photograph of the probe of eddy current sensor mounted in front of the target.

Fig. 3.7: Photograph of the coupling between motor and shaft.

Fig. 3.8 depicts the 3D model of the experimental setup which was developed by SolidWorks. This design was necessary to check all the centers of motor, rigid disk, bearings and shaft whether they were on the same line. This design ensured the proper alignment of each and every part of the experimental test rig.

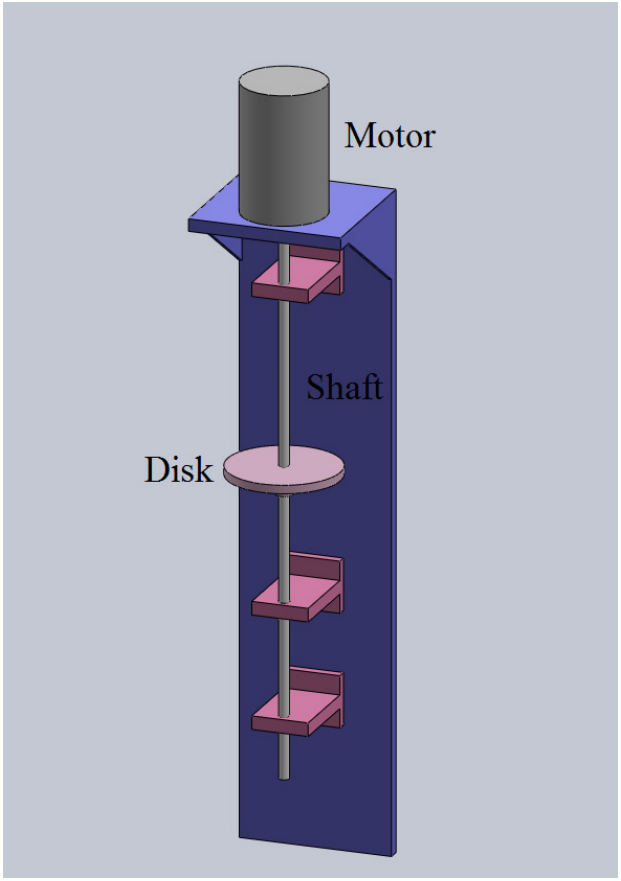

Fig. 3.8: 3D design of the experimental setup.

3.2 Experimental System Block Diagram

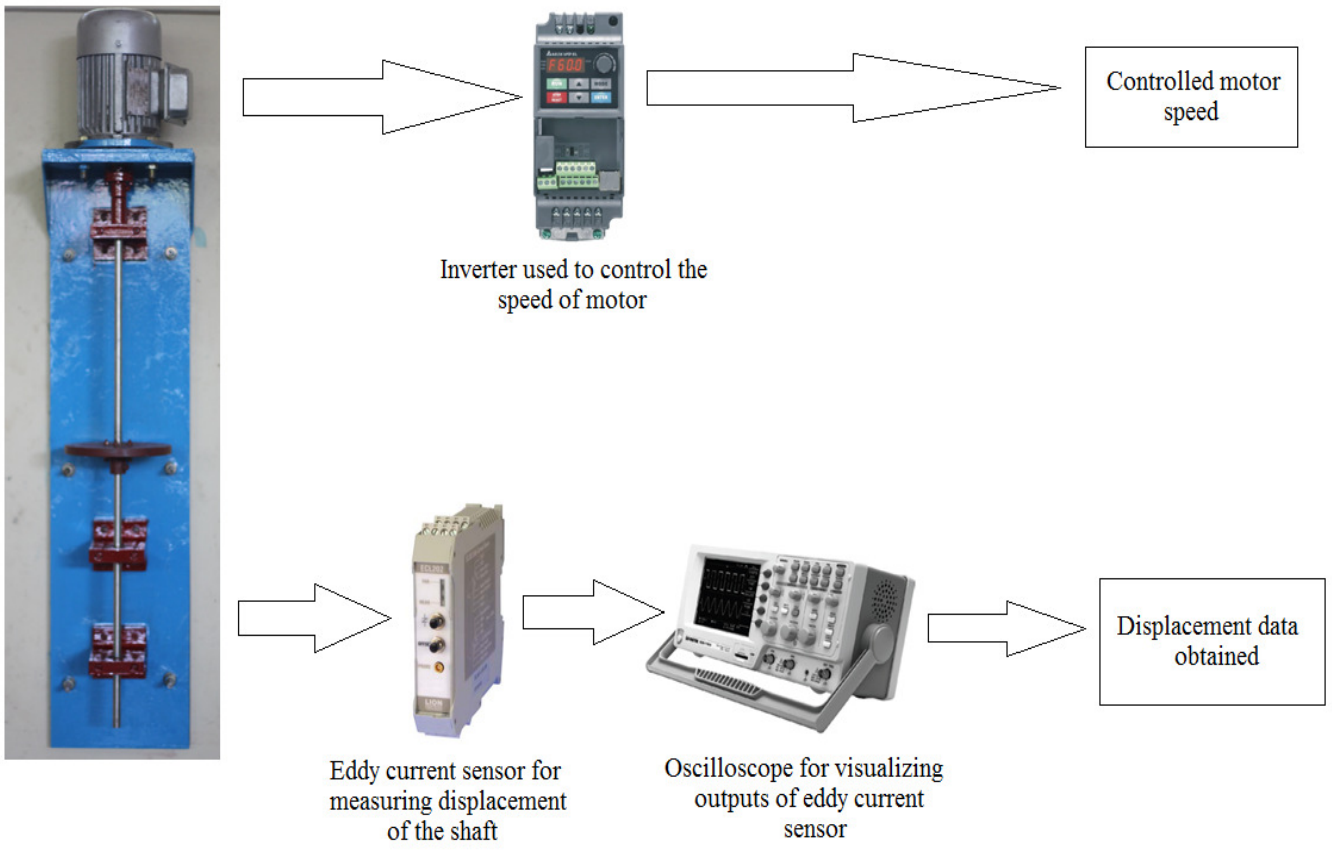

Fig. 3.9: Experimental system block diagram.

Fig. 3.9 represents overall system block diagram. The motor used in this experiment is three phase. So, an inverter is connected with the motor with a view to regulating the motor speed. Using the inverter, it was possible to control the motor precisely and take the data at certain interval. The displacement of the shaft in both x and y directions is measured by the eddy current sensor. The probe is placed in front of the shaft which is then connected to the driver unit of the eddy current sensor. A 15V power supply is used to run the driver unit of the sensor. The measuring range of the eddy current sensor is 3.5 mm. It means the sensor is capable of measuring the displacement if the deflection of the shaft is within 3.5 mm. The driver unit is connected to the oscilloscope which gives the outputs of the sensor. The input to the overall system is the frequency which runs the motor and the output from the system is 0 to 10 VDC from the sensor which is then visualized by the oscilloscope. The displacement data is taken from the oscilloscope.

3.3 Experimental Procedures

The experiments were observed for three types of disk masses. Table 3.2 refers the three different types of disk. And two types of backup bearing were considered for the study such as circular and lemon type. Firstly disk 3 was considered as rotor for the system and the phenomena of rubbing were observed. The motor speed was varied from 0 to 3000 RPM and the rubbing between shaft and the backup bearing started when the rotational speed was 2160 rpm. Secondly disk 2 was considered as rotor for the system and the rubbing started when the rotational speed was 1800 rpm. And finally disk 1 was used as rotor for the system and the rubbing started when the rotational speed was 1440 rpm.

Table 3.2: Length/thickness and masses of the experimental setup components

Component	Material	Length/Thickness (mm)	Diameter (mm)	Mass (kg)
Shaft	Stainless Steel	970	16	1.5
Disk 1	Mild Steel	15	200	3.6
Disk 2	Mild Steel	10	200	2.5
Disk 3	Mild Steel	5	200	1.4

Chapter 4

Mathematical Model of Circular Backup Bearing

4.1 Vibration of Massless Shafts with Rigid Disks [43]

4.1.1 General Considerations

In the vibration analysis of rotating machinery, a lumped parameter system in which a rigid disk is mounted on a massless elastic shaft is often adopted as a mathematical model. Some examples of such fundamental rotor systems are shown in Fig. 4.1. In these rotor systems, a disk is mounted on a shaft of circular cross section. If a rotor is mounted at the center of an elastic shaft supported at both ends, the lateral deflection r and the inclination θ of the rotor are independent of each other and the system is decoupled into two rotor systems with two degrees of freedom (2DOF). Fig. 4.1(a) shows a 2DOF model for the deflection motion of such a system. This simplified mathematical model, called the Jeffcott rotor, is the most widely used model in the theoretical analysis of rotors. Fig. 4.1(b) is a 2DOF model for the inclination motion. Differing from the system in Fig. 4.1(a), the gyroscopic moment acts in this system, and as a result of that, its natural frequencies change as a function of the rotational speed. For some types of vibration problems, this model is more suitable than that of Fig. 4.1(a). Fig. 4.1(c) shows 4DOF models where the deflection motion and the inclination motion couple with each other.

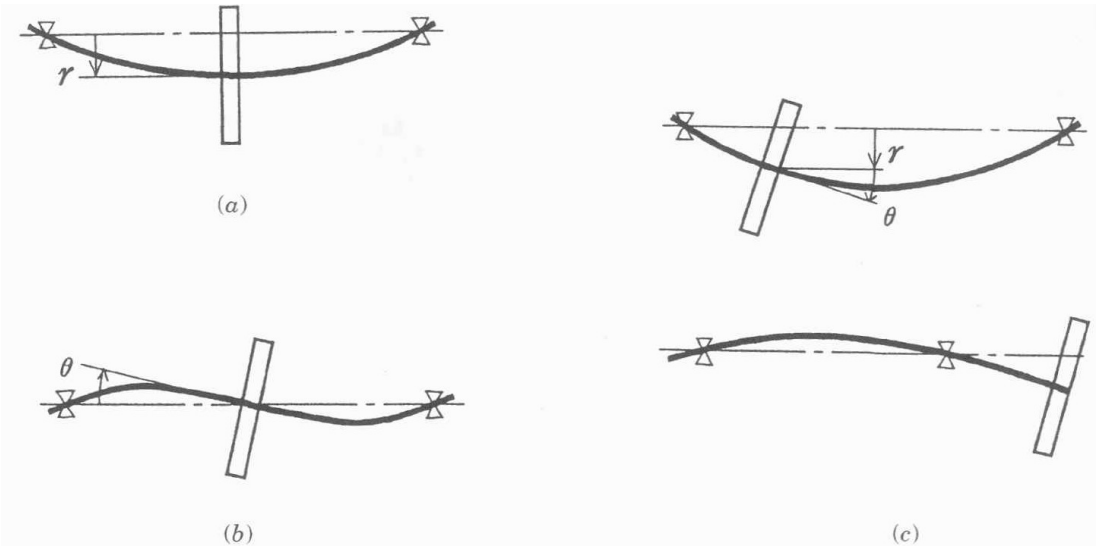

Fig. 4.1: Lumped-parameter rotor models: (a) 2DOF model (deflection); (b) 2DOF model (inclination); (c) 4DOF model [43].

4.1.2 Rotor Unbalance

The main cause of vibration is the excitation due to inevitable mass unbalance of rotors. Residual unbalances occur due to manufacturing error, thermal deformation, material inhomogeneity, and so on.

As shown in Fig. 4.2, two types of unbalance exist in a rotor system consisting of a rigid rotor and a massless elastic shaft. One is *static unbalance,* which is the state represented by a geometric eccentricity e of the center of gravity of a rotor from the centerline of the shaft. This unbalance produces a centrifugal force proportional to the square of the rotational speed. The static unbalance can be detected without operating the rotor because the unbalance is always directed downward if the shaft is supported horizontally by bearings with little friction. The other is *dynamic unbalance,* which is the state represented by the angular misalignment of the principal axis of moment of inertia of the rotor with respect to the centerline of the shaft. The magnitude of the dynamic unbalance is determined by the angle τ as shown in Fig. 4.2(b). This type of unbalance can not be detected without rotating the shaft. As shown in Fig. 4.2, these unbalances are represented by models with one and two concentrated masses, respectively. If the shaft is supported vertically, then there will not be any eccentricity due to the mass of the rotor. But in this case, the eccentricity is produced if the disk is not isotropically uniform. In this research work, the rotor-shaft system is supported vertically and the eccentricity is created because it is difficult to manufacture the rotor as isotropically uniform.

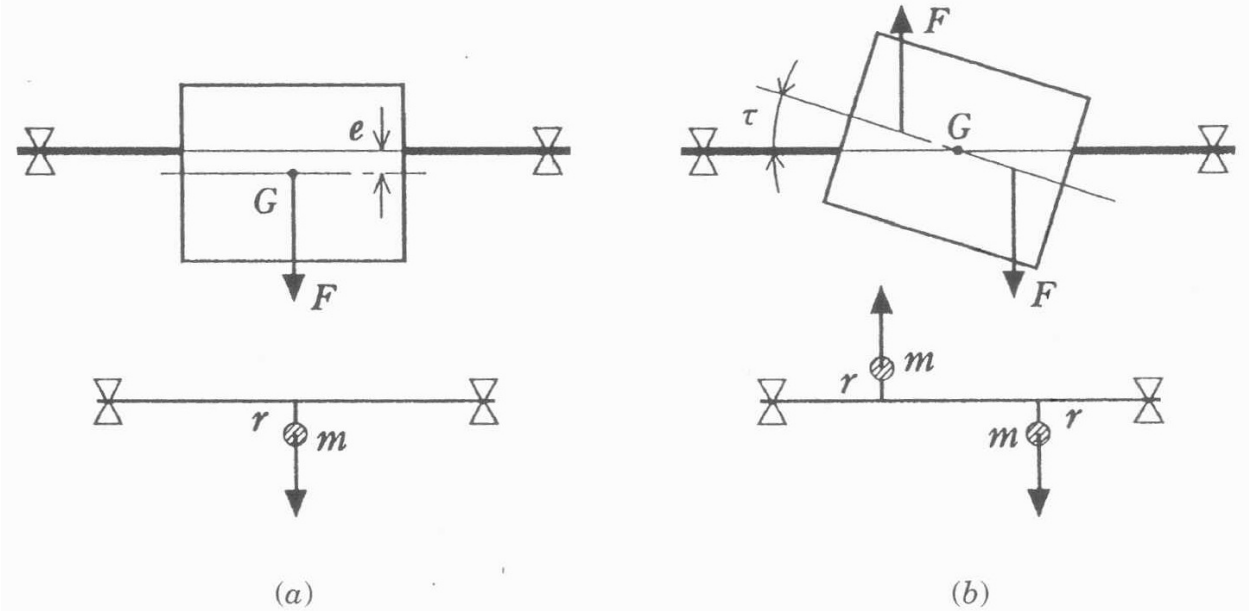

Fig. 4.2: Unbalances in a lumped-parameter rotor system: (a) static unbalance; (b) dynamic unbalance [43].

4.1.3 Lateral Vibrations of an Elastic Shaft with a Disk at Its Center

4.1.3.1 Equations of Motion and Forced Vibrations

Fig. 4.3 shows a vertical rotor in lateral whirling motion and a coordinate system. The gravity force is not considered. The z-axis of the coordinate system O-xyz coincides with the bearing centerline, which connects the centers of the upper and lower bearings. The disk has mass m, and its center of gravity G (x_G, y_G) deviates slightly from the geometrical center M. Due to errors in assembly, this point M does not always coincide with the point S(x, y) through which the shaft centerline passes. The distance $\overline{SG}$ produces the static unbalance. In the following, it is assumed, for simplicity, that the geometrical center M coincides with the shaft center S, and the eccentricity is given by $\overline{MG} = e$.

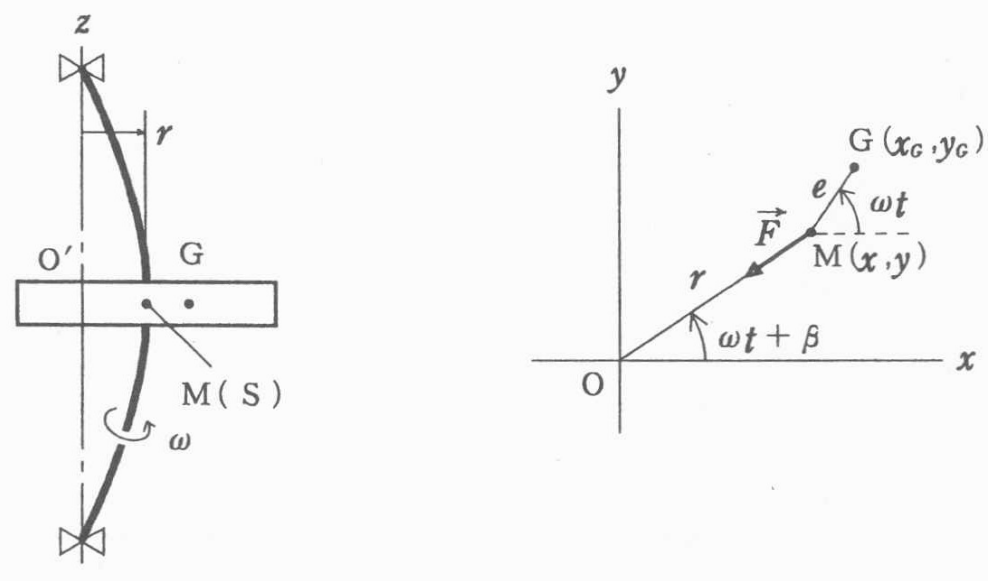

Fig. 4.3: 2DOF rotor system for lateral vibration [43].

Let a rotor spinning with an angular velocity (or rotational speed) ω moves in a circle with a lateral deflection r. This orbital motion is called a *whirl*. The restoring force $\vec{F}(F_x, F_y)$ is expressed by $F_x = -kx$ and $F_y = -ky$, where k is the spring constant. The equations of motion for the undamped system are given by

$$\begin{aligned} m\ddot{x}_G &= -kx \\ m\ddot{y}_G &= -ky \end{aligned} \tag{4.1}$$

Substituting the relations

$$x_G = x + e\cos\omega t$$
$$y_G = y + e\sin\omega t \tag{4.2}$$

Into equation (4.1), we get

$$m\ddot{x} + kx = me\omega^2\cos\omega t$$
$$m\ddot{y} + ky = me\omega^2\sin\omega t \tag{4.3}$$

Which can be rearranged in the form

$$\ddot{x} + \omega_n^2 x = e\omega^2\cos\omega t$$
$$\ddot{y} + \omega_n^2 y = e\omega^2\sin\omega t \tag{4.4}$$

Where $\omega_n = \sqrt{k/m}$. The steady-state response is

$$x = e\frac{\omega^2/\omega_n^2}{1-\omega^2/\omega_n^2}\cos\omega t$$
$$y = e\frac{\omega^2/\omega_n^2}{1-\omega^2/\omega_n^2}\sin\omega t \tag{4.5}$$

In this thesis, the Jeffcott rotor is used as the theoretical model. The massless elastic shaft is supported vertically and the rigid disk is attached at the center of the shaft. The physical model of the rotor-guide system is shown in the Fig. 4.4. Just below the disk the backup bearing is set which has a certain gap with the massless elastic shaft.

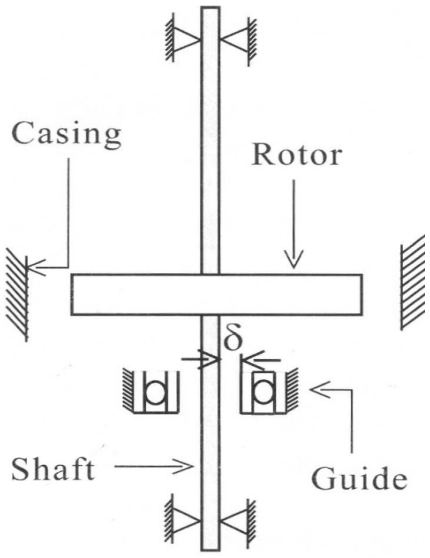

Fig. 4.4: Physical model of the rotor guide system [2].

At around the major critical speed the vibration of the rotating shaft becomes large. Then, the shaft contacts with the backup bearing and the contact vibration occurs. Fig. 4.5 shows the contact models between the shaft and the backup bearing. The contact phenomenon between the shaft and the backup bearing is represented in various models. Li and Paidousis [31] used the instantaneous contact model using the restitution coefficient as shown in Fig. 4.5(a) and performed the numerical simulation with considering the effect of the friction force acting on the rotor. Goldman and Muszynska [44] used the finite time period contact model using the equivalent spring constant and equivalent damping coefficient as shown in Fig. 4.5(b). Symbols k_e and c_e are the equivalent spring constant and the equivalent damping coefficient of the contact phenomena at the backup bearing.

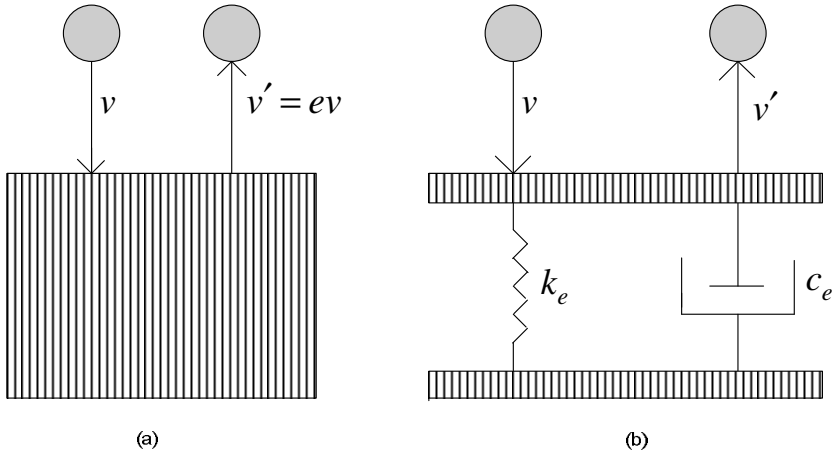

Fig. 4.5: Two types of contact models.

This work considers the contact model of Fig. 4.5(b) and ignores the inner ring rotation of the backup bearing. The friction between the shaft and the inner surface of the backup bearing is considered. The equivalent spring constant k_e is determined from the contact theory and the material characteristics [45]. The equivalent damping coefficient c_e is determined from both the equivalent spring constant k_e and the restitution coefficient e_r. The coordinate of the shaft displacement is denoted by (x, y). The rectangular coordinate O-xy is defined where the origin is situated at the center of the guide. The displacement and the velocity for the radial direction are

$$r = \sqrt{x^2 + y^2}$$
$$\dot{r} = \frac{x\dot{x} + y\dot{y}}{r} \tag{4.6}$$

4.1.4 Impact Condition

(a) From before impact to maximum displacement $\{(x = x_0, v = v_0) \Rightarrow (x = x_{max}, v = 0)\}$

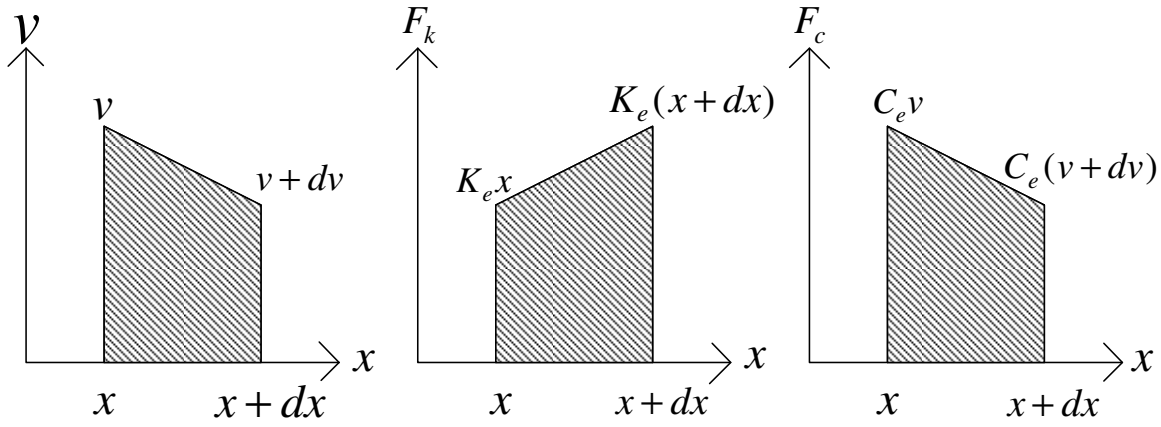

Fig. 4.6: Changing of energy.

During the impact, the displacement changes from x to x+dx, shown in Fig. 4.6. As a result, the spring force, damping force and the velocity change from $k_e x$ to $k_e(x+dx)$, $c_e v$ to $c_e(v+dv)$ and v to (v+dv) respectively. The energy equation for the impact phenomena is

$$\frac{1}{2}mv^2 = \frac{1}{2}mv'^2 + \frac{1}{2}k_e(2x + dx)dx + \frac{1}{2}c_e(2v + dv)dx \tag{4.7}$$

If v' of equation 4.7 is changed to $v + dv$,

$$-mvdv = k_e x dx + c_e v dx \tag{4.8}$$

$$-dv = \frac{k_e x + c_e v}{mv} dx \tag{4.9}$$

Now, considering $v = ux$ in equation 4.9, we get

$$-\frac{dx}{x} = \frac{mu}{k_e + c_e u + mu^2} du \tag{4.10}$$

After integration, we find

$$-\log x = -\frac{c_e \tan^{-1}\left(\frac{c_e + 2mu}{\sqrt{-c_e^{\,2} + 4k_e m}}\right)}{\sqrt{-c_e^{\,2} + 4k_e m}} + \frac{1}{2}\log(k_e + c_e u + mu^2) + \log C_1$$

$$-\log x = -\frac{c_e \tan^{-1}\left(\frac{c_e + 2m\left(\frac{v}{x}\right)}{\sqrt{-c_e^{\,2} + 4k_e m}}\right)}{\sqrt{-c_e^{\,2} + 4k_e m}} + \frac{1}{2}\log\left(k_e + c_e\left(\frac{v}{x}\right) + m\left(\frac{v}{x}\right)^2\right) + \log C_1 \qquad \} \qquad (4.11)$$

$$C_1\sqrt{k_e x^2 + c_e vx + mv^2} = \exp\left(\frac{\tan^{-1}\left(\frac{c_e + 2m\left(\frac{v}{x}\right)}{\sqrt{-c_e^{\,2} + 4k_e m}}\right)}{\sqrt{-c_e^{\,2} + 4k_e m}} c_e\right) \qquad (4.12)$$

Taking the condition as $x = 0, v = v_0$ and $x = x_{\max}, v = 0,$ we find

$$x_{\max} = \frac{\exp\left(\frac{\tan^{-1}\left(\frac{c_e}{\sqrt{-c_e^{\,2} + 4k_e m}}\right)}{\sqrt{-c_e^{\,2} + 4k_e m}} c_e\right)}{C_1\sqrt{k_e}}$$

$$v_0 = \frac{\exp\left(\frac{\frac{\pi}{2}}{\sqrt{-c_e^{\,2} + 4k_e m}} c_e\right)}{C_1\sqrt{m}} \qquad \} \qquad (4.13)$$

(b) From maximum displacement to after impact $\{(x = x_{\max}, v = 0) \Rightarrow (x = 0, v = v_0')\}$

The energy equation for this condition is from Fig. 4.7.

$$\frac{1}{2}k_e(2x + dx)dx = \frac{1}{2}m\{v^2 - (v + dv)^2\} + \frac{1}{2}c_e(2v + dv)dx \qquad (4.14)$$

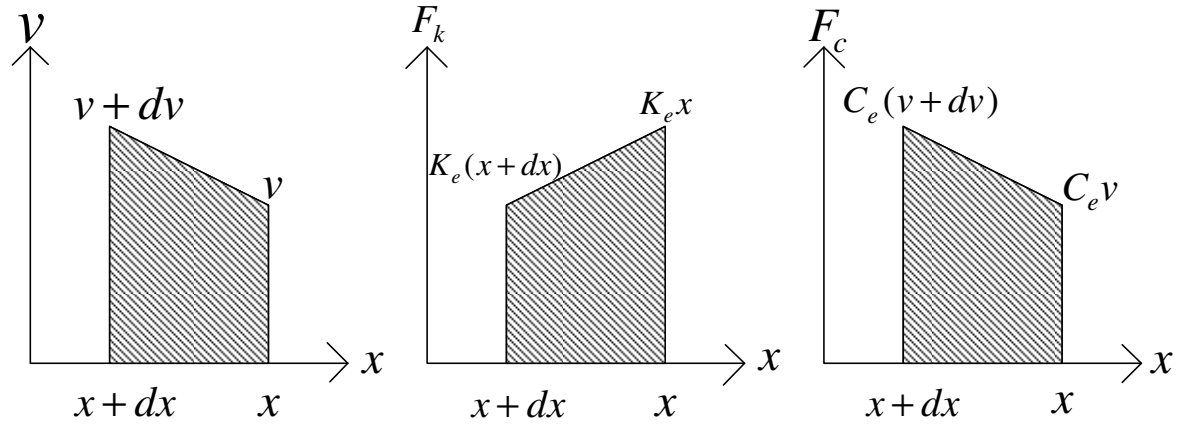

Fig. 4.7: Changing of energy

After simplification

$$k_e x dx = -mvdv + c_e v dv \tag{4.15}$$

Again considering $v = ux$, we get

$$-\frac{dx}{x} = \frac{mu}{k_e - c_e u + mu^2} du \tag{4.16}$$

Taking the condition as ($x = x_{\max}, v = 0$) and ($x = 0, v = v_0'$)

$$\left.\begin{aligned} x_{\max} &= \frac{\exp\left(-\frac{\tan^{-1}\left(\frac{-c_e}{\sqrt{-c_e^2 + 4k_e m}}\right)}{\sqrt{-c_e^2 + 4k_e m}} c_e\right)}{C_2\sqrt{k_e}} \\ v_0' &= \frac{\exp\left(\frac{\frac{\pi}{2}}{\sqrt{-c_e^2 + 4k_e m}} c_e\right)}{C_2\sqrt{m}} \end{aligned}\right\} \tag{4.17}$$

From equation 4.13 and 4.17, we find

$$e_r = \frac{v_0'}{v_0} = \frac{\exp\left(-\frac{-c_e \frac{\pi}{2}}{\sqrt{-c_e{}^2 + 4k_e m}}\right)}{\exp\left(-\frac{c_e \frac{\pi}{2}}{\sqrt{-c_e{}^2 + 4k_e m}}\right)} \tag{4.18}$$

$$e_r = \exp\left(\frac{-c_e \pi}{\sqrt{-c_e{}^2 + 4k_e m}}\right) \tag{4.19}$$

Where e_r is the coefficient of restitution.

So, we find the value of c_e as below:

$$c_e = \sqrt{\frac{4mk_e (\ln e_r)^2}{\pi^2 + (\ln e_r)^2}} \tag{4.20}$$

4.2 Equations of Motion for the Circular Backup Bearing [42]

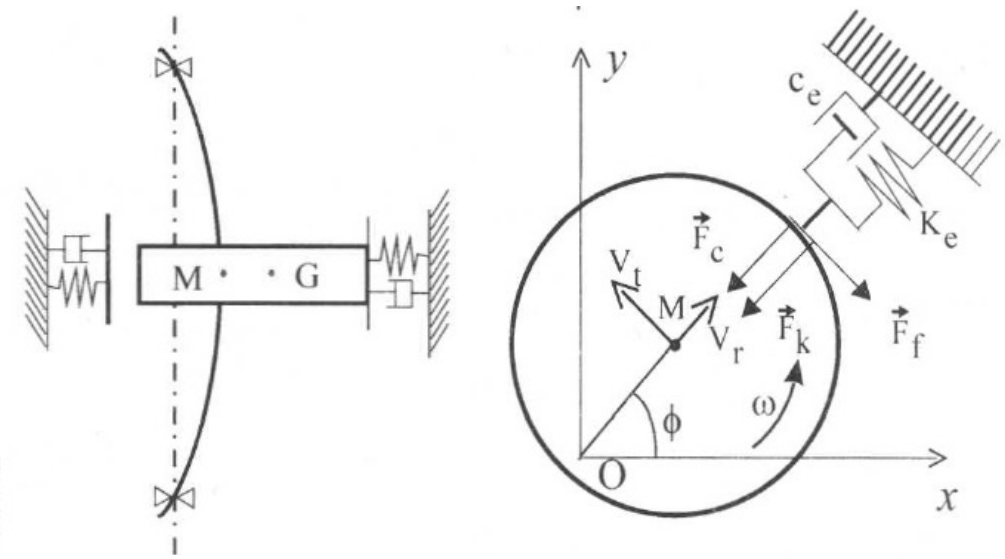

(a) Rotor System (b) Contact Forces

Fig. 4.8: Mathematical model for a rotor-guide system [2].

Fig. 4.8 shows the mathematical model for a rotor-guide system. Due to contact with the guide restoring force F_k, damping force F_c and friction force F_f are generated. V_t and V_r are the tangential and radial velocities of the rotor respectively.

The restoring force is

$$F_k = k_e(r - \delta') \tag{4.21}$$

Here, k_e is the spring constant of the backup bearing and δ' is the gap between the shaft and the backup bearing.

The damping force is

$$F_c = c_e \dot{r} \tag{4.22}$$

Here, c_e is the damping coefficient of the backup bearing.

The friction force is

$$F_f = \pm\mu(F_k + F_c) \tag{4.23}$$

The $\pm$ sign depends on forward and backward rubbing condition. If the rub is forward then the sign of the above equation is positive and if the rub is backward then the sign is negative.

The transferred value of F_k in the x direction is

$$F_{kx} = k_e(r - \delta')\frac{x}{r} \tag{4.24}$$

The transferred value of F_k in the y direction is

$$F_{ky} = k_e(r - \delta')\frac{y}{r} \tag{4.25}$$

The transferred value of F_c in the x direction is

$$F_{cx} = c_e \dot{r}\frac{x}{r} \tag{4.26}$$

The transferred value of F_c in the y direction is

$$F_{cy} = c_e \dot{r}\frac{y}{r} \tag{4.27}$$

The transferred value of F_f in the x direction is

$$F_{fx} = \mu(F_k + F_c)\frac{y}{r} \tag{4.28}$$

The transferred value of F_f in the y direction is

$$F_{fy} = -\mu(F_k + F_c)\frac{x}{r} \tag{4.29}$$

The condition for both the restoring force F_k and the damping force F_c is represented below.

$$\left.\begin{aligned} F_k &= k_e(r-\delta') \\ F_c &= c_e\dot{r} \end{aligned}\right\} \text{ for } r \geq \delta' \tag{4.30}$$

When $r < \delta'$ then both the restoring force F_k and the damping force F_c will become zero. This scenario represents the non contact condition between the shaft and the backup bearing.

The following step equation is considered to make a one equation:

$$u(x) = \begin{cases} 0 & (x < 0) \\ 1 & (x \geq 0) \end{cases} \tag{4.31}$$

So, the restoring force and the damping force become as

$$\begin{aligned} F_k &= k_e(r-\delta')u(r-\delta') \\ F_c &= c_e\dot{r}u(r-\delta') \end{aligned} \tag{4.32}$$

The stepping equation is further simplified as:

$$u(x) = \frac{1+\dfrac{x}{|x|}}{2} \tag{4.33}$$

And consequently the restoring force and the damping force become:

$$\begin{aligned} F_k &= k_e(r-\delta')\frac{1+\dfrac{r-\delta'}{|r-\delta'|}}{2} \\ F_c &= c_e\dot{r}\frac{1+\dfrac{r-\delta'}{|r-\delta'|}}{2} \end{aligned} \tag{4.34}$$

When the rotor with the rotating velocity ω contacts with the guide, the friction force F_f works against the rotation of the rotor. Now this friction force is represented as:

$$F_f = \pm\mu(F_k + F_c) \tag{4.35}$$

If $V_t + \omega R_s > 0$ then F_f is positive.

If $V_t + \omega R_s < 0$ then F_f is negative.

Where R_s is the radius of the shaft and V_t is the tangential velocity of the geometrical center of rotor. The tangential velocity V_t can be obtained below:

From figure 4.8, we can write

$$\begin{aligned} x &= r\cos\phi \\ y &= r\sin\phi \end{aligned} \tag{4.36}$$

And

$$\tan\phi = \frac{y}{x}$$

By differentiating the above equation

$$\sec^2\phi\dot{\phi} = \frac{x\dot{y} - y\dot{x}}{x^2} \tag{4.37}$$

$$\begin{aligned} \dot{\phi} &= \frac{x\dot{y} - y\dot{x}}{x^2(1+\tan^2\phi)} \\ &= \frac{x\dot{y} - y\dot{x}}{x^2(1+\frac{y^2}{x^2})} \\ &= \frac{x\dot{y} - y\dot{x}}{x^2 + y^2} \\ &= \frac{x\dot{y} - y\dot{x}}{r^2} \end{aligned}$$

$$\dot{\phi}r = \frac{x\dot{y} - y\dot{x}}{r} \tag{4.38}$$

So the tangential velocity $V_t = \frac{x\dot{y} - y\dot{x}}{r}$

The friction force can be positive or negative. This scenario can be represented by the following equation which is also applied to the simulation.

$$F_f = \mu(F_k + F_c)\left[\frac{1+\frac{(R_s\omega + V_t)}{|R_s\omega + V_t|}}{2} - \frac{1-\frac{(R_s\omega + V_t)}{|R_s\omega + V_t|}}{2}\right] \tag{4.39}$$

So, from Fig. 4.8 the equations of motion for the circular backup bearing during contact can be obtained below:

$$m\ddot{x} = -c\dot{x} - kx - F_{kx} - F_{cx} \pm F_{fx} + me\omega^2 \cos\omega t \tag{4.40}$$

$$m\ddot{y} = -c\dot{y} - ky - F_{ky} - F_{cy} \pm F_{fy} + me\omega^2 \sin\omega t \tag{4.41}$$

Where m is the mass of the rotor, ω is the angular velocity of the rotor and e is the unbalance of the rotor. Due to unbalance e, $me\omega^2 \cos\omega t$ and $me\omega^2 \sin\omega t$ forces are generated along the x and y axis respectively.

After simplification equations 4.40 and 4.41 can be represented below:

$$\ddot{x} = -c\dot{x} - x - k_e(r-\delta)\frac{x}{r} - c_e\dot{r}\frac{x}{r} \pm \mu(F_k + F_c)\frac{y}{r} + e\omega^2 \cos\omega t \tag{4.42}$$

$$\ddot{y} = -c\dot{y} - y - k_e(r-\delta)\frac{y}{r} - c_e\dot{r}\frac{y}{r} \mp \mu(F_k + F_c)\frac{x}{r} + e\omega^2 \sin\omega t \tag{4.43}$$

The representations of the non dimensional parameters are as follows:

$$x' = \frac{x}{D_s},\ y' = \frac{y}{D_s},\ \delta = \frac{\delta'}{D_s},\ r' = \frac{r}{D_s},\ e' = \frac{e}{D_s},\ t' = \omega_n t,$$

$$\omega' = \frac{\omega}{\omega_n},\ c' = \frac{c}{m\omega_n},\ F_k' = \frac{F_k}{m\omega_n D_s},\ F_c' = \frac{F_c}{m\omega_n D_s},\ F_f' = \frac{F_f}{m\omega_n D_s},\ R' = \frac{R_s}{D_s}$$

After rearranging equations 4.42 and 4.43 and also converting in non dimensional form can be again represented below:

$$\ddot{x}' + c'\dot{x}' + x' + F_k'\frac{x'}{r'} + F_c'\frac{x'}{r'} - F_f'\frac{y'}{r'} = e'\omega'^2 \cos\omega' t' \tag{4.44}$$

$$\ddot{y}' + c'\dot{y}' + y' + F_k'\frac{y'}{r'} + F_c'\frac{y'}{r'} + F_f'\frac{x'}{r'} = e'\omega'^2 \sin\omega' t' \tag{4.45}$$

Chapter 5

Simulation and Experimental Results of Circular Backup Bearing

The mathematical model for circular backup bearing shown in the previous chapter is simulated in MATLAB SIMULINK software. The solver is used here for solution is ODE 4 (Runge-Kutta method). This chapter will highlight the development of the SIMULINK model and the results obtained from the model. Also the experimental results are discussed in brief for comparison with the simulation results. The following section 5.1 discusses the SIMULINK model, section 5.2 discusses the simulation results and at the end section 5.3 discusses the experimental results.

5.1 The SIMULINK Model

The mathematical model for circular backup bearing has been simulated in MATLAB SIMULINK software. Fig. 5.1 represents the overall SIMULINK block diagram to obtain the solutions from equations 4.44 and 4.45. Five subsystems are used to build the model precisely. All the required connections in subsystem 1, 2, 3, 4 and 5 are shown in Fig. 5.2, 5.3, 5.4, 5.5 and 5.6 respectively. The outputs from subsystem 3 are r and F_k. The outputs from the subsystems 4 and 5 are F_c and F_f. All the outputs r, F_k, F_c and F_f obtained from subsystems 3,4 and 5 are then fed to subsystems 1 and 2. The input force for subsystem 1 (Fig. 5.2) is cosine wave (phase changed in block parameter) and the input force for subsystem 2 (Fig. 5.3) is sinusoidal wave. Integrators in subsystem 1 (Fig. 5.2) and 2 (Fig. 5.3) are used to integrate the acceleration parameters ($\ddot{x}$ in subsystem 1 and $\ddot{y}$ in subsystem 2) to displacements (x and y). Many addition, subtraction, multiplication, division, gain and different other blocks (from SIMULINK library browser) are used to represent the equations 4.44 and 4.45. The parameters considered in simulation are $e' = 0.035, c' = 0.13$, $k_e' = 3800000$, $c_e' = 400$ and $R' = 0.5$ [2]. Initial conditions are given in the integrator blocks of subsystems 1 and 2. Initial conditions are changed according to the different clearances (gap between shaft and inner surface of the bearing). The clearance is represented in SIMULINK model by d. In modeling the circular backup bearing system, the clearance d is constant for a specific scenario. Moreover, initial conditions have also influence for forward and backward rubbing. Two hundred output data points are obtained from the simulation. The outputs from the overall SIMULINK model are visualized by graphical forms (which is basically the graph of amplitude against rotational speed). A small program is written in MATLAB M-file to run the overall SIMULINK block diagram. The program is given below.

```
close all;
clear all;
format long;
e=0.035;
k=1.0;
```

```
ke=3800000;
d=0.2;
c=0.13;
ce=400;
uk=0.0;
step=0.001;
open new.mdl;
w=8.0;

for q=1:800;
    w=w-0.04;
    sim new.mdl;
    a(q,1)=w;
    a(q,2)=max(rout(200001:end));
    figure(1)
    plot(a(:,1),a(:,2),'.')
    hold on

end
plot(a(:,1),a(:,2),'.')
save test.txt a -ascii;
```

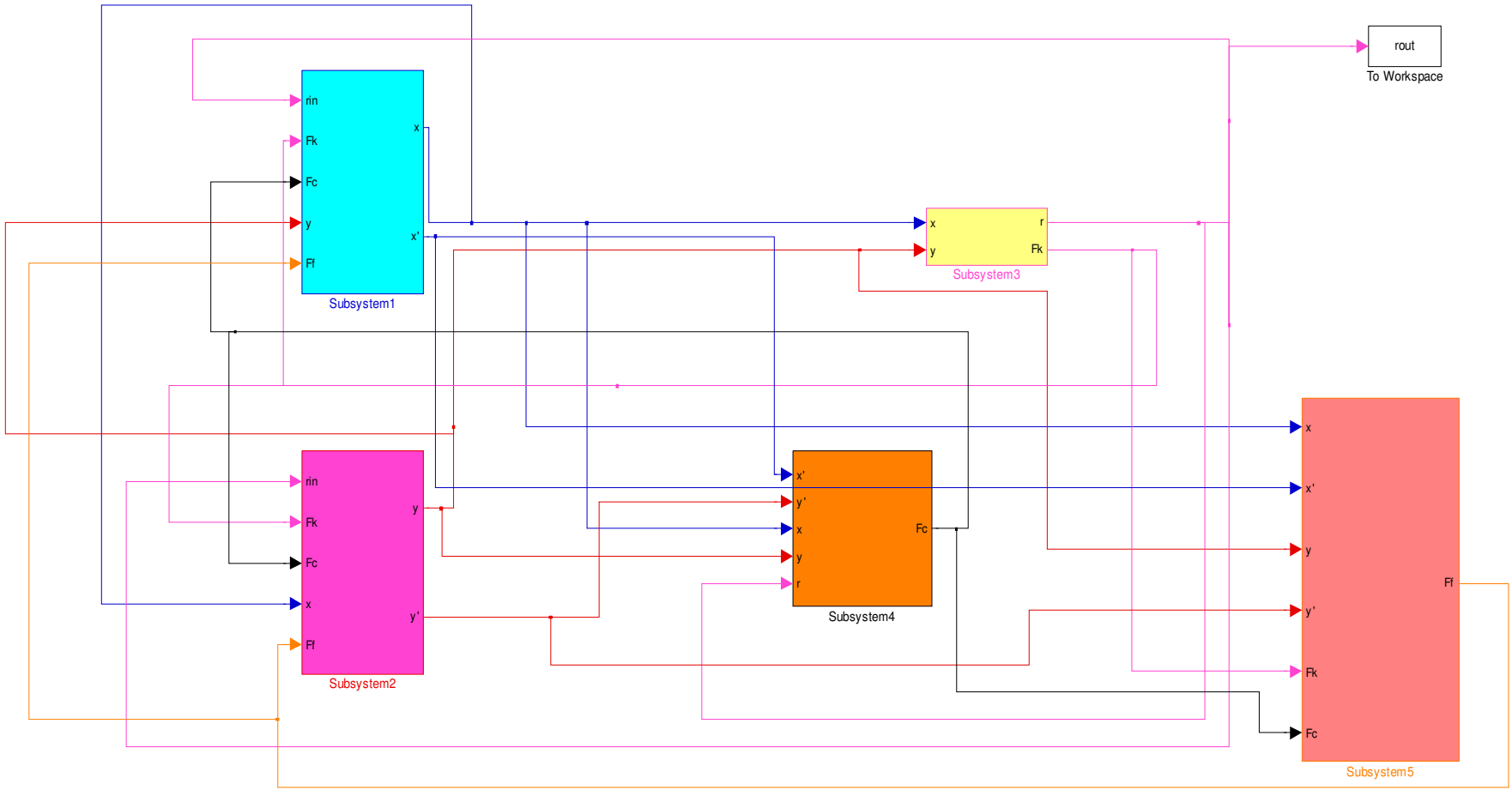

Fig. 5.1: Overall SIMULINK block diagram.

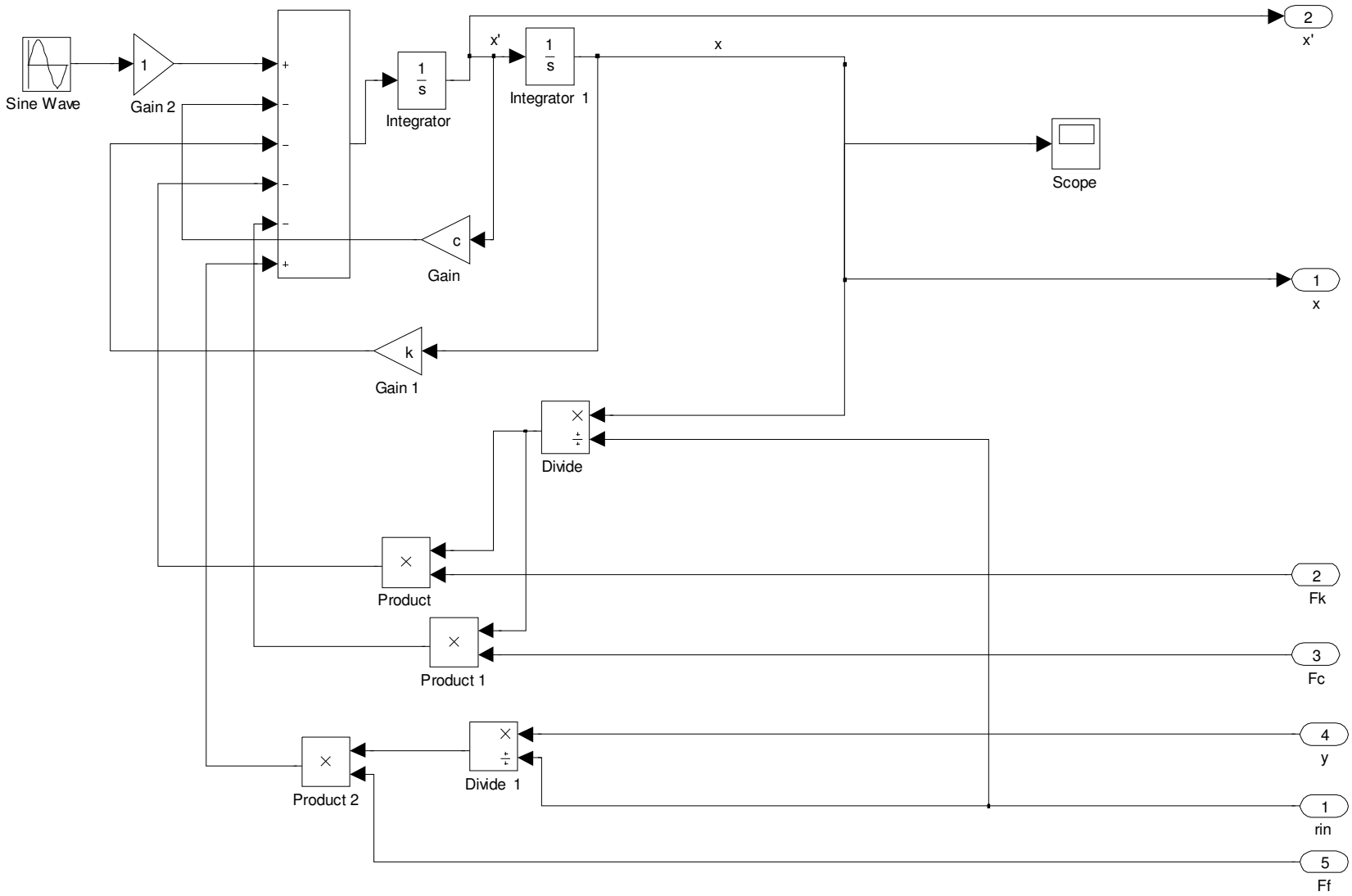

Fig. 5.2: Subsystem 1.

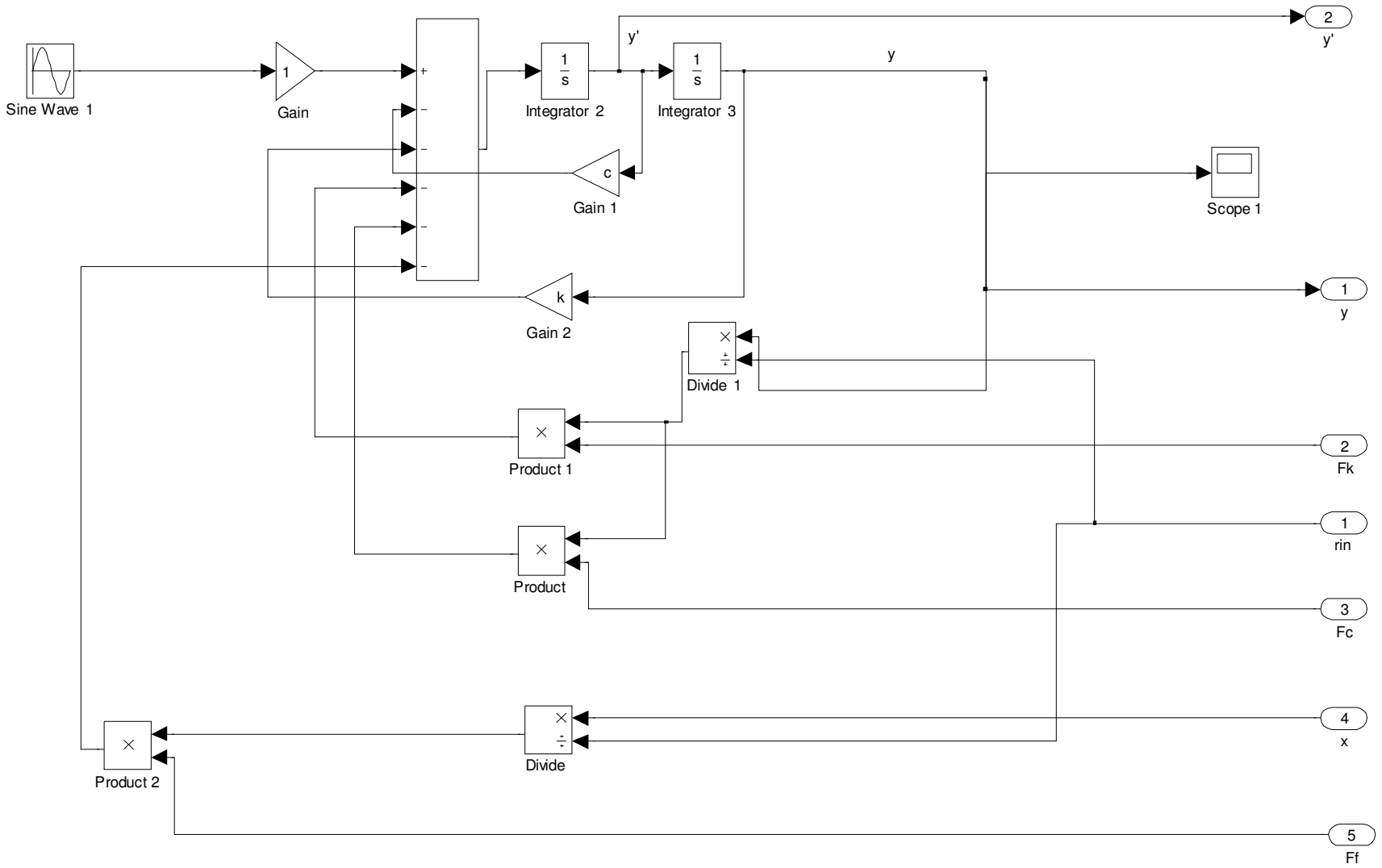

Fig. 5.3: Subsystem 2.

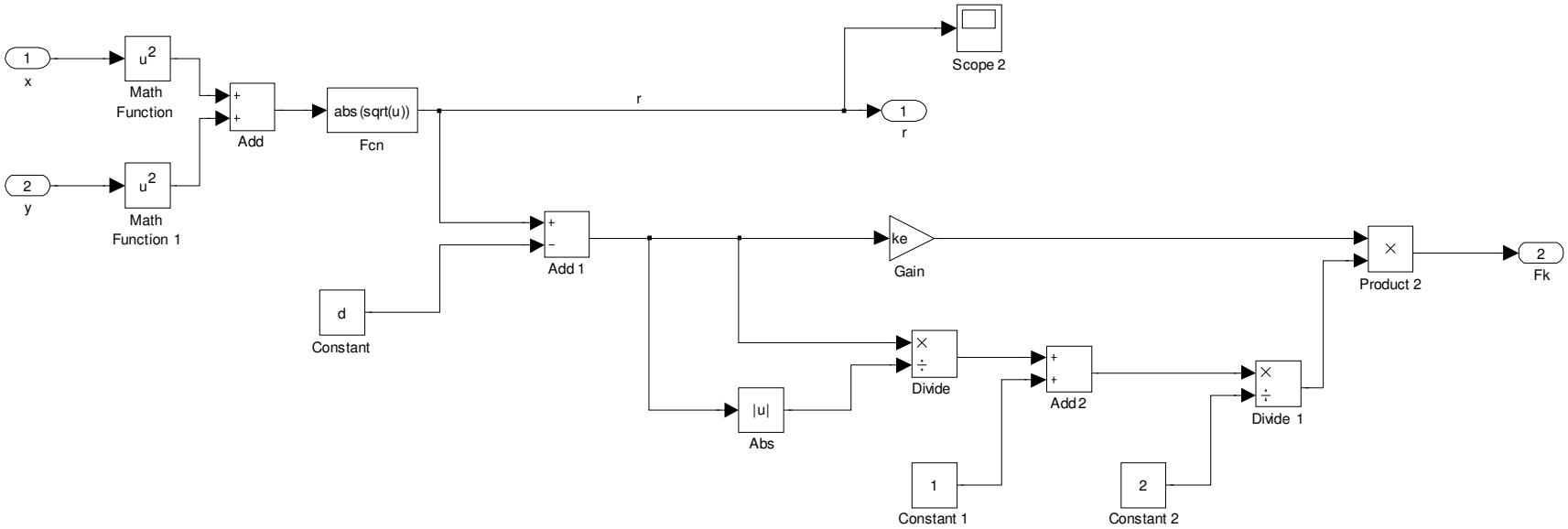

Fig. 5.4: Subsystem 3.

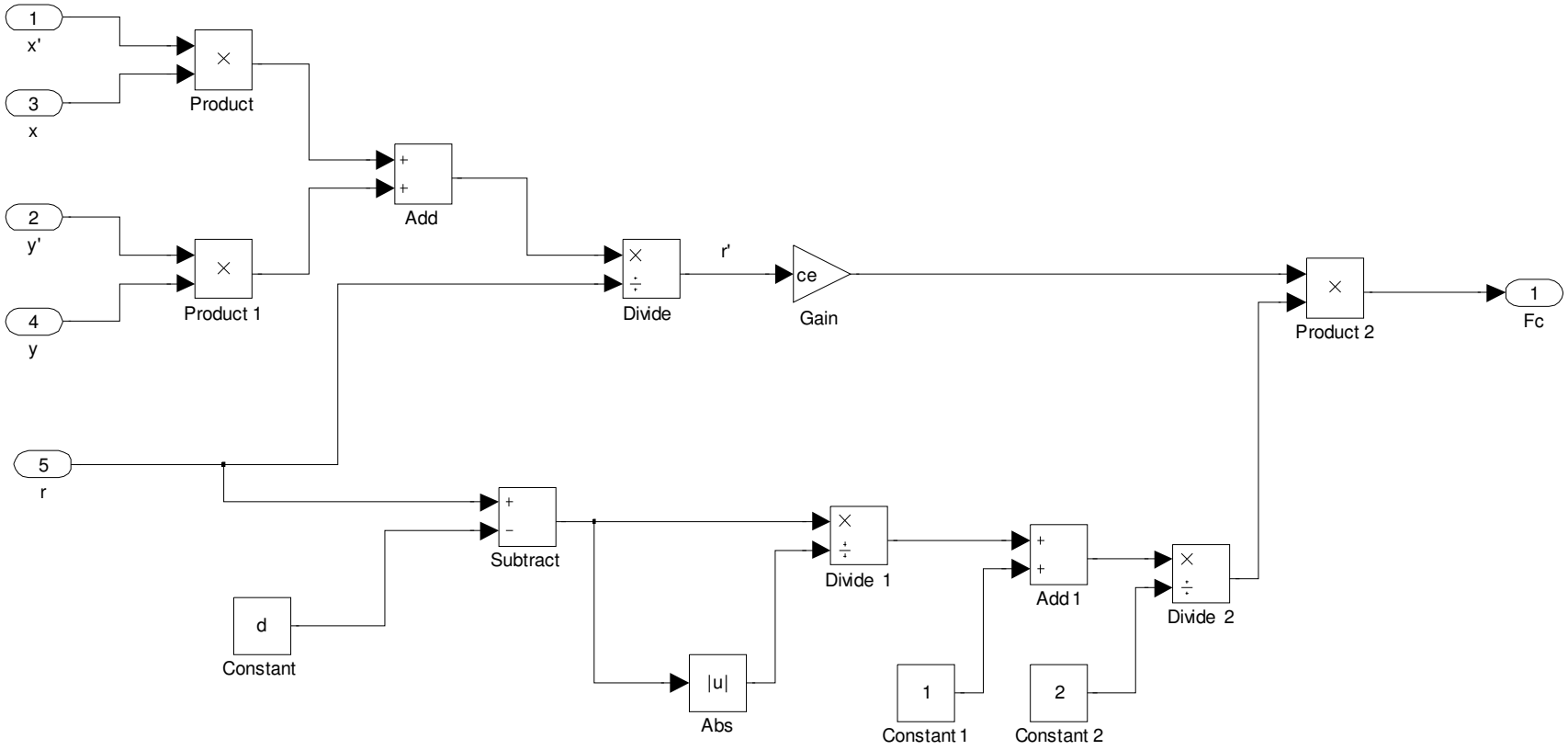

Fig. 5.5: Subsystem 4.

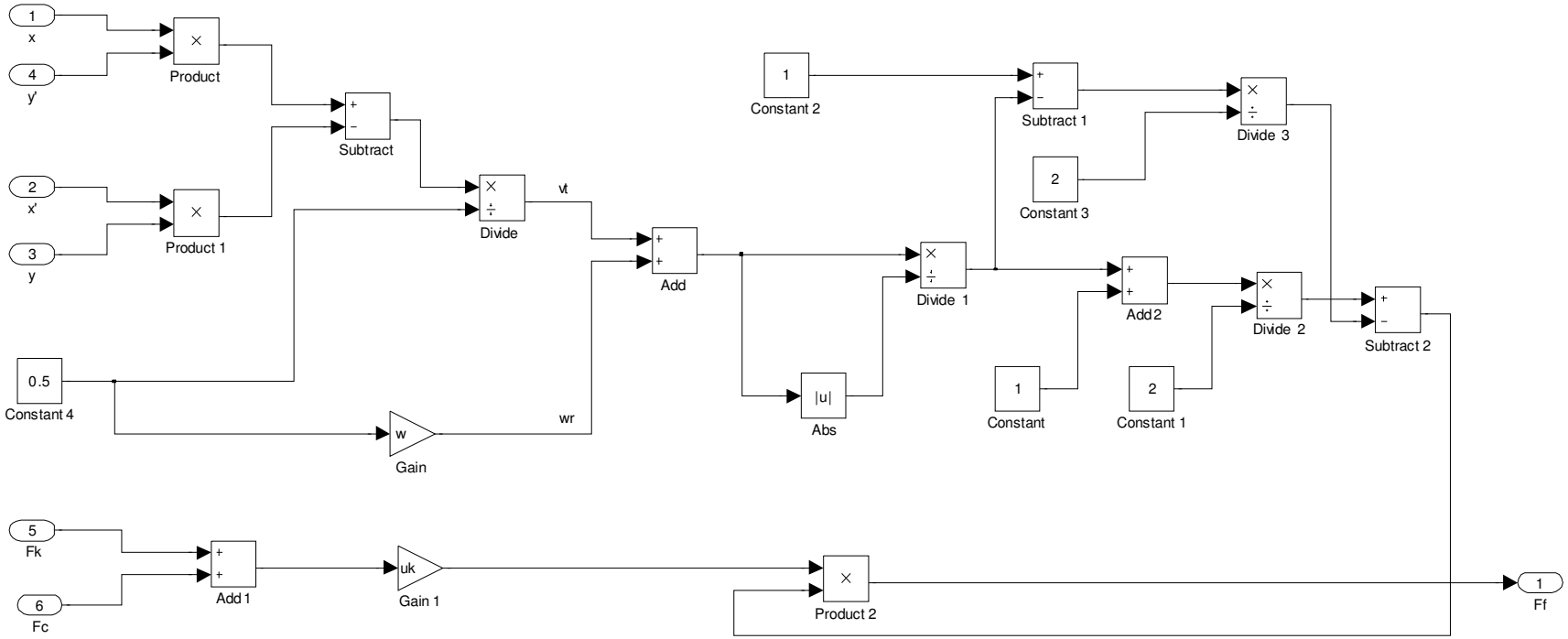

Fig. 5.6: Subsystem 5.

5.2 Simulation Results for Circular Backup Bearing

The following figures enlighten the simulation results for circular backup bearing. Friction effect has also been considered in analysis. Both the forward rub and backward rub phenomena are discussed elaborately with comparison of different clearances (gap between shaft and inner surface of backup bearing). And resonance curves, whirling speed diagrams, phase diagrams and rotor orbits are presented here to illustrate the overall scenarios present in rotor-to-stator contact. The symbol (o) denotes the resonance curves, whirling speed diagrams, phase diagrams and rotor orbits while there is no guide, i.e. no contact motion, and the symbol (●) denotes the resonance curves, whirling speed diagrams, phase diagrams and rotor orbits upon contact while the guide exists. All the parameters are dimensionless in simulation. Therefore, dimensionless analysis is performed in simulations.

5.2.1 Resonance Curves

5.2.1.1 When $\delta = 0.4$

The following figures are considered for $\delta = 0.4$. The friction coefficient is further varied in this case. Fig. 5.7 is considered when there is no friction force. And it is observed from the figure that the contact between rotor and guide drops down when rotational speed is 1.48. The interesting observation from Fig. 5.7 is although the maximum amplitude for the rotor-shaft system is 0.27 at critical speed 1.0, but the amplitude is 0.4 from rotational speed 8.0 to 1.52. This happens because of the initial conditions given in the simulation.

Fig. 5.8 to 5.14 represents the contact phenomena when friction is present. It is obvious from these figures that increasing the friction coefficient the contact between rotor and guide drops down earlier with the rotating speed up to certain friction coefficient. From the Fig. 5.11 when the friction coefficient is 0.07, the contact drops down at rotational speed 6.72. It is also observed that from Fig. 5.7 to 5.11, the rubbing phenomenon is forward which is confirmed by the whirling speed diagram shown in Fig. 5.15. From Fig. 5.15, it is clear that the rotational speed and the whirling speed of the rotor are same. Moreover, the direction of both the speed is same and the scenario is considered as forward rub. But when the friction coefficient is 0.1 and above, the rubbing phenomenon is backward. Fig. 5.12 to 5.14 show the backward rubbing phenomenon which is again confirmed by the whirling speed [see the appendix] diagram as shown in Fig. 5.16. Fig. 5.16 is considered when the friction coefficient is 0.2. From this figure, the rotational speed and the whirling speed are not same and the direction of one is opposite to the other. Therefore, this ensures the phenomenon of backward rub. And in this case, increase in the friction coefficient will increase the probability of the contact between rotor and guide. Fig. 5.14 shows that the contact drops down when rotational speed is 1.

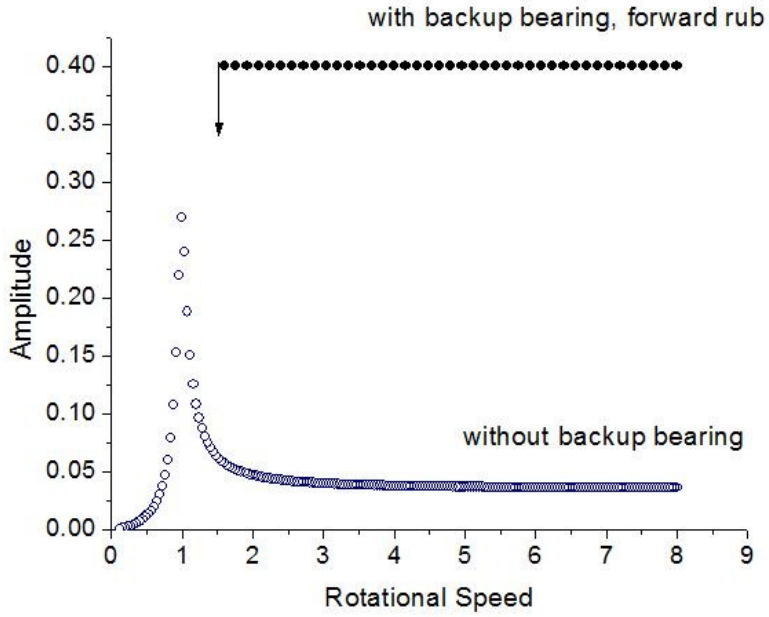

Fig. 5.7: Resonance Curve $\delta = 0.4, \mu = 0.0$

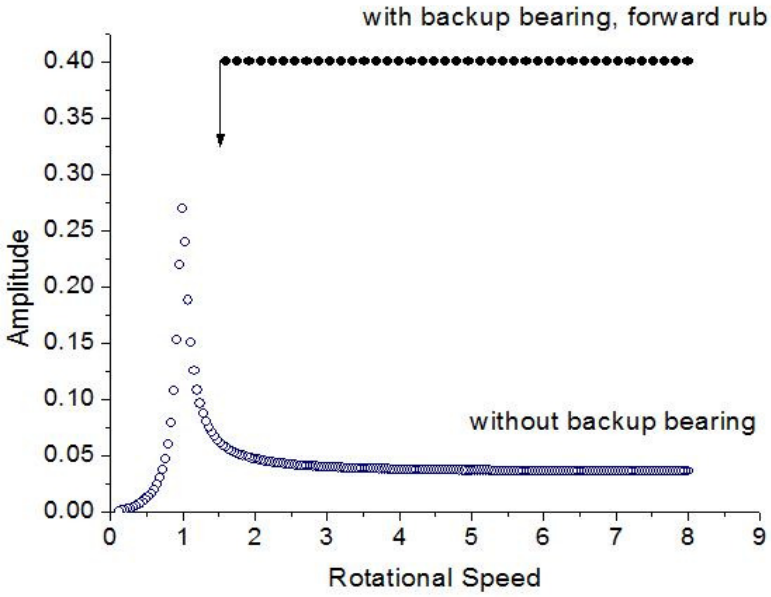

Fig. 5.8: Resonance Curve $\delta = 0.4, \mu = 0.01$

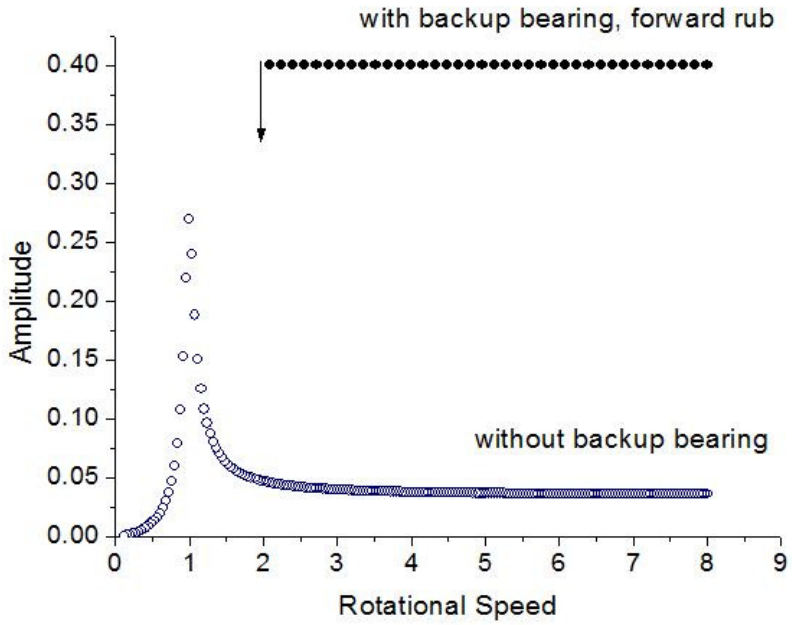

Fig. 5.9: Resonance Curve $\delta = 0.4, \mu = 0.03$

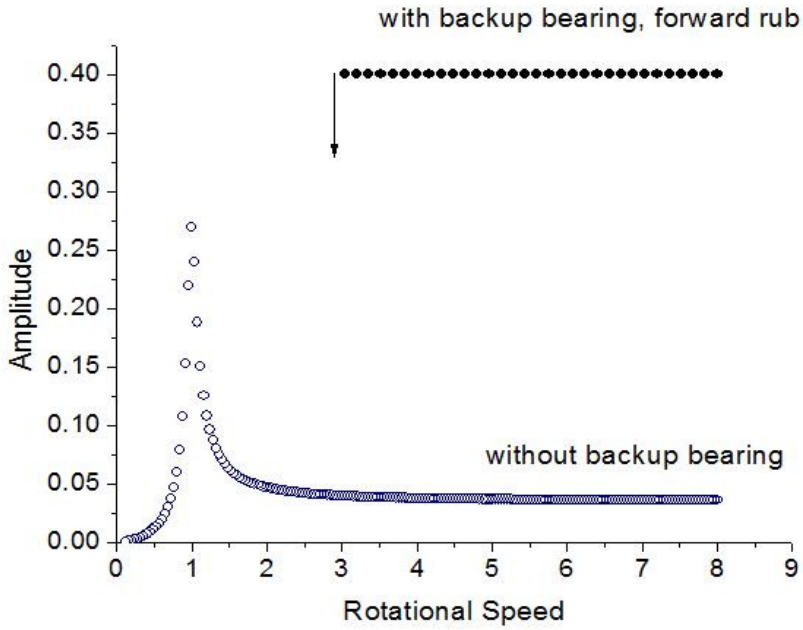

Fig.5.10: Resonance Curve $\delta = 0.4, \mu = 0.05$

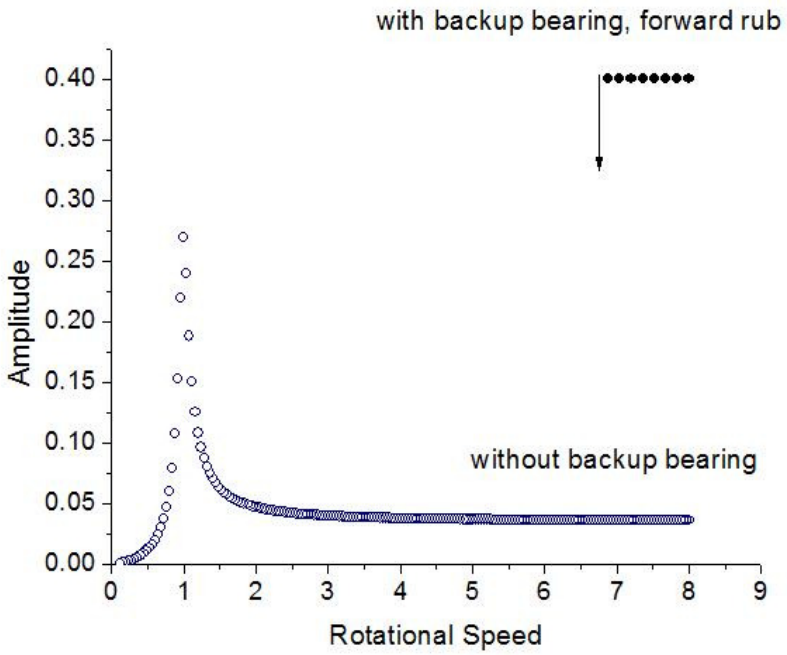

Fig. 5.11: Resonance Curve $\delta = 0.4, \mu = 0.07$

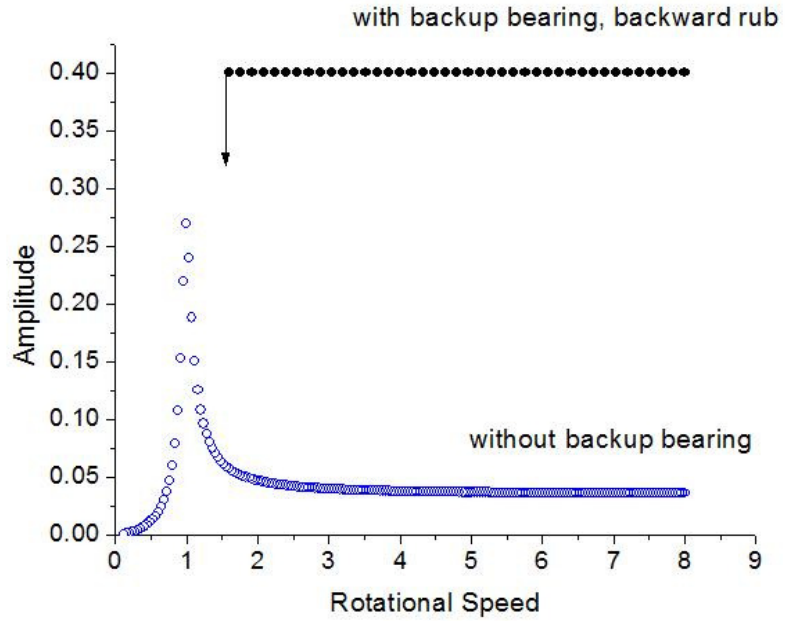

Fig. 5.12: Resonance Curve $\delta = 0.4, \mu = 0.1$

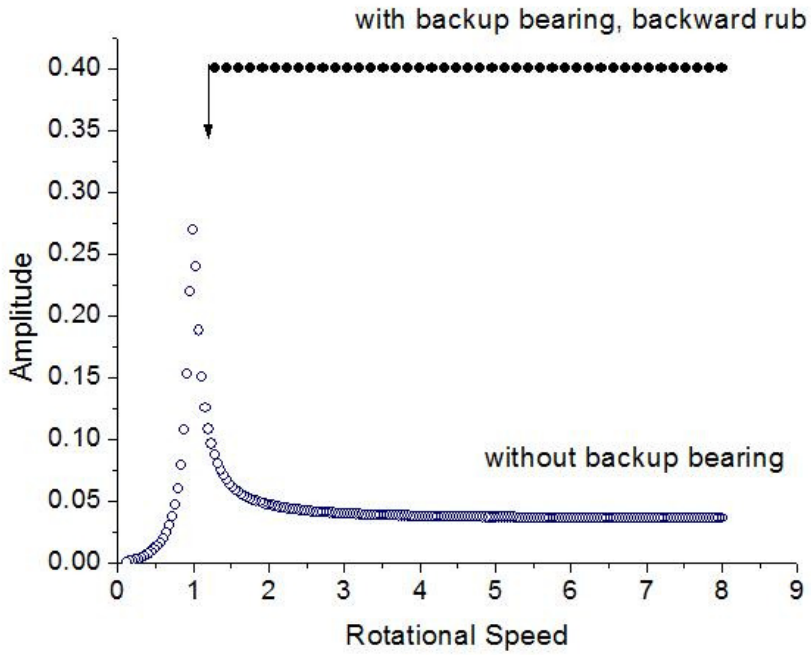

Fig. 5.13: Resonance Curve $\delta = 0.4, \mu = 0.2$

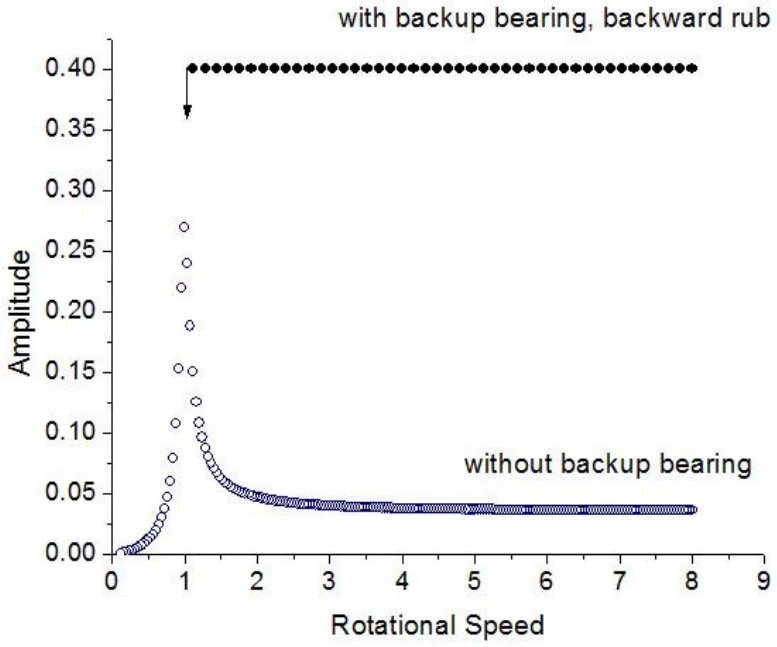

Fig. 5.14: Resonance Curve $\delta = 0.4, \mu = 0.3$

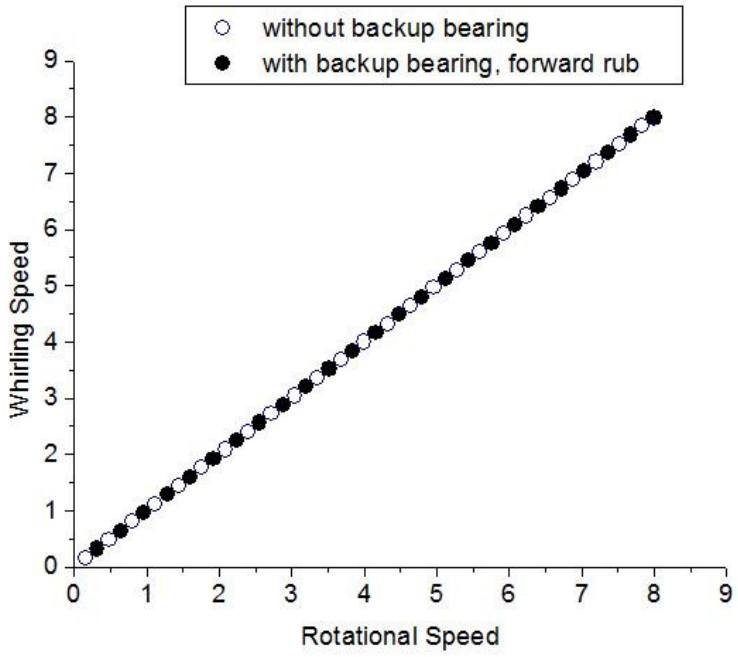

Fig. 5.15: Whirling speed diagram $\delta = 0.4, \mu = 0.01$

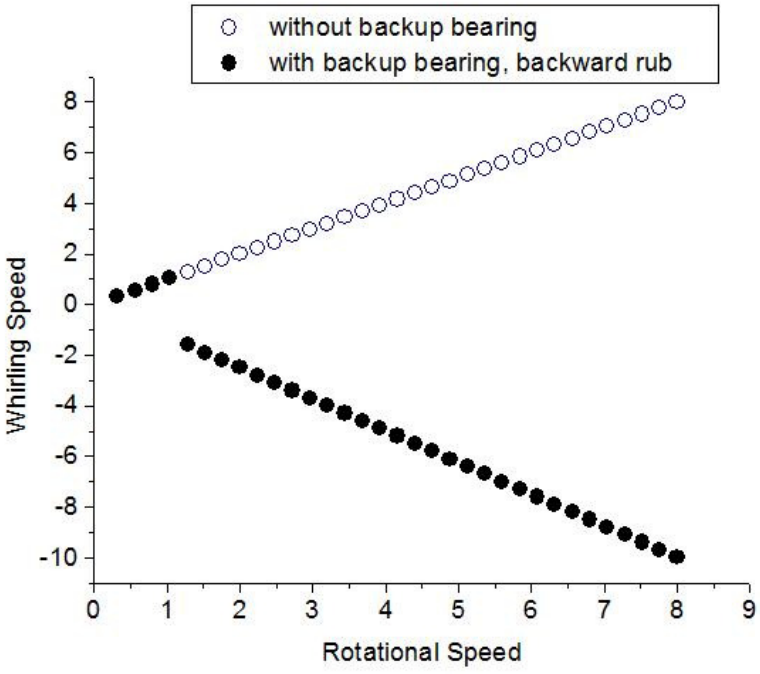

Fig. 5.16: Whirling speed diagram $\delta = 0.4, \mu = 0.2$

5.2.1.2 When $\delta = 0.3$

The following figures are considered for $\delta = 0.3$. The friction coefficient is also varied in this case. Fig. 5.17 is considered when there is no friction force. And it is observed from this figure that the contact between rotor and guide drops down when the rotational speed is 1.08. The interesting observation from Fig. 5.17 is although the maximum amplitude for the rotor-shaft system is 0.27 at critical speed 1.0, but the amplitude is 0.3 from rotational speed 8.0 to 1.12. This happens because of the initial conditions given in the simulation.

Fig. 5.18 to 5.24 represents the scenario of contact between rotor and guide when friction is present. It is clear from the figures that increasing the friction coefficient the contact between rotor and guide drops down earlier with the rotating speed for up to certain friction coefficient. From the Fig. 5.21 when the friction coefficient is 0.07 the contact drops down at rotational speed 2.0. It is also observed that from Fig. 5.17 to 5.21, the rubbing phenomenon is forward which is confirmed by the whirling speed diagram shown in Fig. 5.25. From Fig. 5.25, it is clear that the rotational speed and the whirling speed of the rotor are same. Moreover, the direction of both the speed is same and the scenario is considered as forward rub. But when the friction coefficient is 0.1 and above, the rubbing phenomenon is backward. Fig. 5.22 to 5.24 show the backward rubbing phenomenon which is again confirmed by the whirling speed diagram as shown in Fig. 5.26. Fig. 5.26 is considered when the friction coefficient is 0.2. From this figure, the rotational speed and the whirling speed are not same and the direction of both the speed is opposite. Therefore, this ensures the phenomenon of backward rub. So in this case, increase in the friction coefficient will definitely increase the probability of the contact between rotor and guide. Fig. 5.24 shows that the contact drops down when rotational speed is 0.76.

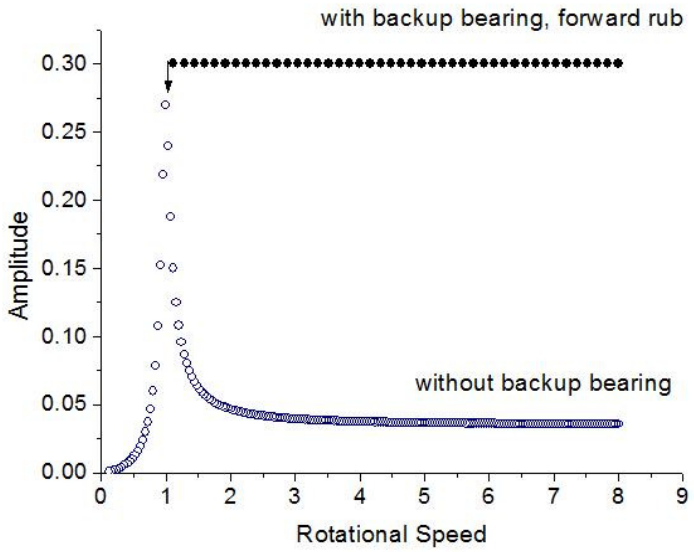

Fig. 5.17: Resonance Curve $\delta = 0.3, \mu = 0.0$

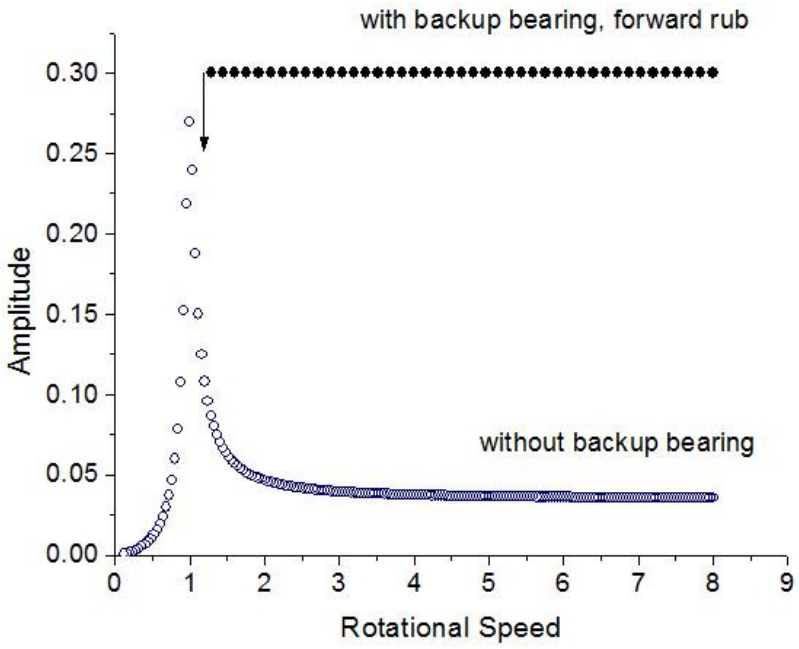

Fig. 5.18: Resonance Curve $\delta = 0.3, \mu = 0.01$

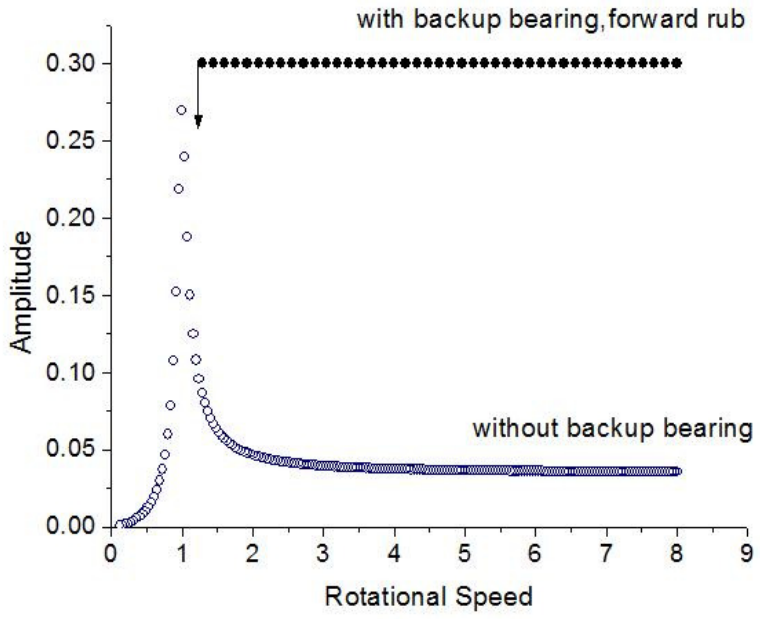

Fig. 5.19: Resonance Curve $\delta = 0.3, \mu = 0.03$

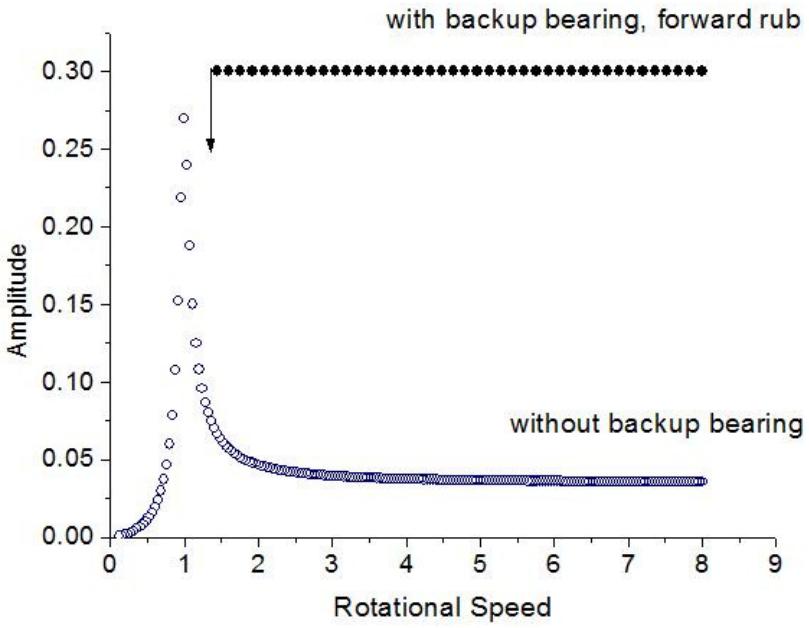

Fig. 5.20: Resonance Curve $\delta = 0.3, \mu = 0.05$

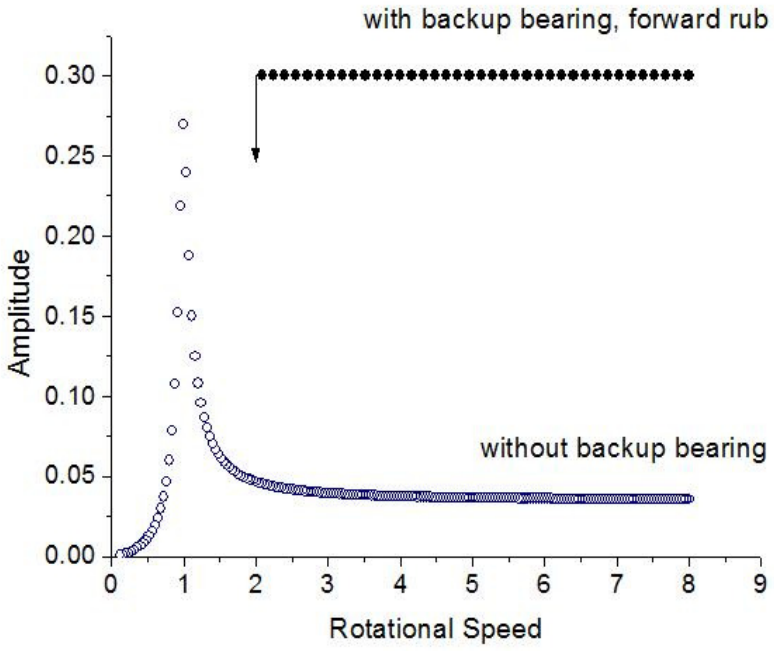

Fig. 5.21: Resonance Curve $\delta = 0.3, \mu = 0.07$

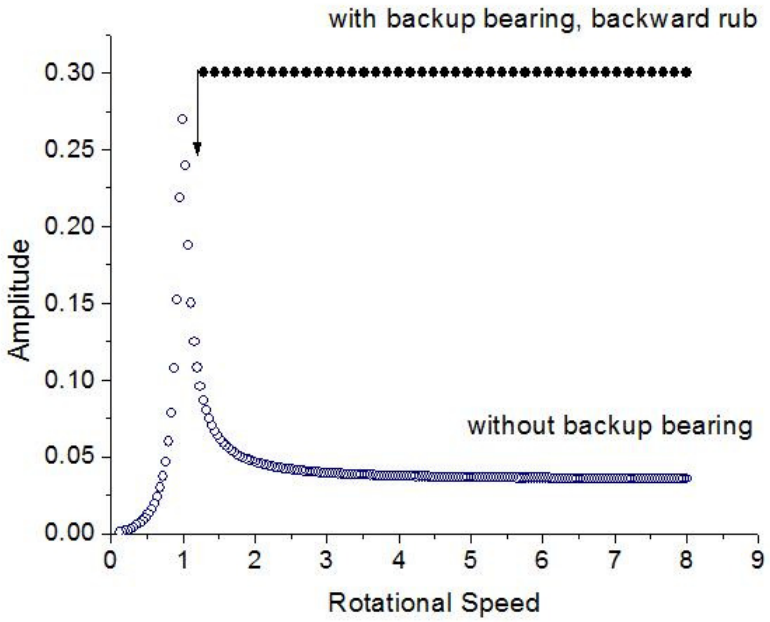

Fig. 5.22: Resonance Curve $\delta = 0.3, \mu = 0.1$

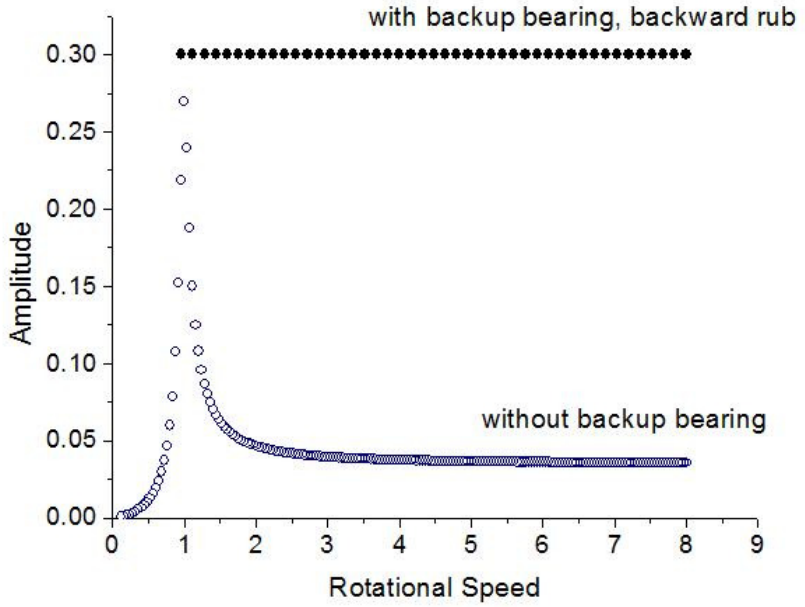

Fig. 5.23: Resonance Curve $\delta = 0.3, \mu = 0.2$

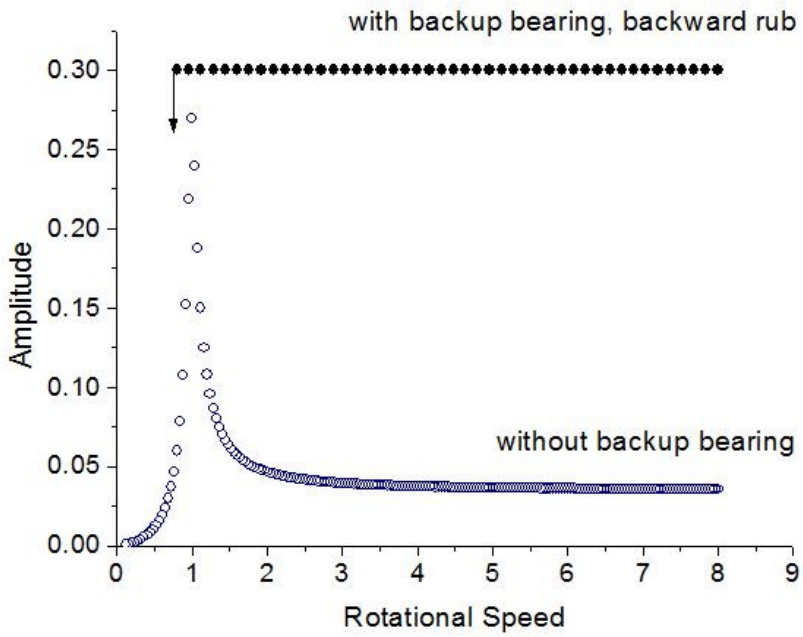

Fig. 5.24: Resonance Curve $\delta = 0.3, \mu = 0.3$

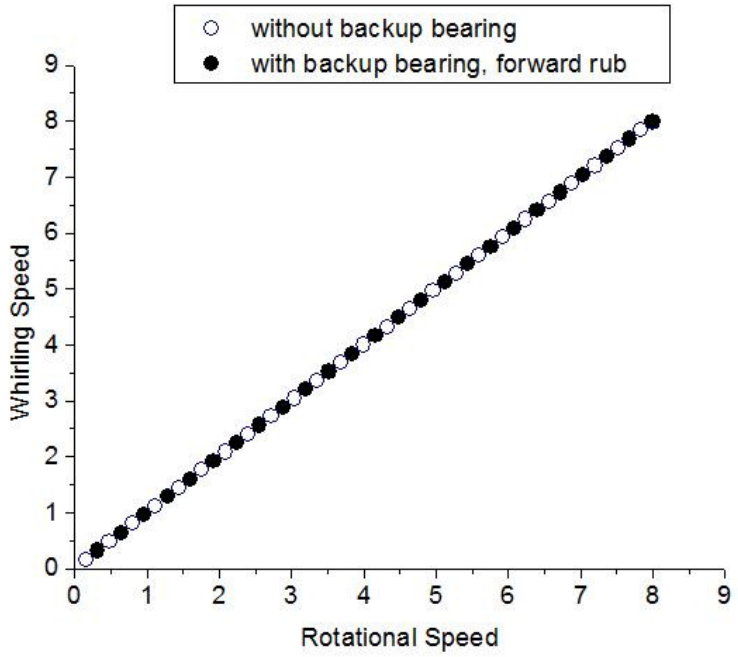

Fig. 5.25: Whirling speed diagram $\delta = 0.3, \mu = 0.01$

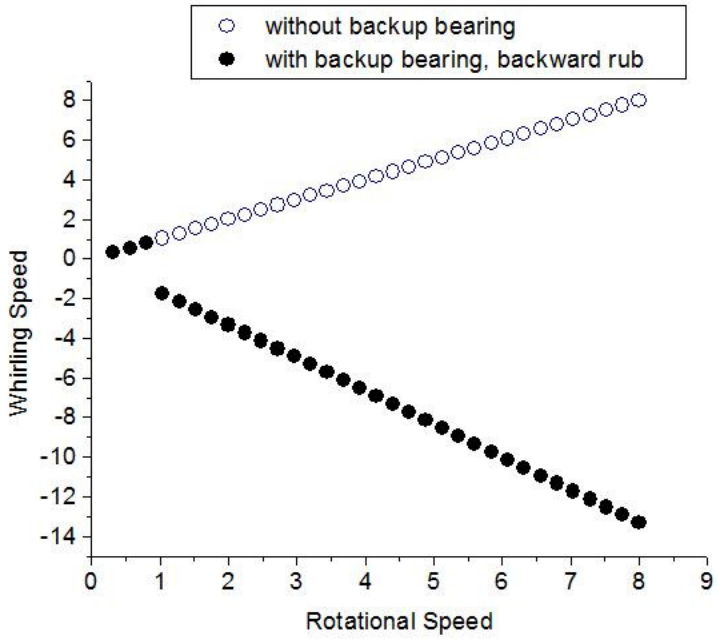

Fig. 5.26: Whirling speed diagram $\delta = 0.3$, $\mu = 0.2$

5.2.1.3 When $\delta = 0.2$

In this section, the following figures are considered for $\delta = 0.2$. The friction coefficient is again varied in this case. Fig. 5.27 is considered when there is no friction force. And it is observed from the figure that the contact between rotor and guide drops down when rotational speed is 0.92.

Fig. 5.28 to 5.34 represents the contact phenomena when friction is present. It is clear from the figures that although the friction coefficient is increased the contact between rotor and guide drops down at a certain the rotating speed which is 0.92. It is also observed that from Fig. 5.27 to 5.32, the rubbing phenomenon is forward which is confirmed by the whirling speed diagram shown in Fig. 5.35. From Fig. 5.35, it is clear that the rotational speed and the whirling speed of the rotor are same. Moreover, the direction of both the speed is same and the scenario is considered as forward rub. But when the friction coefficient is 0.2 and above, the rubbing phenomenon is backward. Fig. 5.33 and 5.34 show the backward rubbing phenomenon which is again confirmed by the whirling speed diagram as shown in Fig. 5.36. Fig. 5.36 is considered when the friction coefficient is 0.2. From this figure, the rotational speed and the whirling speed are not same and the direction of both the speed is opposite. Therefore, this ensures the phenomenon of backward rub. So in this case, increase in the friction coefficient will definitely increase the probability of the contact between rotor and guide. Fig. 5.34 shows that the contact drops down when rotational speed is 0.48.

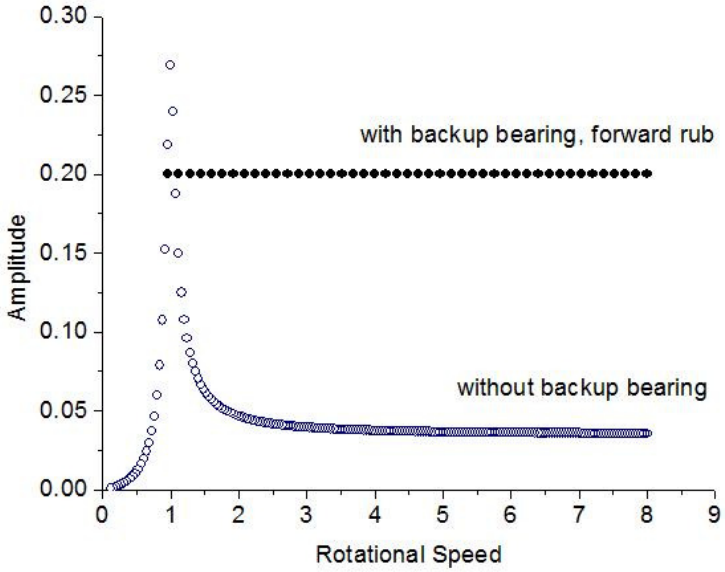

Fig. 5.27: Resonance Curve $\delta = 0.2, \mu = 0.0$

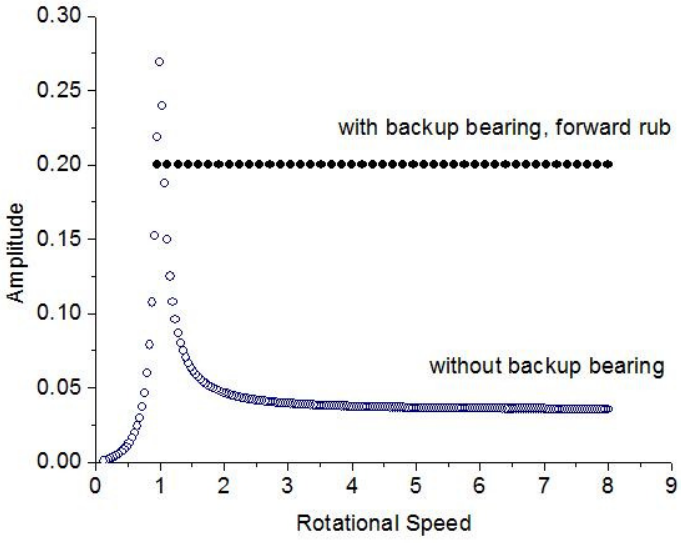

Fig. 5.28: Resonance Curve $\delta = 0.2, \mu = 0.01$

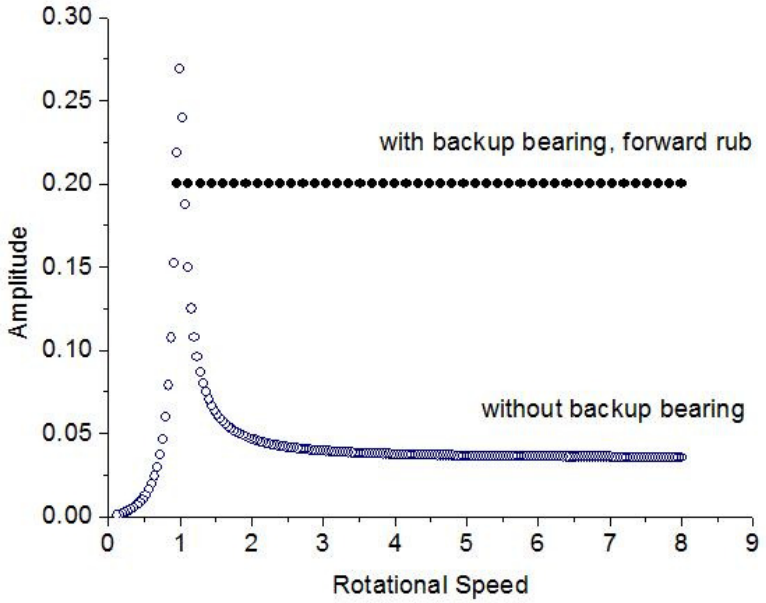

Fig. 5.29: Resonance Curve $\delta = 0.2, \mu = 0.03$

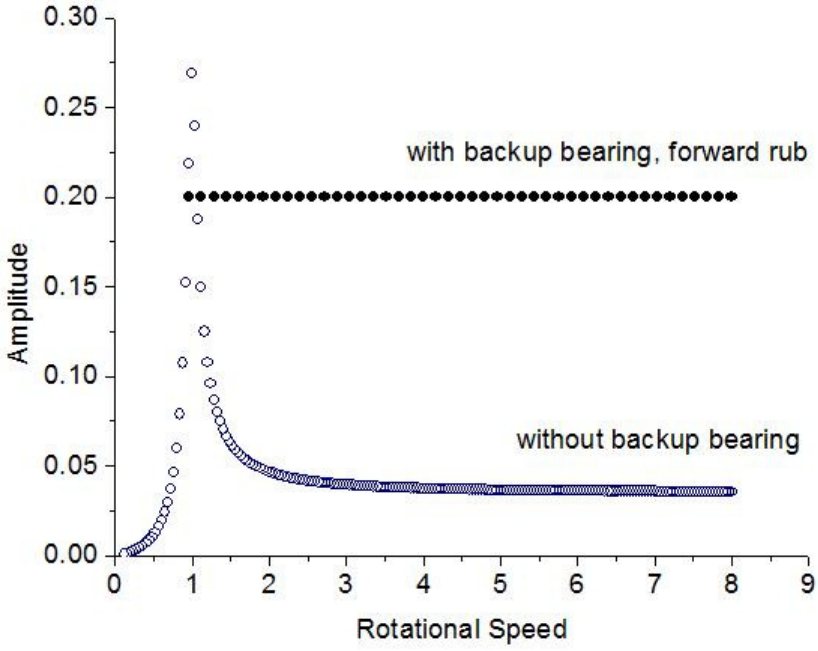

Fig. 5.30: Resonance Curve $\delta = 0.2, \mu = 0.05$

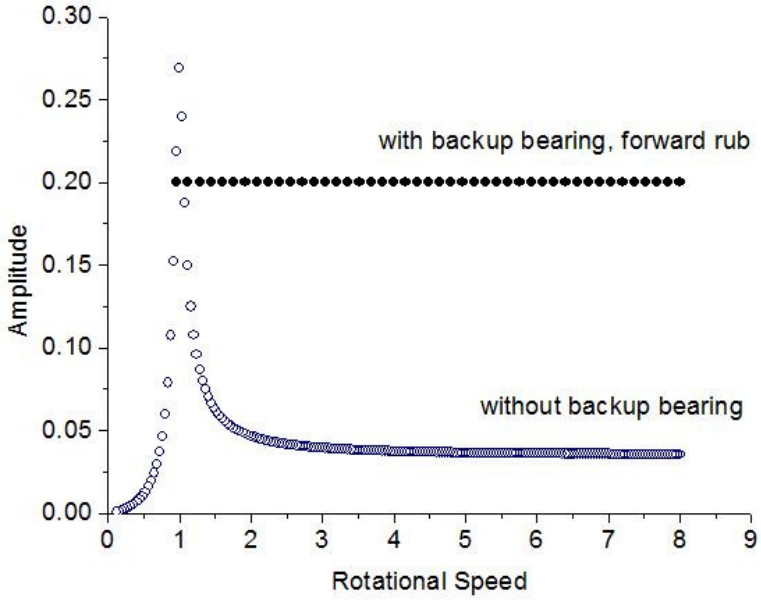

Fig. 5.31: Resonance Curve $\delta = 0.2, \mu = 0.07$

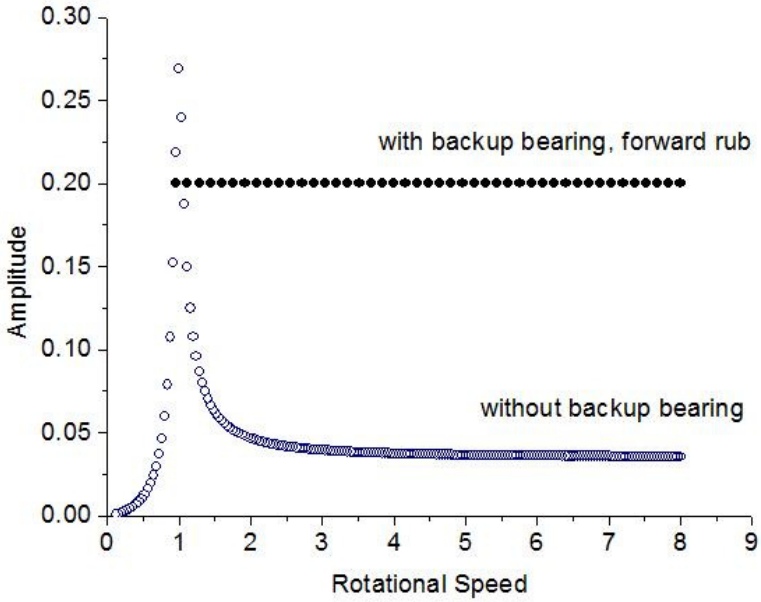

Fig.5.32: Resonance Curve $\delta = 0.2, \mu = 0.1$

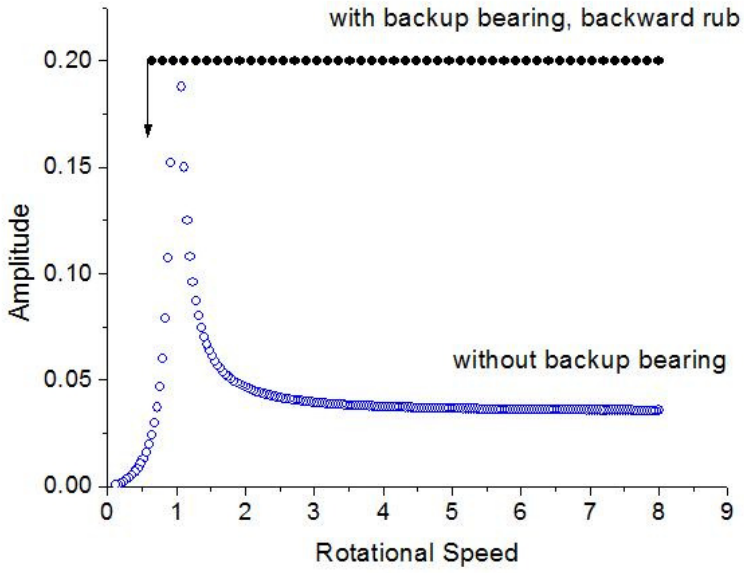

Fig. 5.33: Resonance Curve $\delta = 0.2, \mu = 0.2$

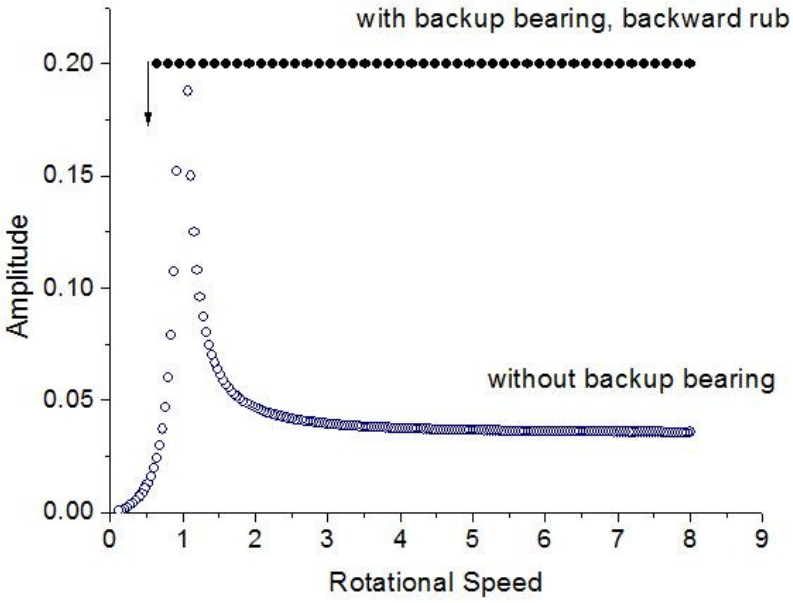

Fig. 5.34: Resonance Curve $\delta = 0.2, \mu = 0.3$

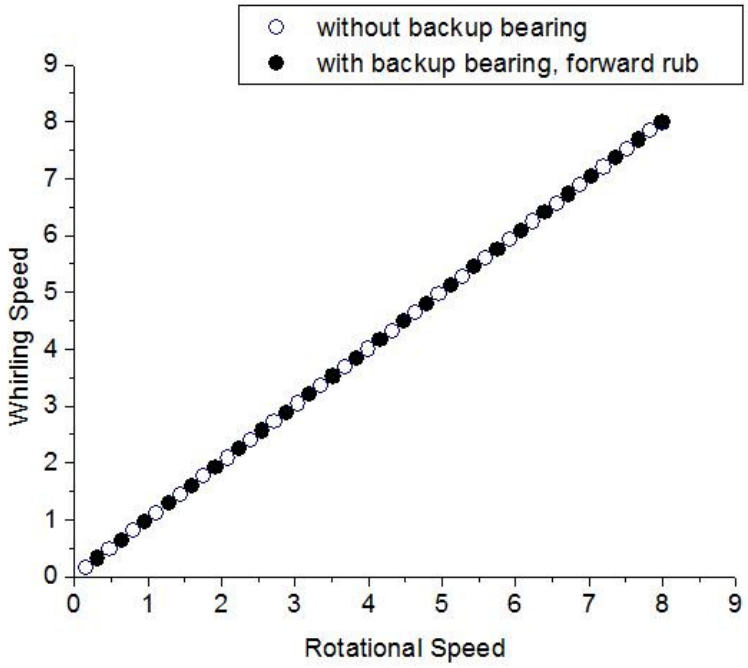

Fig. 5.35: Whirling speed diagram $\delta = 0.2, \mu = 0.01$

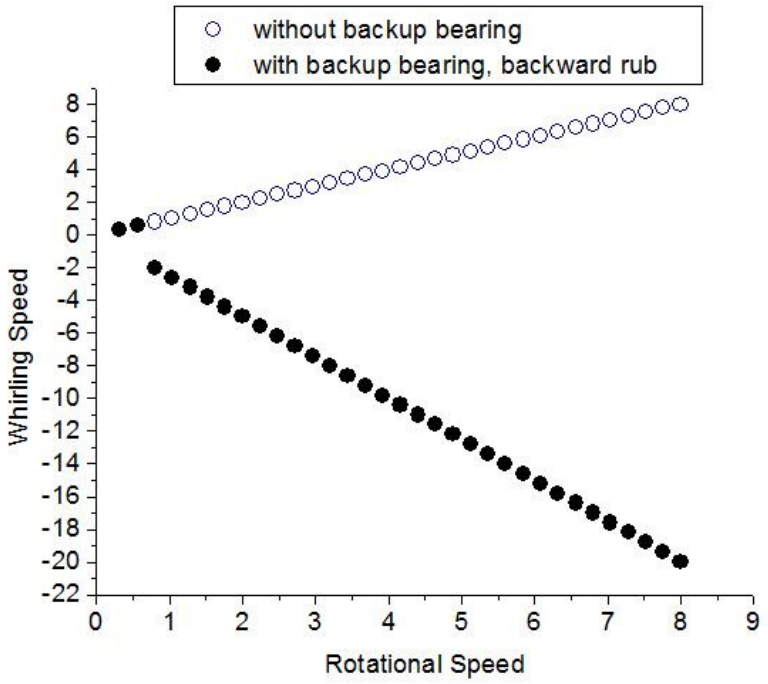

Fig. 5.36: Whirling speed diagram $\delta = 0.2, \mu = 0.2$

5.2.1.4 When $\delta = 0.1$

The following figures are considered for $\delta = 0.1$**.** The friction coefficient is also considered in this case. Fig. 5.37 is considered when there is no friction force. And it is observed from the figure that the contact between rotor and guide drops down when rotational speed is 0.84.

It was observed that although the friction coefficient was increased the contact between rotor and guide drops down at a certain the rotating speed which is 0.84. And effect was same as it was in the case of $\delta = 0.2$ where changing the friction coefficient from 0.01 to 0.1 did not change the dropping down behavior of the contact between rotor and guide. It is also observed from the Fig. 5.37 that the rubbing phenomenon is forward which is confirmed by the whirling speed diagram shown in Fig. 5.39. From Fig. 5.39, it is clear that the rotational speed and the whirling speed of the rotor are same. Moreover, the direction of both the speed is same and the scenario is considered as forward rub. But when the friction coefficient is 0.1 and above, the rubbing phenomenon becomes backward. Fig. 5.38 shows the backward rubbing phenomenon which is again confirmed by the whirling speed diagram as shown in Fig. 5.40. Fig. 5.40 is considered when the friction coefficient is 0.1. From this figure, the rotational speed and the whirling speed are not same and the direction of both the speed is opposite. Therefore, this ensures the phenomenon of backward rub. So in this case, increase in the friction coefficient will definitely increase the probability of the contact between rotor and guide. Fig. 5.38 shows that the contact drops down when the rotational speed is 0.36.

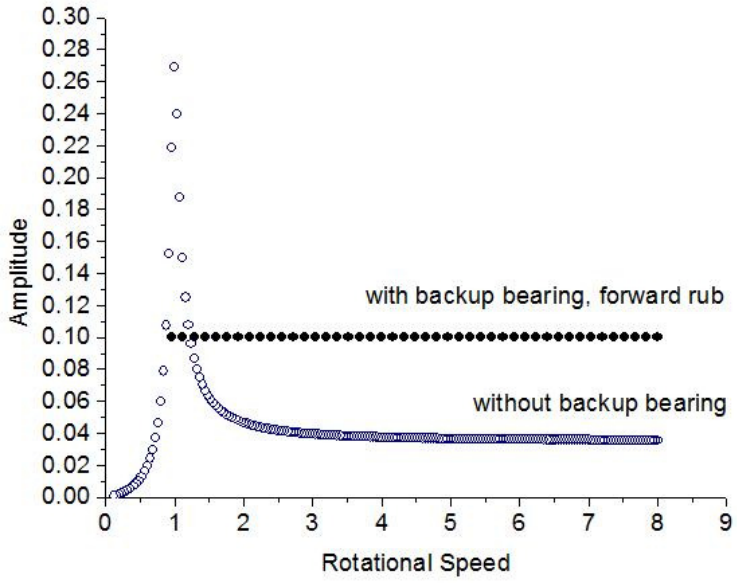

Fig. 5.37: Resonance Curve $\delta = 0.1, \mu = 0.0$

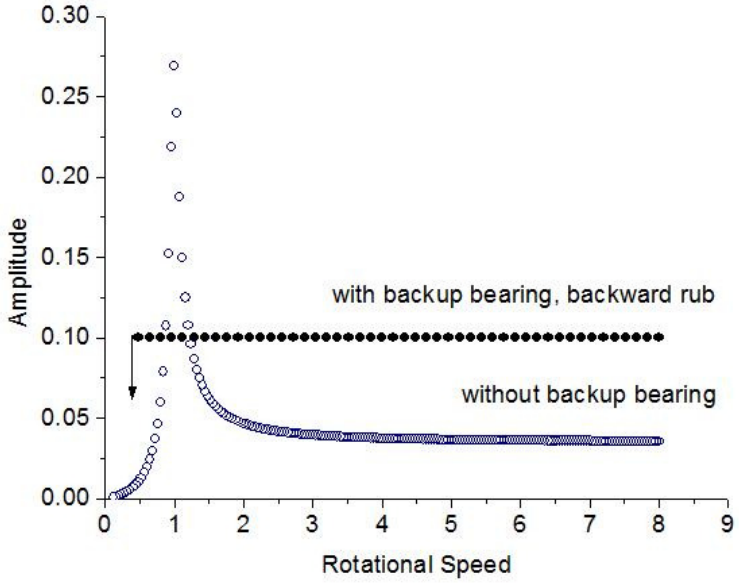

Fig. 5.38: Resonance Curve $\delta = 0.1, \mu = 0.1$

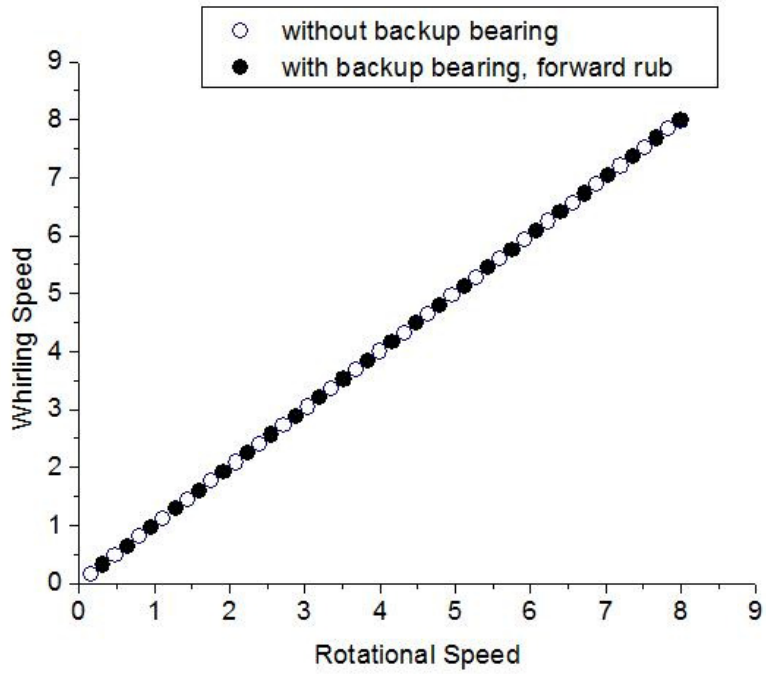

Fig. 5.39: Whirling speed diagram $\delta = 0.1, \mu = 0.01$

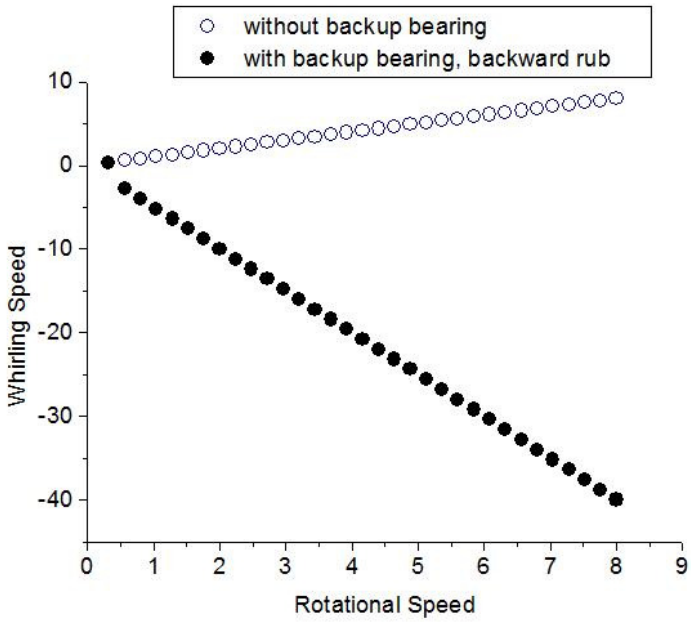

Fig. 5.40: Whirling speed diagram $\delta = 0.1, \mu = 0.1$

5.2.2 Phase Diagrams

5.2.2.1 When $\delta = 0.4$

The following figures represent the phase [see the appendix] diagram for $\delta = 0.4$. It is observed from Fig. 5.41 to 5.45 that when there is no backup bearing, then the phase angle is varied from -179.06 to -0.91 degree. But in case of implementing the backup bearing, the variation of phase angle range is observed. It is obvious from Fig. 5.41 that the phase angle varies from -171.95 to -0.91 degree. And during rubbing between rotor and guide, the phase angle varies from -17.92 to -87.10 degree and after that the contact between rotor and stator drops down and the phase angle then shifted to the lower value. Fig. 5.42 confirms that with the increase in the friction coefficient up to certain value, the contact drops down earlier in the higher rotating speed range which was also confirmed by the earlier resonance curves. In Fig. 5.42, it is noticeable that during rubbing between rotor and guide, the phase angle varies from -80.14 to -92.98 degree and then the contact between rotor and guide drops down and the phase angle is shifted to the lower value which then follows the path of phase angle of without using the backup bearing. When the friction coefficient is 0.1 and above, from Fig. 5.43 to 5.45 the phase angle is almost 0 during contact and the scenario is backward rubbing which was confirmed previously by showing the whirling speed diagram. These figures also ensure that increasing the friction coefficient from 0.1 will certainly delay the contact dropdown between rotor and guide.

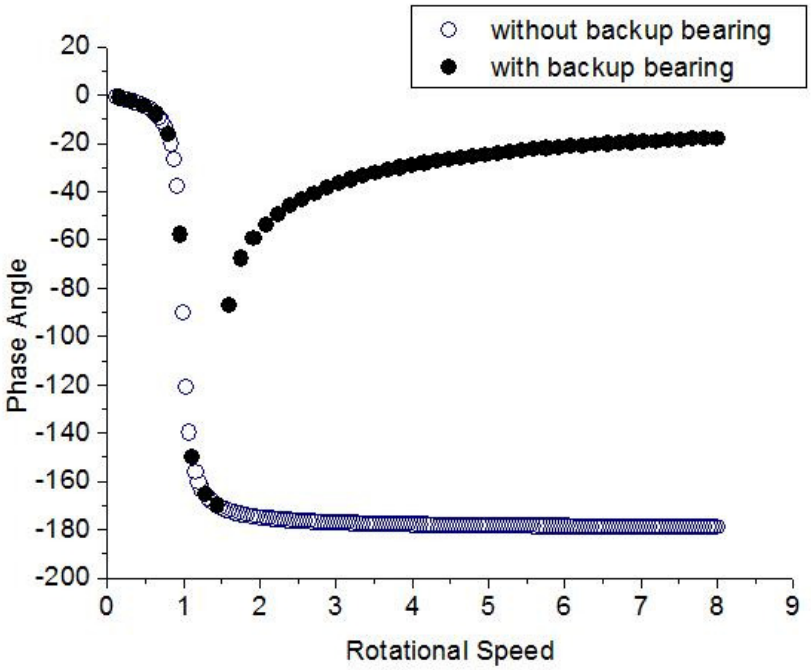

Fig. 5.41: Phase diagram $\delta = 0.4$, $\mu = 0.01$

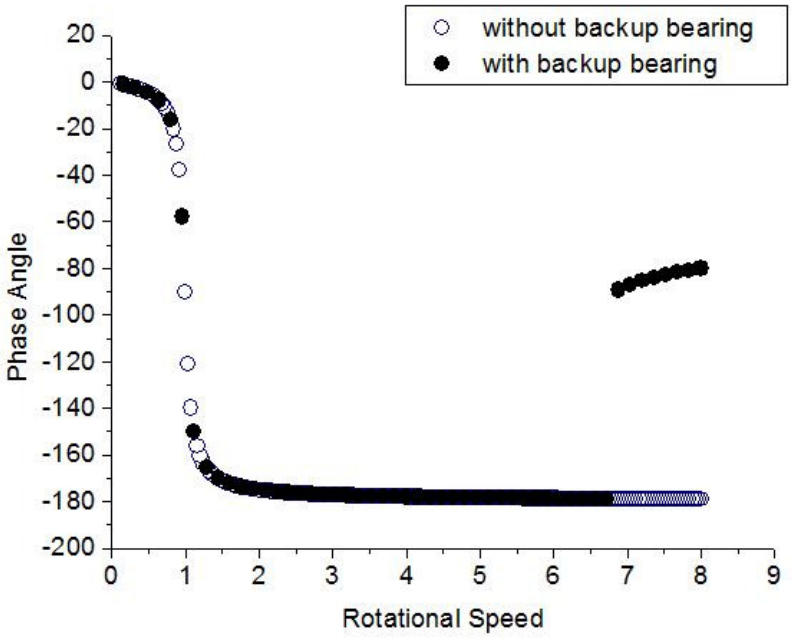

Fig. 5.42: Phase diagram $\delta = 0.4$, $\mu = 0.07$

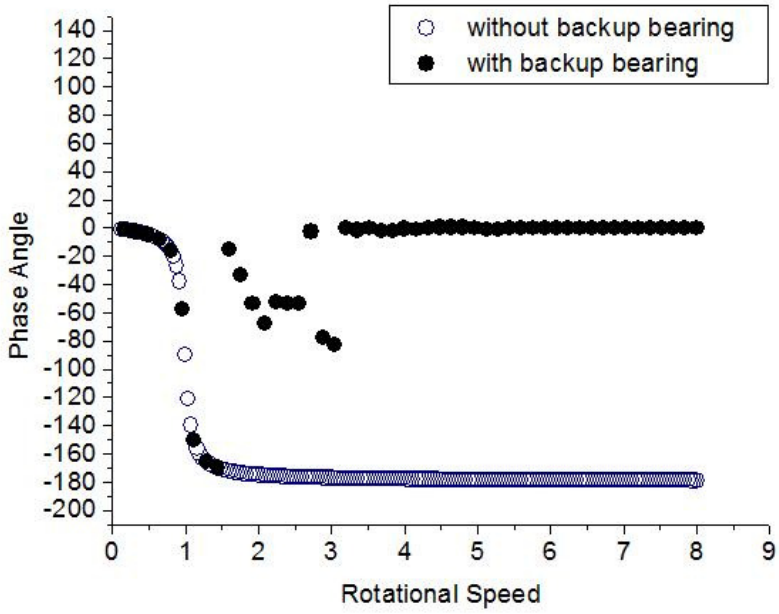

Fig. 5.43: Phase diagram $\delta = 0.4$, $\mu = 0.1$

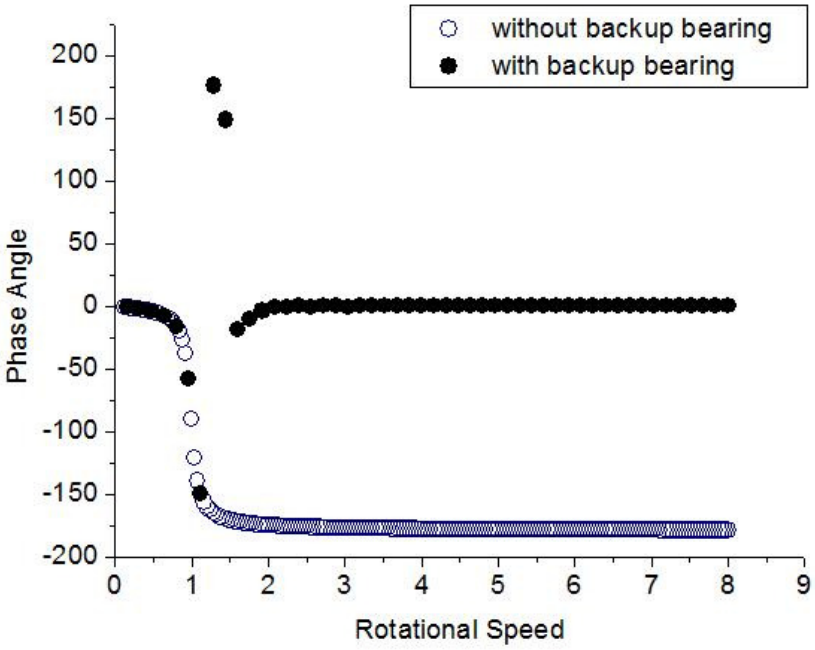

Fig. 5.44: Phase diagram $\delta = 0.4$, $\mu = 0.2$

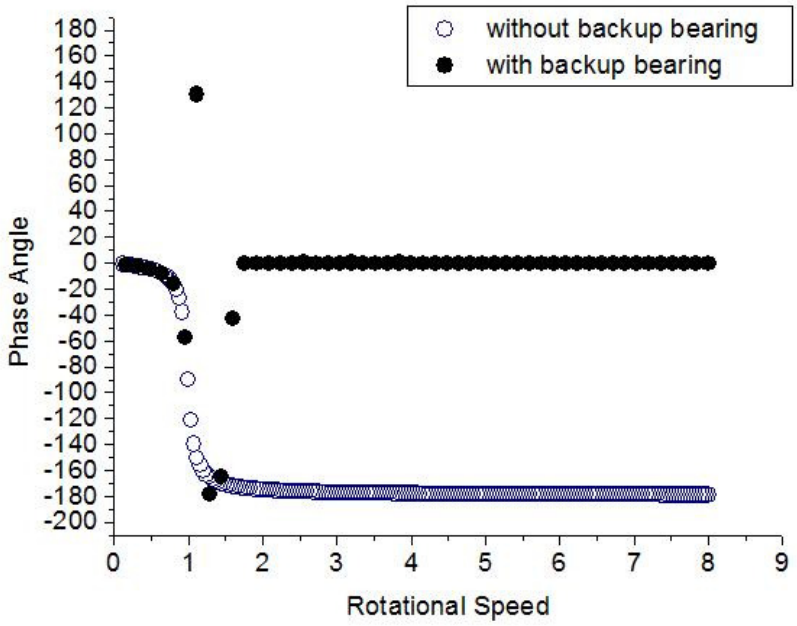

Fig. 5.45: Phase diagram $\delta = 0.4$, $\mu = 0.3$

5.2.2.2 When $\delta = 0.3$

The following figures represent the phase diagram for $\delta = 0.3$. It is observed from Fig. 5.46 to 5.50 that when there is no backup bearing, then the phase angle is varied from -179.06 to -0.91 degree. But in case of implementing the backup bearing, the variation of phase angle happens. It is obvious from Fig. 5.46 that the phase angle varies from -150.22 to -0.91 degree. And during rubbing between rotor and guide, the phase angle varies from -13.49 to -79.86 degree and after that the contact between rotor and stator drops down and the phase angle then shifted to the lower value. Fig. 5.47 confirms that with the increase in the friction coefficient up to certain value, the contact drops down earlier in the higher rotating speed range which was also confirmed by the earlier resonance curves. In Fig. 5.47, it is noticeable that during rubbing between rotor and guide, the phase angle varies from -50.74 to -92.38 degree and then the contact between rotor and guide drops down and the phase angle is shifted to the lower value which then follows the path of phase angle of without using the backup bearing. When the friction coefficient is 0.1 and above, from Fig. 5.48 to 5.50 the phase angle is almost 0 during contact and the scenario is backward rubbing which was confirmed previously by showing the whirling speed diagram. These figures also ensure that increasing the friction coefficient from 0.1 will certainly delay the contact dropdown between rotor and guide.

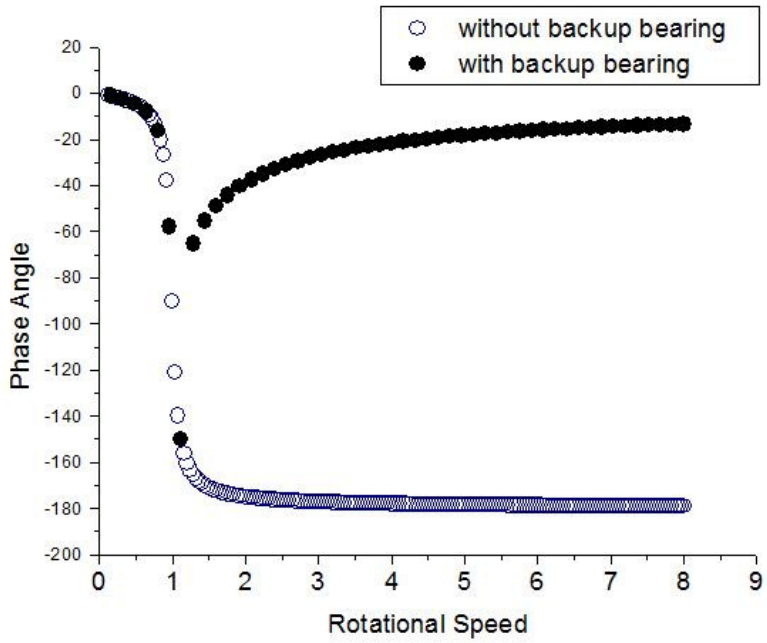

Fig. 5.46: Phase diagram $\delta = 0.3$, $\mu = 0.01$

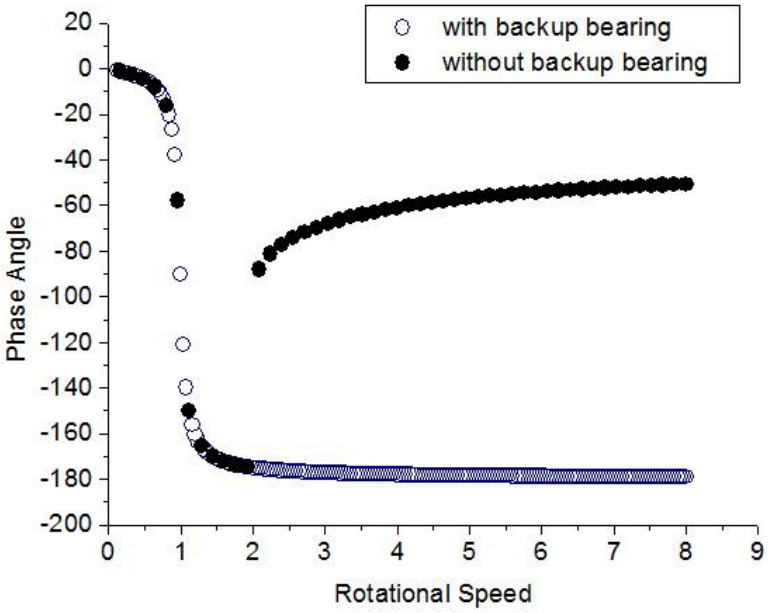

Fig. 5.47: Phase diagram $\delta = 0.3$, $\mu = 0.07$

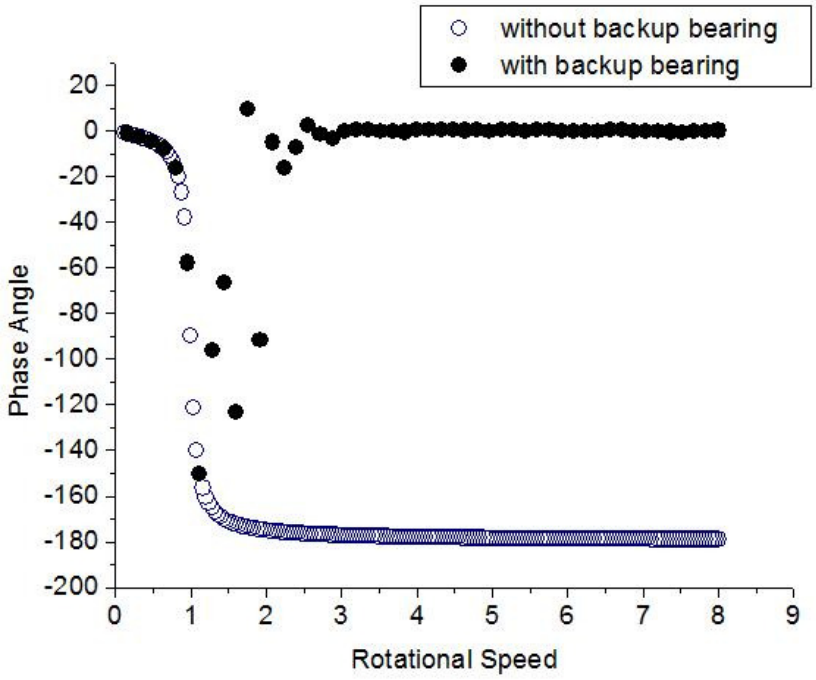

Fig. 5.48: Phase diagram $\delta = 0.3$, $\mu = 0.1$

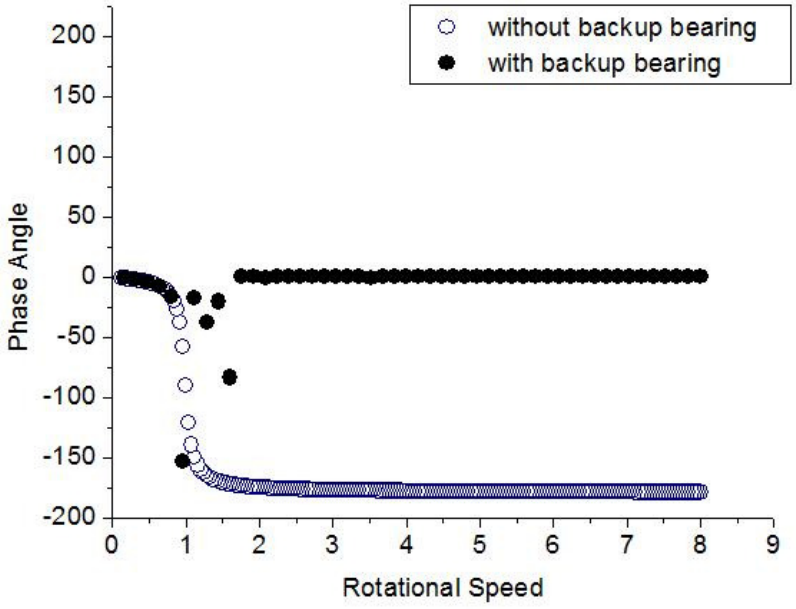

Fig. 5.49: Phase diagram $\delta = 0.3$, $\mu = 0.2$

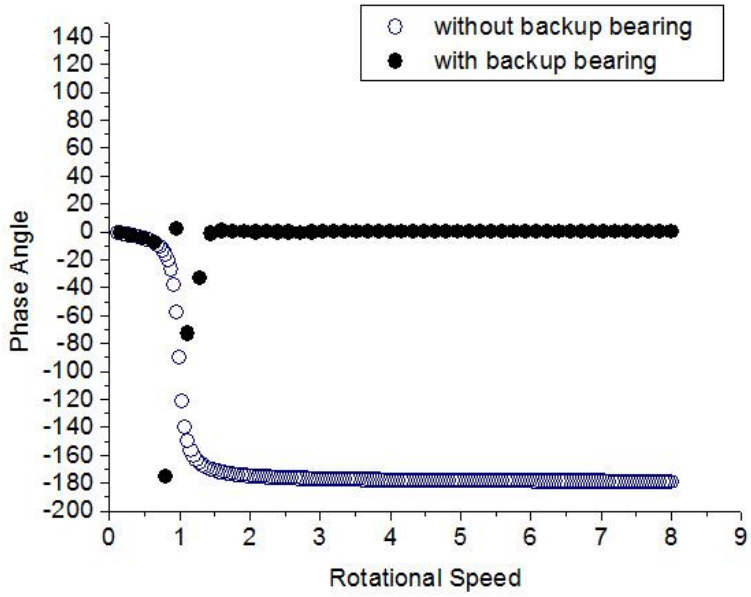

Fig. 5.50: Phase diagram $\delta = 0.3$, $\mu = 0.3$

5.2.2.3 When $\delta = 0.2$

The following figures represent the phase diagram for $\delta = 0.2$. It is observed from Fig. 5.51 to 5.54 that when there is no backup bearing, then the phase angle is varied from -179.06 to -0.91 degree. But in case of implementing the backup bearing, the variation of phase angle range is observed. It is obvious from Fig. 5.51 that the phase angle varies from -50.83 to -0.91 degree. And during rubbing between rotor and guide, the phase angle varies from -9.15 to -50.83 degree and after that the contact between rotor and stator drops down and the phase angle then shifted to the lower value. Fig. 5.52 shows that with the increase in the friction coefficient up to certain value, the contact drops down at fixed rotating speed which is 0.92 and was also confirmed by the earlier resonance curves for $\delta = 0.2$. In Fig. 5.52, it is noticeable that during rubbing between rotor and guide, the phase angle varies from -33.04 to -51.56 degree and then the contact between rotor and guide drops down and the phase angle is shifted to the lower value which then follows the path of phase angle of without using the backup bearing. When the friction coefficient is 0.2 and above, from Fig. 5.53 and 5.54, the phase angle is almost 0 during contact and the scenario is backward rubbing which was confirmed previously by showing the whirling speed diagram. These figures also ensure that increasing the friction coefficient from 0.2 will certainly delay the contact dropdown between rotor and guide.

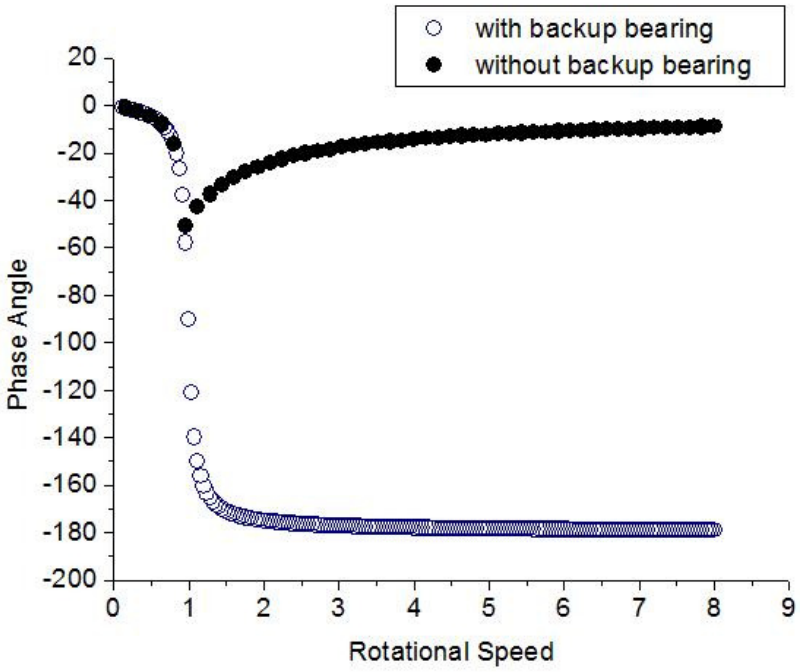

Fig. 5.51: Phase diagram $\delta = 0.2$, $\mu = 0.01$

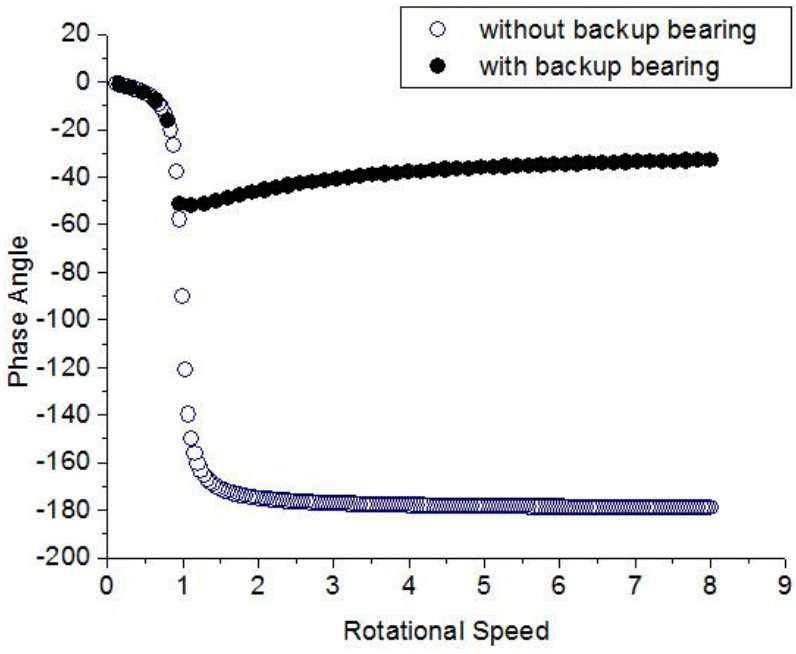

Fig. 5.52: Phase diagram $\delta = 0.2$, $\mu = 0.07$

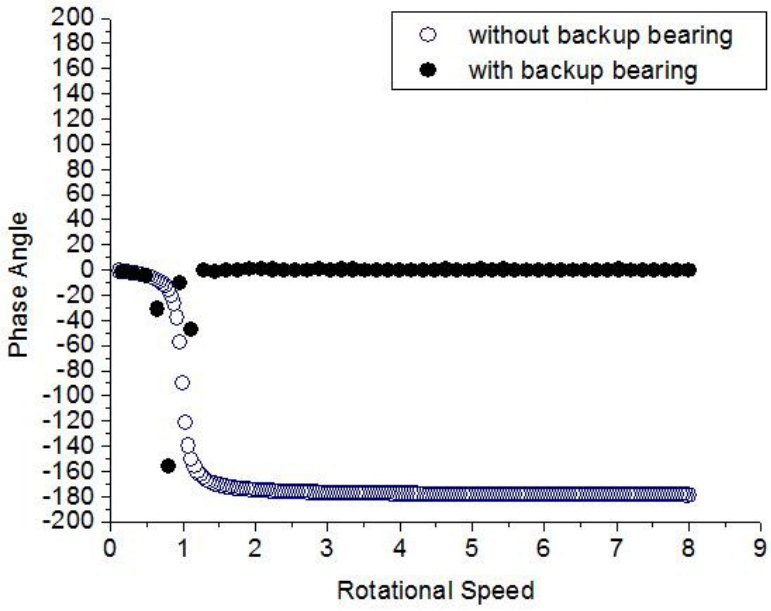

Fig. 5.53: Phase diagram $\delta = 0.2, \mu = 0.2$

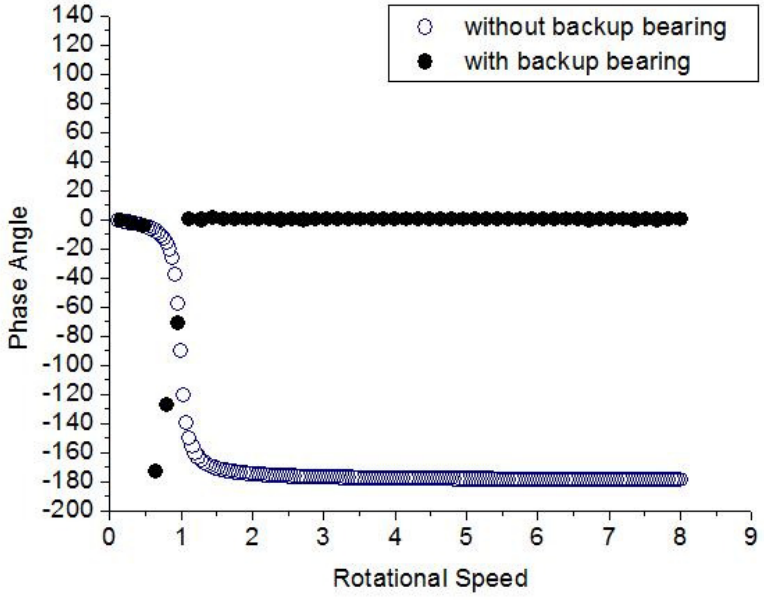

Fig. 5.54: Phase diagram $\delta = 0.2, \mu = 0.3$

5.2.2.4 When $\delta = 0.1$

The following figures represent the phase diagram for $\delta = 0.1$. It is observed from Fig. 5.55 and 5.56 that when there is no backup bearing, then the phase angle is varied from -179.06 to -0.91 degree. But in case of implementing the backup bearing, the variation of phase angle range is observed. It is obvious from Fig. 5.55 that the phase angle varies from -24.73 to -0.91 degree. And during rubbing between rotor and guide, the phase angle varies from -4.85 to -24.73 degree and after that the contact between rotor and stator drops down and the phase angle then shifted to the lower value. In this case also with the increase in the friction coefficient up to certain value, the contact drops down at fixed rotating speed which is 0.84. When the friction coefficient is 0.1 and above, from Fig. 5.56, the phase angle is almost 0 during contact and the scenario is backward rubbing which was confirmed previously by showing the whirling speed diagram. And in this case also increasing the friction coefficient from 0.1 will certainly delay the contact dropdown between rotor and guide.

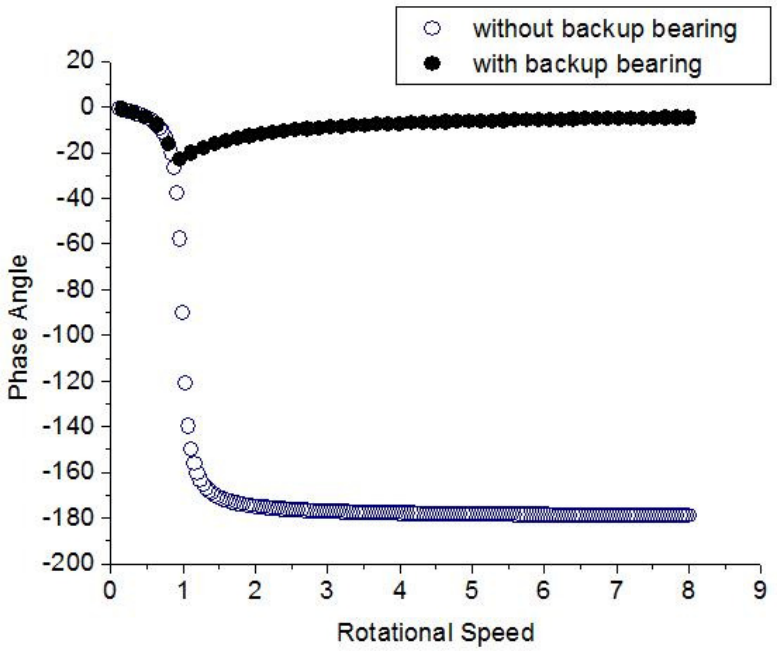

Fig. 5.55: Phase diagram $\delta = 0.1, \mu = 0.01$

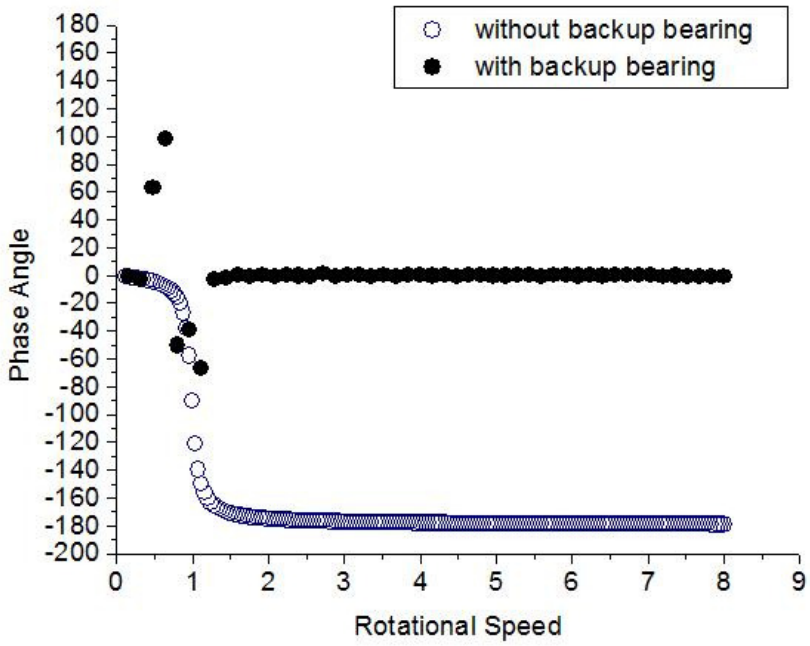

Fig. 5.56: Phase diagram $\delta = 0.1, \mu = 0.1$

5.2.3 Rotor Orbits

This section describes the orbits of the rotor for clearance $\delta = 0.3, \delta = 0.2$ and $\delta = 0.1$. All the orbits for different clearances are visualized when the rotating speed is 8.0 and friction coefficient is 0. From Fig. 5.57, a smooth circular rotor orbit is obtained. In this case, the rubbing continues throughout the speed. In Fig. 5.58, the rotor trajectories are pretty much denser than that of in Fig. 5.57. Fig. 5.58 depicts the rotor trajectories for $\delta = 0.2$. It is seen from this figure that continuous rub occurs during the entire rotating speed. Fig. 5.59 shows the rotor orbit when $\delta = 0.3$. Due to the increase in clearance, the rotor does not follow the same trajectories all the time. Although the orbit pattern is regular, but there are some impacts of the rotor with the guide. So, increase in clearance will certainly increase the probability of impact phenomenon.

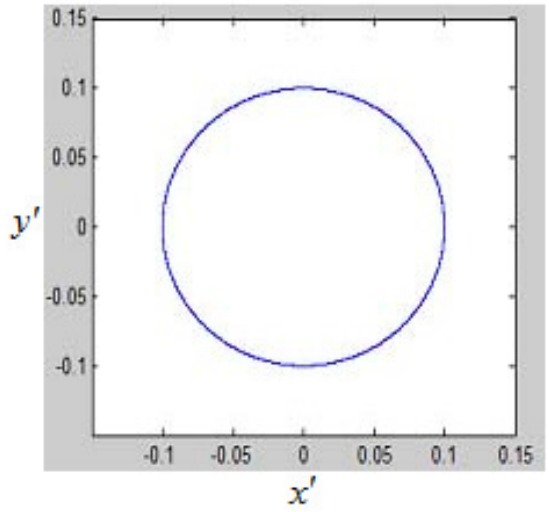

Fig. 5.57: Rotor orbit, $\delta = 0.1, \mu = 0.0,\ \omega' = 8.0$

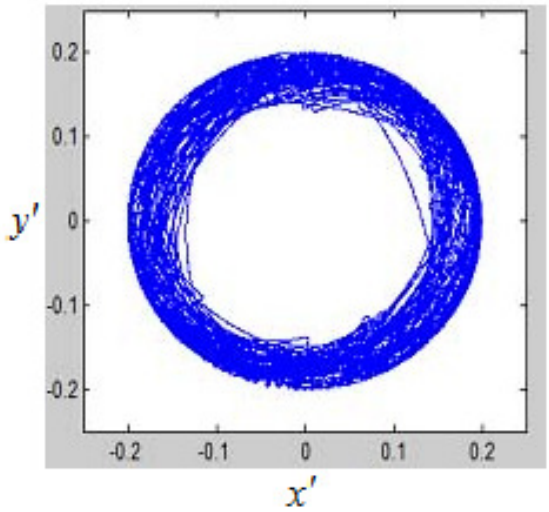

Fig. 5.58: Rotor orbit, $\delta = 0.2, \mu = 0.0,\ \omega' = 8.0$

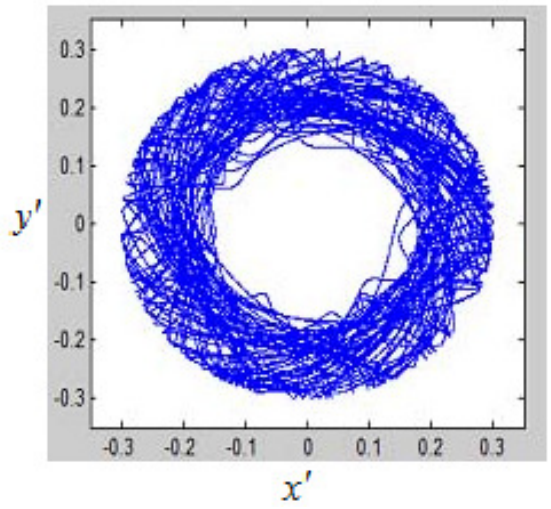

Fig. 5.59: Rotor orbit, $\delta = 0.3$, $\mu = 0.0$, $\omega' = 8.0$

5.2.4 Comparison among the Results of Different Clearances of Circular Backup Bearing

Fig. 5.60 shows the comparison among the simulation results of different clearances for $\delta = 0.4, \delta = 0.3, \delta = 0.2$ and $\delta = 0.1$. For all these four clearances, the friction coefficient is kept same which is 0.07. From the Fig. 5.60, it is clear that when the clearance between rotor and guide is $\delta = 0.4$, then the contact between rotor and guide drops down earliest in the higher rotating speed range compared with the clearances $\delta = 0.3, \delta = 0.2$ and $\delta = 0.1$. In case of $\delta = 0.4$, the contact drops down when the rotational speed is 6.72. For $\delta = 0.3$, the contact between rotor and guide drops down earlier than the clearances $\delta = 0.2$ and $\delta = 0.1$. In case of $\delta = 0.3$, the contact between rotor and guide drops down at rotational speed 2.0. The contact drops down earlier for $\delta = 0.2$ than $\delta = 0.1$. In case of $\delta = 0.2$, the contact between rotor and guide drops down at rotational speed 0.92. So, with the decrease in the rotational speed, the rubbing occurs between rotor and guide for longest period in case of $\delta = 0.1$. For $\delta = 0.1$, the contact between rotor and guide drops down when the rotational speed is 0.84. So, from this discussion, it is inevitable that when the clearance between rotor and guide is higher then there is less rubbing where the contact between rotor and guide drops down earlier in the higher rotating speed range. On the other hand, if the clearance is smaller then the contact drops down very late with the decrease in the rotational speed and the rubbing between rotor and guide is severe which is very dangerous for rotating machineries.

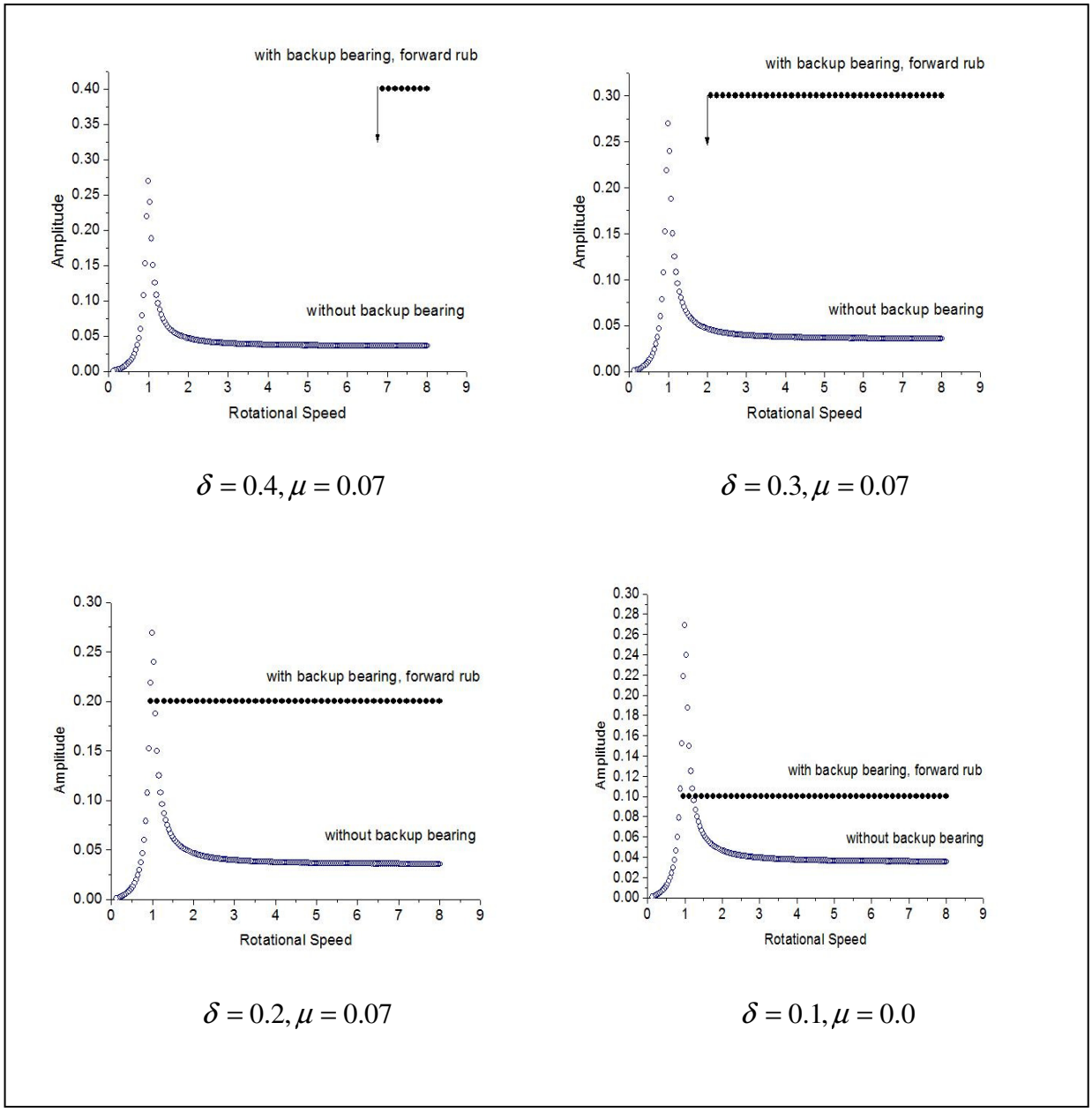

Fig. 5.60: Comparison among the results of different clearances for $\delta = 0.4, \delta = 0.3, \delta = 0.2$ and $\delta = 0.1$

5.3 Experimental results of Circular Backup Bearing

Fig. 5.61 to 5.63 shows the results of rotor-shaft system when the disk thickness is 5 mm, 10 mm and 15 mm respectively. Here the clearance between the shaft and backup bearing is 2 mm. Fig. 5.61 to 5.63 confirms that decreasing the rotating speed will certainly drop down the contact between rotor and guide. These results show that the rubbing occurs up to certain rotating speed, then the contact between rotor and guide drops down which validate the simulation results qualitatively discussed in previous sections. In this thesis, the quantitative analysis is not performed to compare the simulation results with the experimental results. Rather a qualitative research is made to validate the simulation results.

It is also observed from Fig. 5.61 to 5.63 that by increasing the mass of the rotor, the system critical speed decreases accordingly.

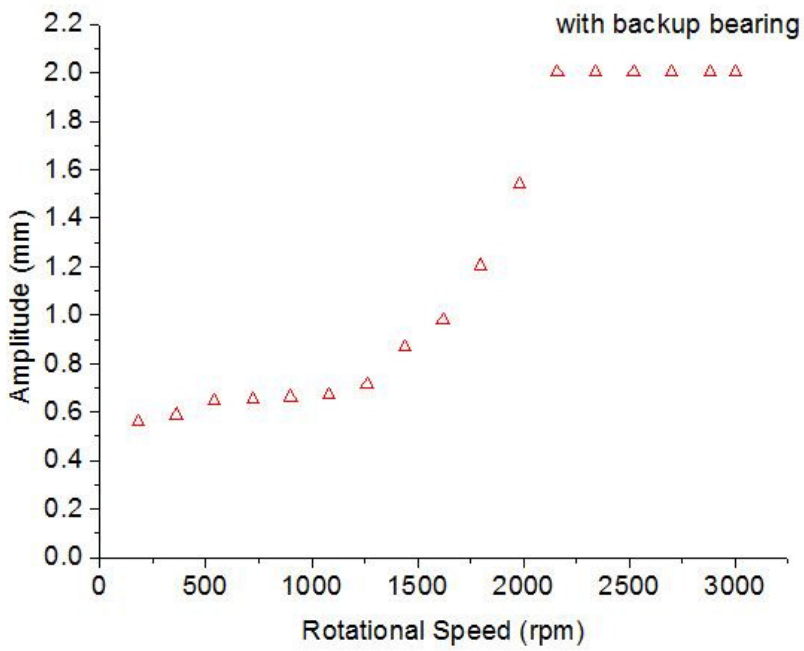

Fig. 5.61: Resonance Curve, disk thickness 5 mm.

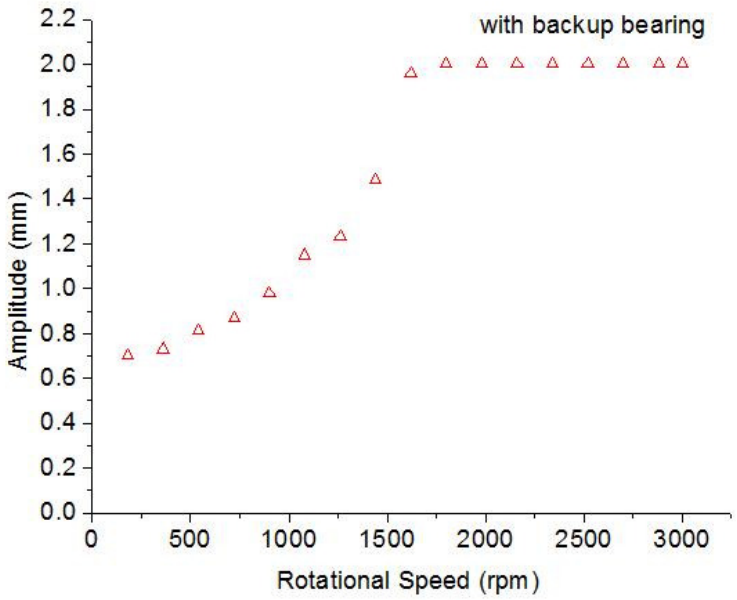

Fig. 5.62: Resonance Curve, disk thickness 10 mm.

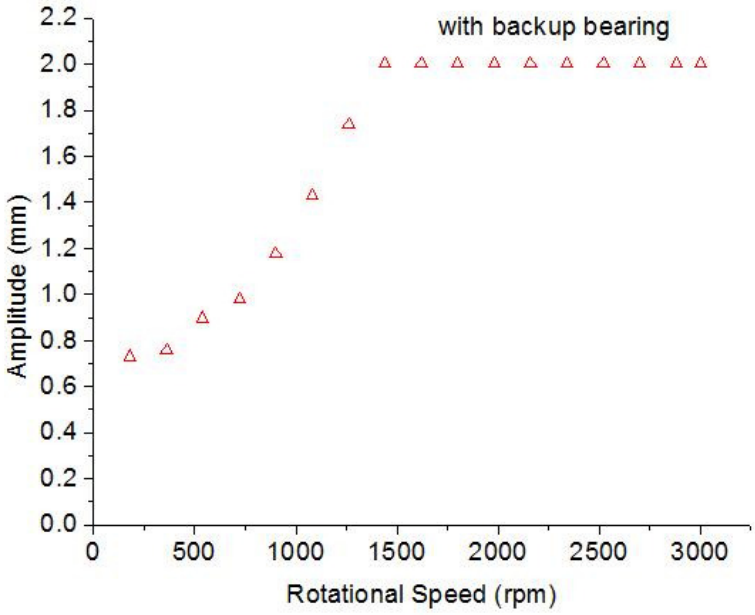

Fig. 5.63: Resonance Curve, disk thickness 15 mm.

Chapter 6

Minimization of Rubbing

Chapter 4 and chapter 5 discussed the minimization of excessive vibration by implementing circular backup bearing. From the simulation as well as experimental result, it has already been proved that by using this type of bearing excessive vibration can be minimized easily. However, in all the cases discussed earlier in chapter 4 and 5, rubbing was present between the shaft and inner surface of the backup bearing which is not good for rotating machineries. So this chapter will enlighten the implementation of a special type of bearing (in this case, the type is lemon shaped) which is basically used as back up bearing. Section 6.1 will discuss the theoretical model development for lemon shaped backup bearing, section 6.2 will discuss the SIMULINK model for the lemon type guide, section 6.3 will illustrate the simulation results of lemon type backup bearing and section 6.4 will discuss the experimental results of the lemon type backup bearing.

6.1 Theoretical Model Development for Lemon Shaped Guide

The design of the lemon shaped backup bearing is depicted in Fig. 6.1. The lemon shaped is formed by drawing the two circles (circle 1 and circle 2 in the following figure). Circle 1 and circle 2 have the same radius R.

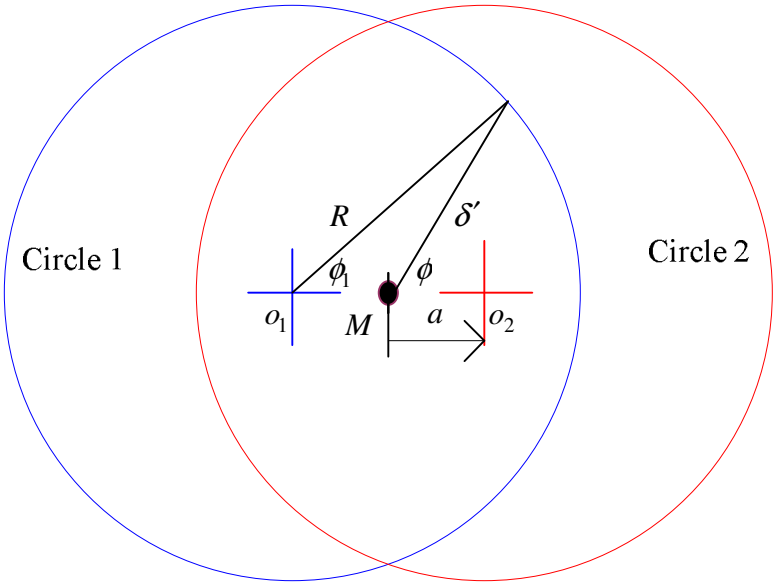

Fig. 6.1: Lemon Type Guide.

o_1 is the center point of circle 1 and o_2 is the center point of circle 2. ϕ_1 is the angle between R and O_1M and ϕ is the angle between δ' and MO_2. M is the center point of the lemon shaped guide. a is the distance between points M and o_2, points M and o_1 . The equations of circle 1 and 2 are $(x+a)^2 + y^2 = R^2$ and $(x-a)^2 + y^2 = R^2$. From this figure, subtraction of R and a is

the nearest gap from the center M to the wall of the lemon shaped guide. The lemon shaped can be modified by changing the two parameters R and a. So, these two are the most significant parameters for designing a lemon type backup bearing.

From Fig. 6.1, the following equations are obtained. All the following equations are used to derive a general equation for the clearance δ' which is variable in case of lemon type bearing.

$$R\sin\phi_1 = \delta'\sin\phi \tag{6.1}$$

$$R\cos\phi_1 = a + \delta'\cos\phi \tag{6.2}$$

$$R^2 = \delta'^2\sin^2\phi + a^2 + 2\delta' a\cos\phi + \delta'^2\cos^2\phi$$
$$R^2 = \delta'^2 + a^2 + 2\delta' a\cos\phi$$

$$\delta'^2 + 2\delta' a\cos\phi + a^2 - R^2 = 0 \tag{6.3}$$

$$\delta' = \frac{-2a\cos\phi \pm \sqrt{4a^2\cos^2\phi - 4(a^2 - R^2)}}{2}$$

$$\delta' = -a\cos\phi \pm \sqrt{a^2\cos^2\phi + R^2 - a^2}$$

$$\delta' = -a\frac{x}{r} \pm \sqrt{R^2 - a^2 + a^2(\frac{x}{r})^2}$$

As δ' can not be negative

$$\delta' = -a\frac{x}{r} + \sqrt{R^2 - a^2 + a^2(\frac{x}{r})^2} \tag{6.4}$$

So now we can put the condition considering 'M' point (Fig. 6.1) of the rotor is just middle of the lemon shape.

$$\left.\begin{aligned} F_k &= k_e(r - \delta') \\ F_c &= c_e\dot{r} \end{aligned}\right\} \quad \text{for} \quad \begin{aligned} x > 0, r > \delta' \\ x > 0, r' > R \end{aligned} \tag{6.5}$$

$r' = \sqrt{(x+a)^2 + y^2}$ (Considering first circle)

And

$$\left.\begin{aligned} F_k &= k_e(r-\delta') \\ F_c &= c_e\dot{r} \end{aligned}\right\} \quad \text{for} \quad \begin{aligned} &x<0, r>\delta' \\ &x<0, r'>R \end{aligned} \tag{6.6}$$

$r' = \sqrt{(x-a)^2 + y^2}$ (Considering second circle)

If x>0 then x is always positive (first circle) and if x<0 then x is always negative (second circle). So, r' for both the circles will be same and if we write

$$\delta' = -a\frac{|x|}{r} + \sqrt{R^2 - a^2 + a^2(\frac{x}{r})^2} \tag{6.7}$$

We can find the conditions for both the circles.

$$\left.\begin{aligned} F_k &= k_e(r-\delta') \\ F_c &= c_e\dot{r} \end{aligned}\right\} \quad \text{for} \quad \begin{aligned} &r>\delta' \\ &or \\ &r'>R \end{aligned} \tag{6.8}$$

Where $r' = \sqrt{(|x|+a)^2 + y^2}$

$r = \sqrt{x^2 + y^2}$

Now, before the experiment or simulation the value of 'R' and 'a' will be always known.

Conditions have been applied in simulation as before

$$F_k = k_e(r-\delta')\frac{1+\frac{r'-R}{|r'-R|}}{2} \tag{6.9}$$

$$F_c = c_e\dot{r}\frac{1+\frac{r'-R}{|r'-R|}}{2} \tag{6.10}$$

Or

$$F_k = k_e(r-\delta')\frac{1+\frac{r-\delta'}{|r-\delta'|}}{2} \tag{6.11}$$

$$F_c = c_e\dot{r}\frac{1+\frac{r-\delta'}{|r-\delta'|}}{2} \tag{6.12}$$

$$F_f = \mu(F_k + F_c)\frac{1+\frac{(R_s\omega+V_t)}{|R_s\omega+V_t|}}{2} - \frac{1-\frac{(R_s\omega+V_t)}{|R_s\omega+V_t|}}{2} \quad (6.13)$$

Where Rs is the radius of the shaft and V_t is the tangential velocity.

6.2 The SIMULINK Model

The mathematical model for lemon type backup bearing has been simulated in MATLAB SIMULINK software. Fig. 6.2 represents the overall SIMULINK block diagram to obtain the solutions from equations 4.44 and 4.45. Five subsystems are used to build the model precisely. All the required connections in subsystem 1, 2, 3, 4 and 5 are shown in Fig. 6.3, 6.4, 6.5, 6.5 and 6.7 respectively. The outputs from subsystem 3 are r and F_k. The outputs from the subsystems 4 and 5 are F_c and F_f. All the outputs r, F_k, F_c and F_f obtained from subsystems 3,4 and 5 are then fed to subsystems 1 and 2. The input force for subsystem 1 (Fig. 6.3) is cosine wave (phase changed in block parameter) and the input force for subsystem 2 (Fig. 6.4) is sinusoidal wave. Integrators in subsystem 1 (Fig. 6.3) and 2 (Fig. 6.4) are used to integrate the acceleration parameters ($\ddot{x}$ in subsystem 1 and $\ddot{y}$ in subsystem 2) to displacements (x and y). Many addition, subtraction, multiplication, division, gain and different other blocks (from SIMULINK library browser) are used to represent the equations 4.44 and 4.45. The parameters considered in simulation are same as used before to model the circular backup bearing system which are $e' = 0.035$, $c' = 0.13$, $k_e' = 3800000$, $c_e' = 400$ and $R' = 0.5$ [2]. Initial conditions are given in the integrator blocks of subsystems 1 and 2. Initial conditions are changed according to the different clearances (gap between shaft and inner surface of the lemon type bearing). The clearance is represented in SIMULINK model by d. In modeling the lemon shaped backup bearing system, the clearance d is not constant at all rather it is a variable. This variable is obtained from subsystem 3 in Fig. 6.5. In Fig. 6.5 actually equation 6.7 is represented to obtain the variable clearance. Moreover, initial conditions have also influence for forward and backward rubbing. Two hundred output data points are obtained from the simulation. The outputs from the overall SIMULINK model are visualized by graphical forms (which is basically the graph of amplitude against rotational speed). A small program is written in MATLAB M-file to run the overall SIMULINK block diagram for lemon type guide. The program is given below.

```
close all;
clear all;
format long;
e=0.035;
k=1.0;
```

```
ke=3800000;
c=0.13;
ce=400;
uk=0.0;
a=0.3;
R=0.5;
step=0.001;
open delta.mdl;
w=8.0;

for q=1:800;
    w=w-0.04;
    sim delta.mdl;
    z(q,1)=w;
    z(q,2)=max(rout(200001:end));
    figure(1)
    plot(z(:,1),z(:,2),'.')
    hold on

end
plot(z(:,1),z(:,2),'.')
save test.txt a -ascii;
```

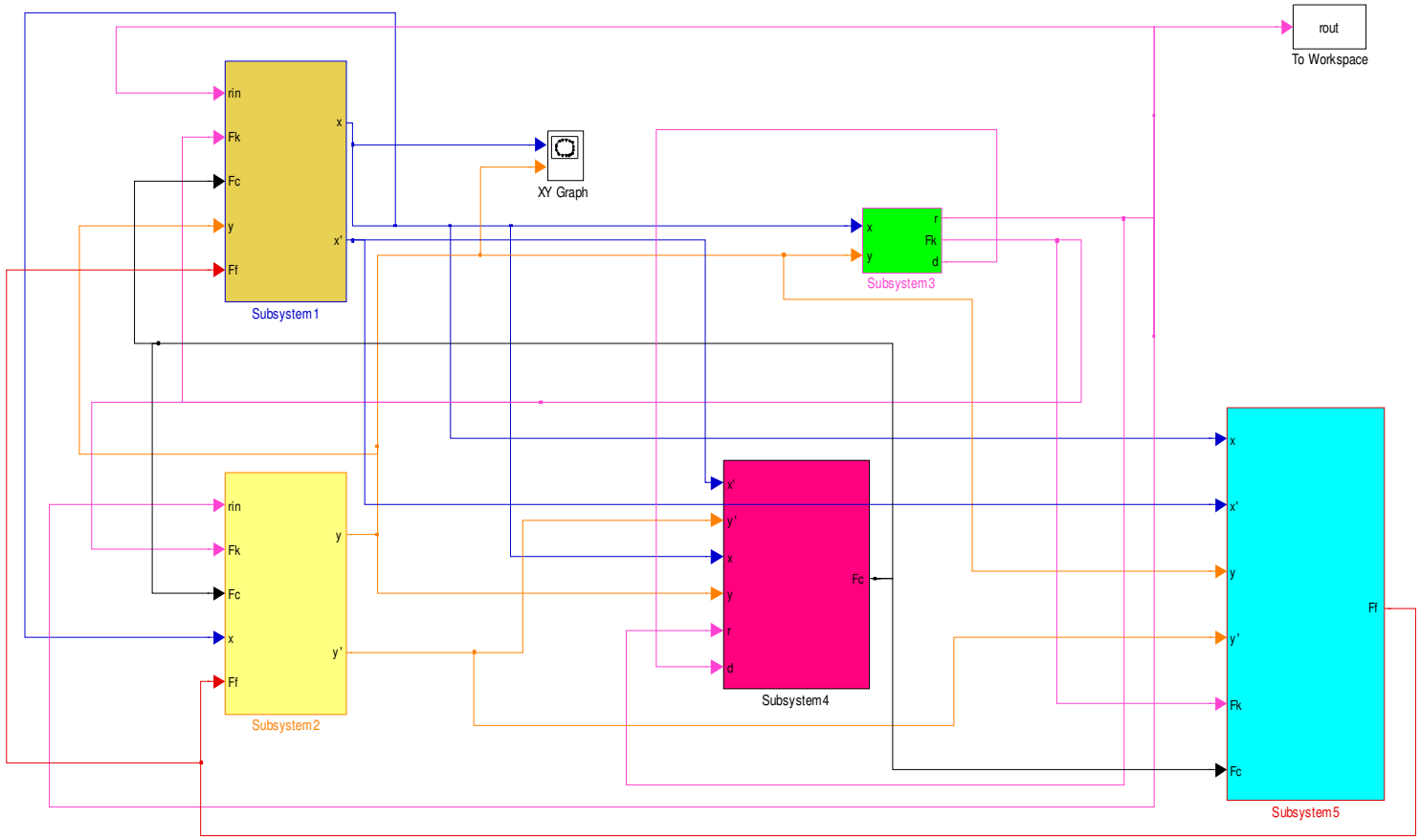

Fig. 6.2: Overall SIMULINK block diagram.

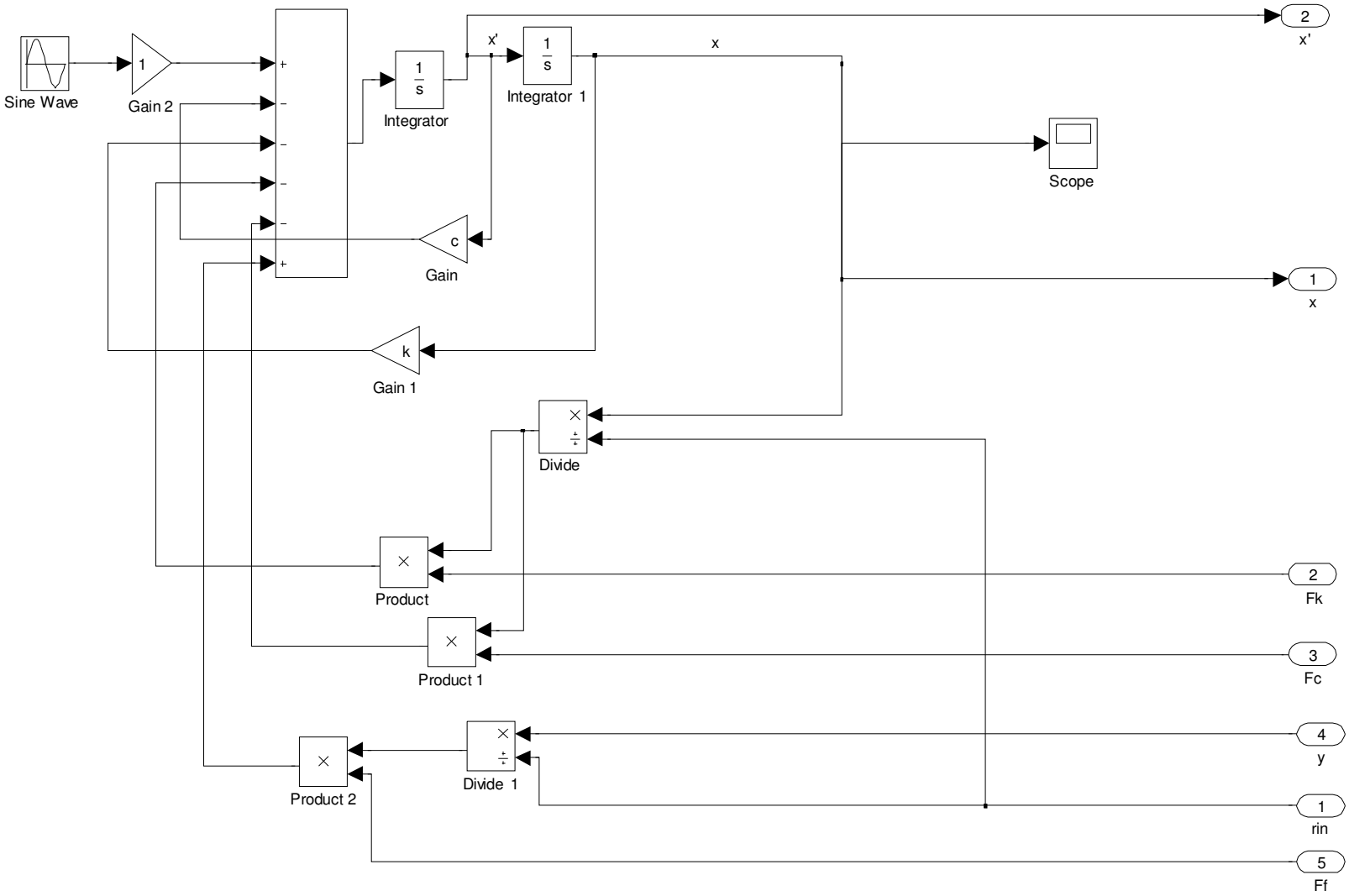

Fig. 6.3: Subsystem 1.

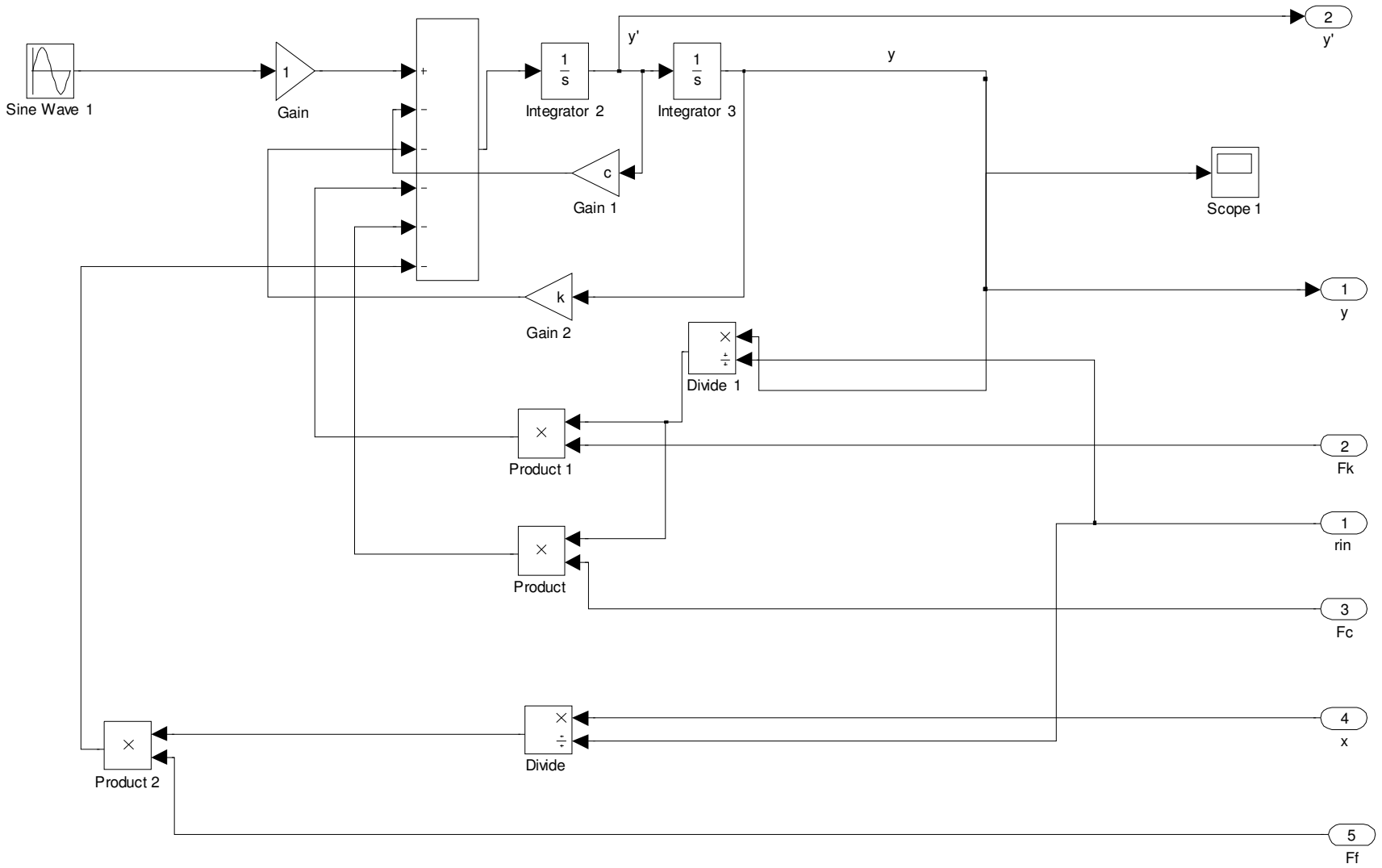

Fig. 6.4: Subsystem 2.

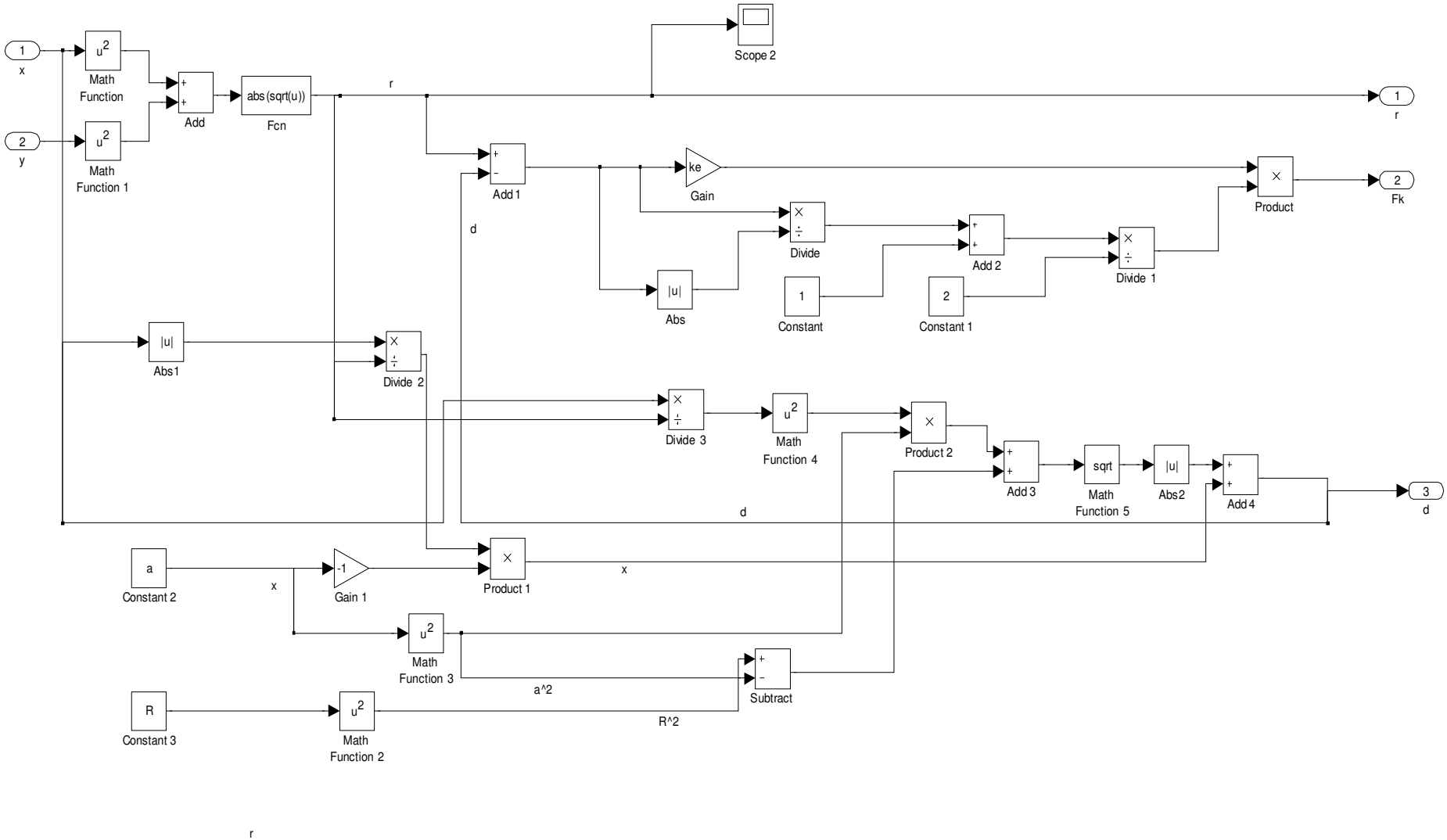

Fig. 6.5: Subsystem 3.

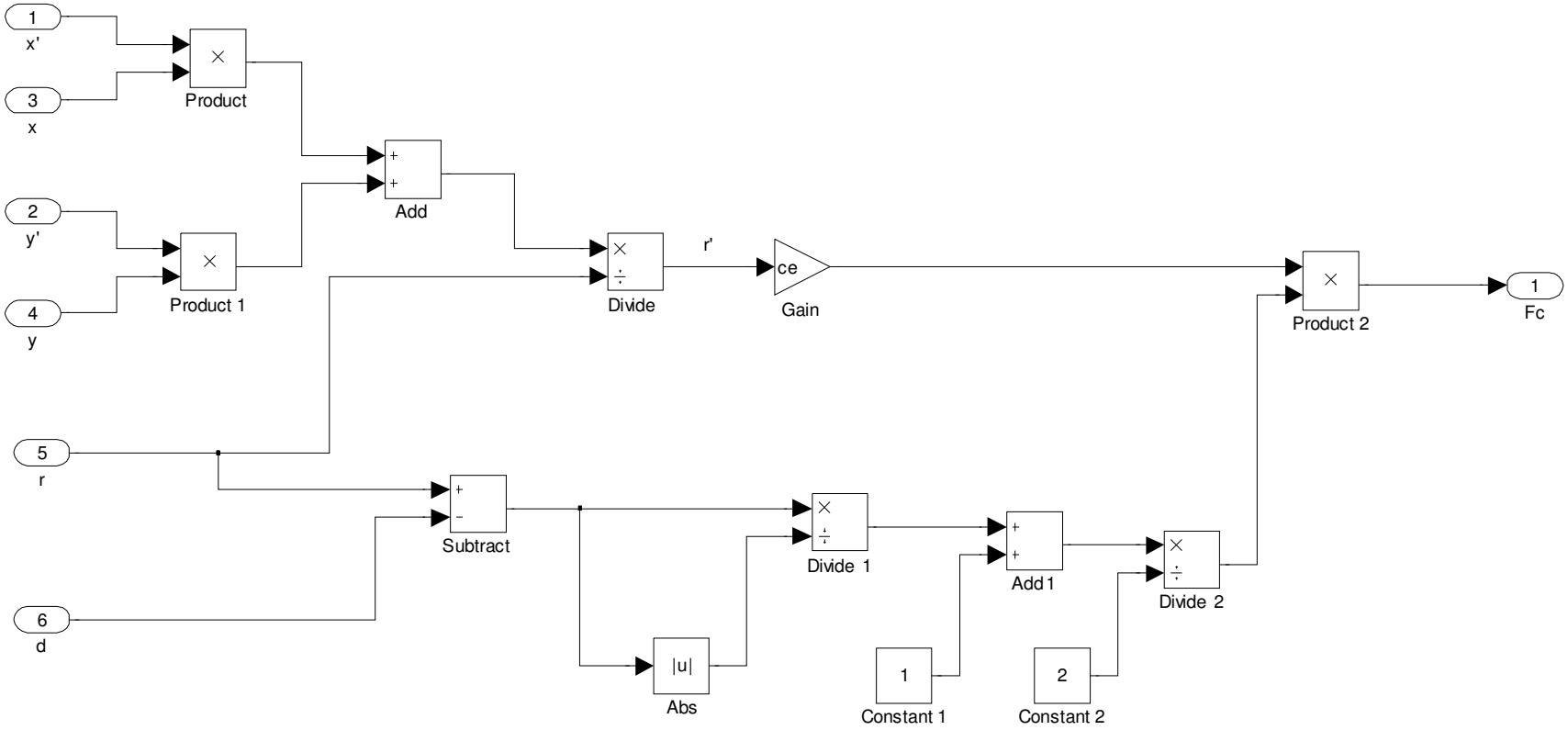

Fig. 6.6: Subsystem 4.

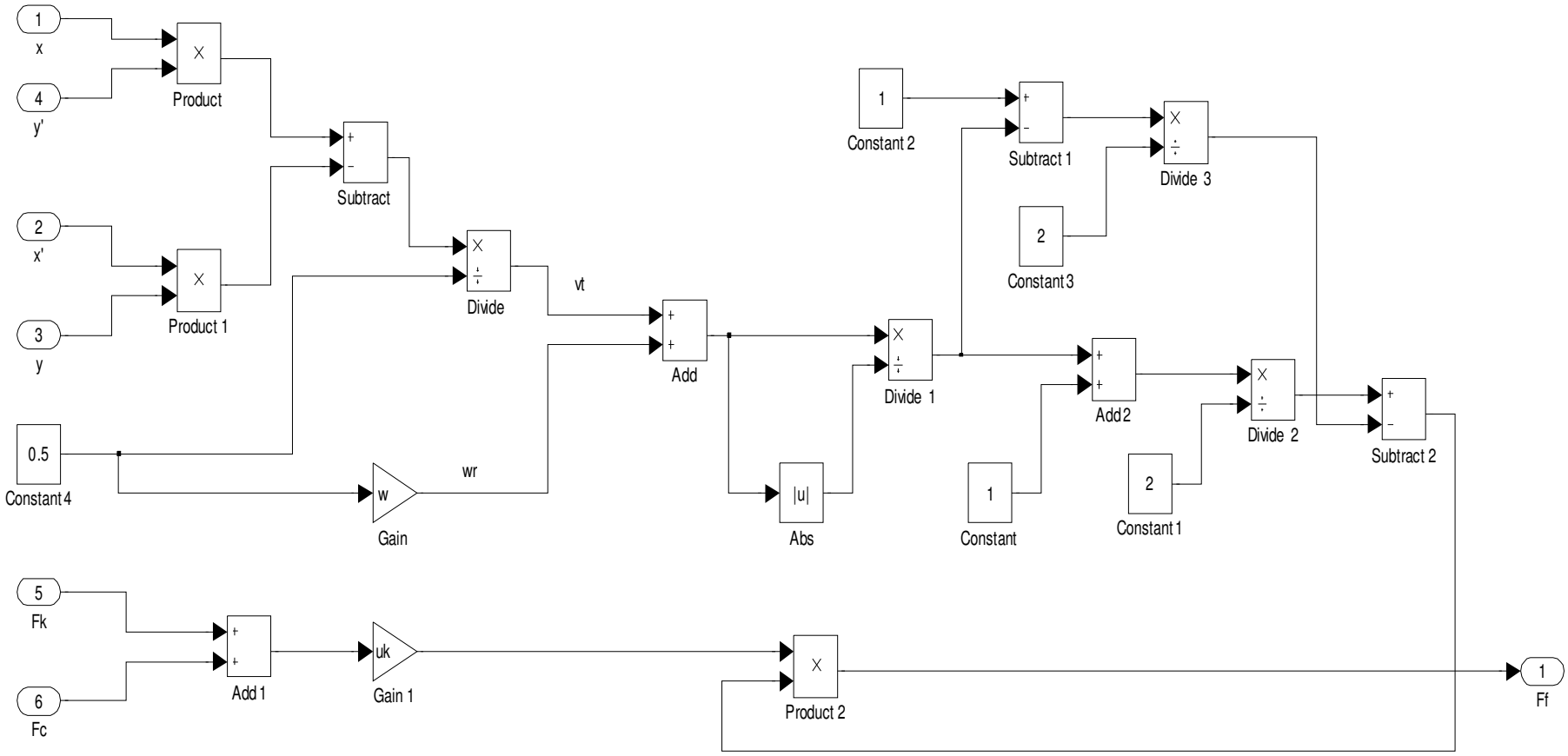

Fig. 6.7: Subsystem 5.

6.3 Simulation Results for Lemon Type Backup Bearing

This section enlightens the simulation results for lemon type backup bearing. From Fig. 6.1, it is certain that the subtracted value from 'R' and 'a' is δ which was used in previous chapter for the clearance between the shaft and inner surface of the circular backup bearing. So, the simulation results from the lemon type backup bearing will be compared with the circular backup bearing on the basis of the subtracted value from 'R' and 'a'. All the parameters are also dimensionless in simulation. So, dimensionless analysis is performed in simulations.

6.3.1 Resonance Curves

6.3.1.1 When R=0.5 and a=0.1

In this case, the subtracted value 'R' and 'a' is 0.4. So the nearest gap between the shaft and inner surface of the lemon type backup bearing is 0.4 which was δ in the previous chapter's simulation for circular backup bearing. Fig. 6.8 enlightens this scenario. Here the clearance for the circular type guide is the nearest gap between the shaft and the inner surface of the guide for lemon type guide. Fig. 6.9 depicts that when the rotating speed is higher the contact between the rotor and guide drops down. Here the system reaches to the lower valued amplitude line. And this scenario is completely opposite from the circular backup bearing result where $\delta = 0.4$ and $\mu = 0.0$ which is enlightened in Fig. 6.10. From Fig. 6.10, it is certain that when the rotating speed is higher the contact between rotor and guide drops down and there is no rubbing in case of lemon type backup bearing whereas in case of circular backup bearing there is continuous rubbing between rotor and guide even in the lower rotational speed range. So, the amplitude of vibration is less in case of lemon type backup bearing. And the interesting phenomenon is increasing the friction coefficient will not increase the probability of contact between rotor and guide which is confirmed by Fig. 6.11 where friction coefficient is 0.05. Fig. 6.12 shows that the rotational speed and the whirling speed of the rotor are same and the direction of both the speed is same. So, this scenario is forward rubbing. Fig. 6.13 depicts the phase diagram which is exactly the same with the phase diagram where there is no guide. The phase angle varies from -179.04 to -0.60. So, in this case there is no rubbing between rotor and guide after the resonance.

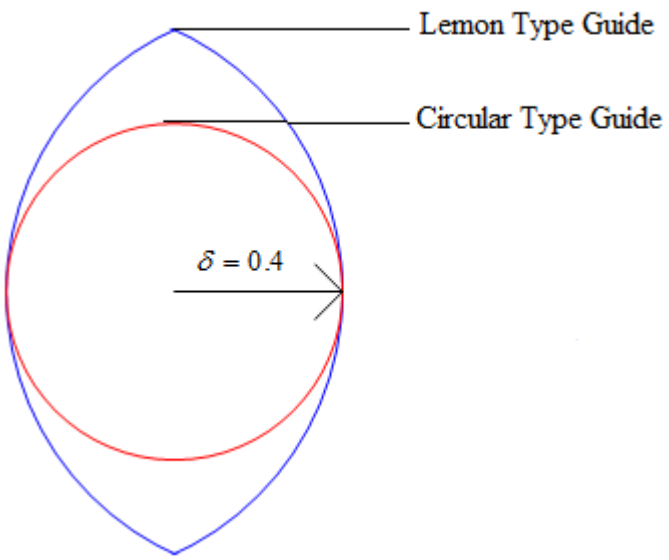

Fig. 6.8: Comparison between lemon and circular type guide.

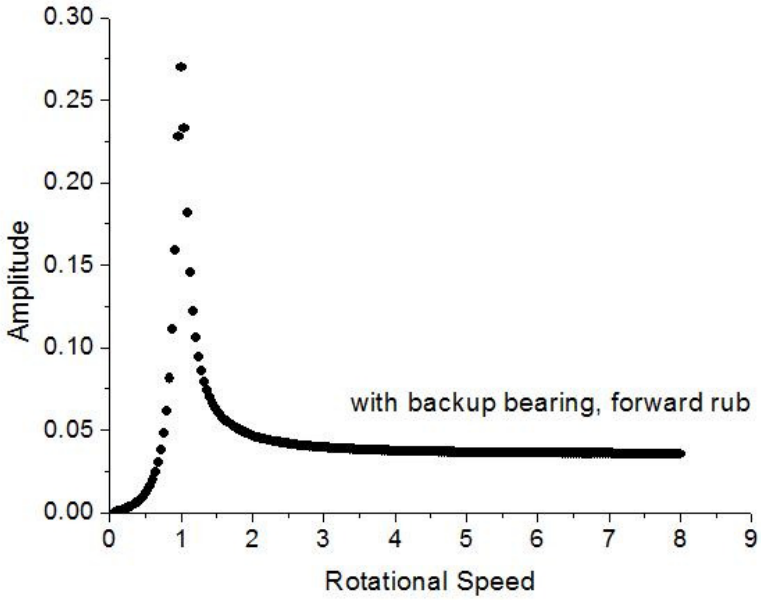

Fig. 6.9: Resonance Curve $R = 0.5, a = 0.1, \mu = 0.0$.

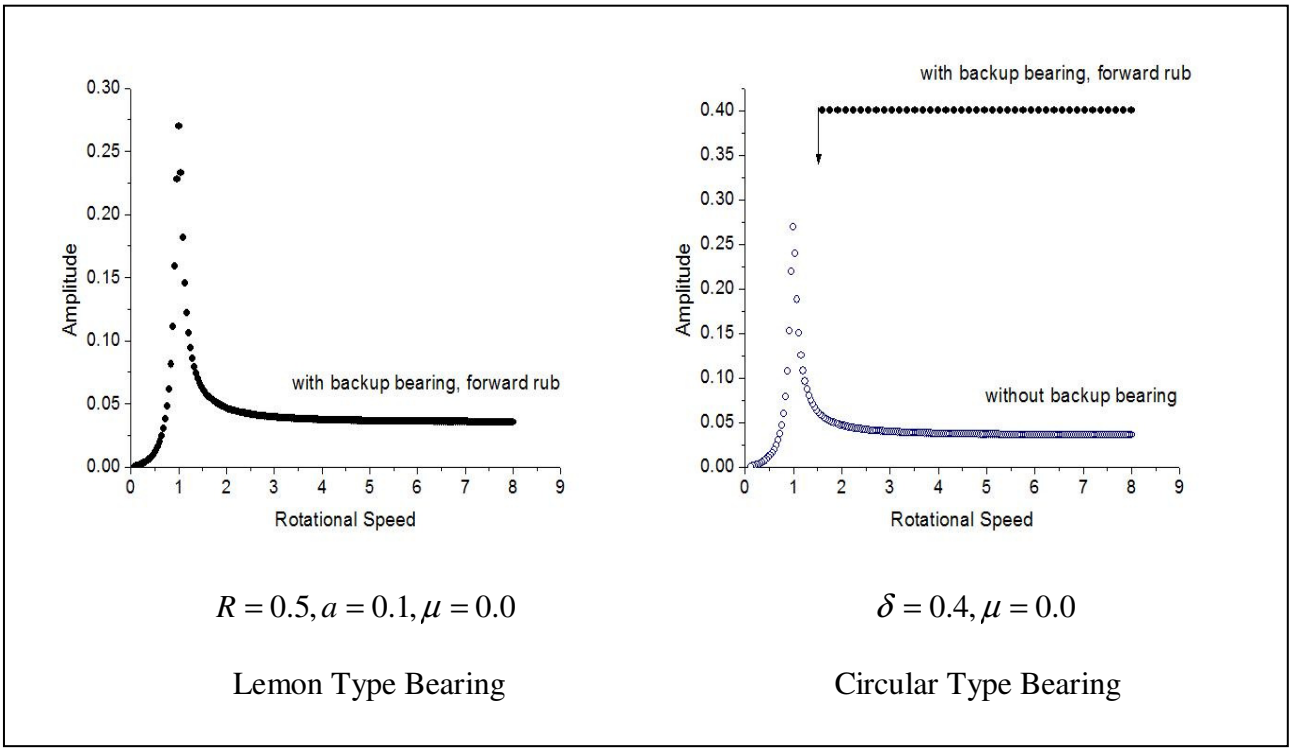

Fig. 6.10: Comparison between the simulation results of lemon and circular type bearing.

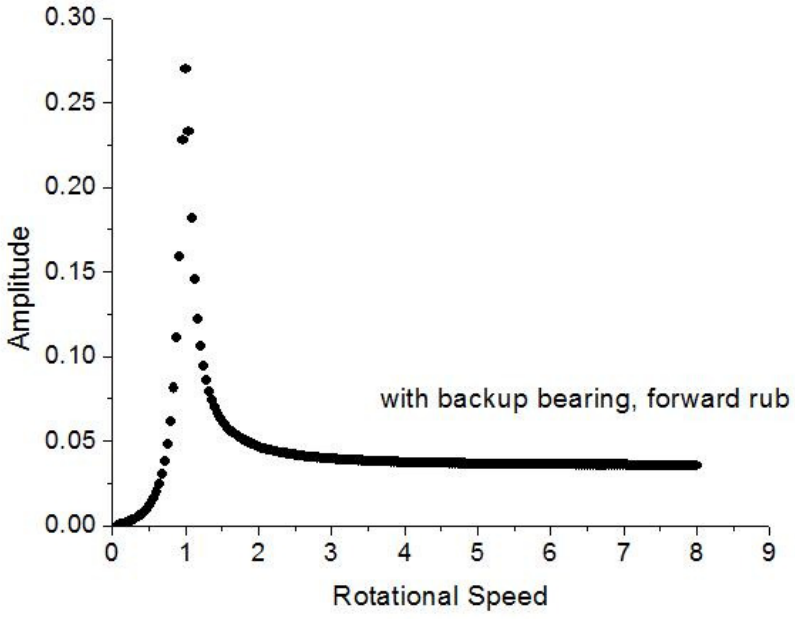

Fig. 6.11: Resonance Curve $R = 0.5, a = 0.1, \mu = 0.05$.

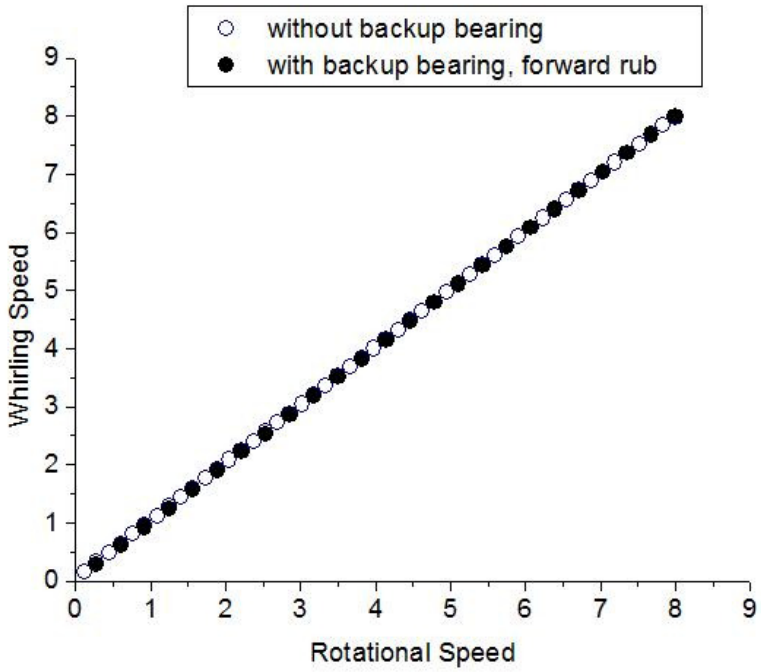

Fig. 6.12: Whirling speed diagram $R = 0.5, a = 0.1, \mu = 0.0$

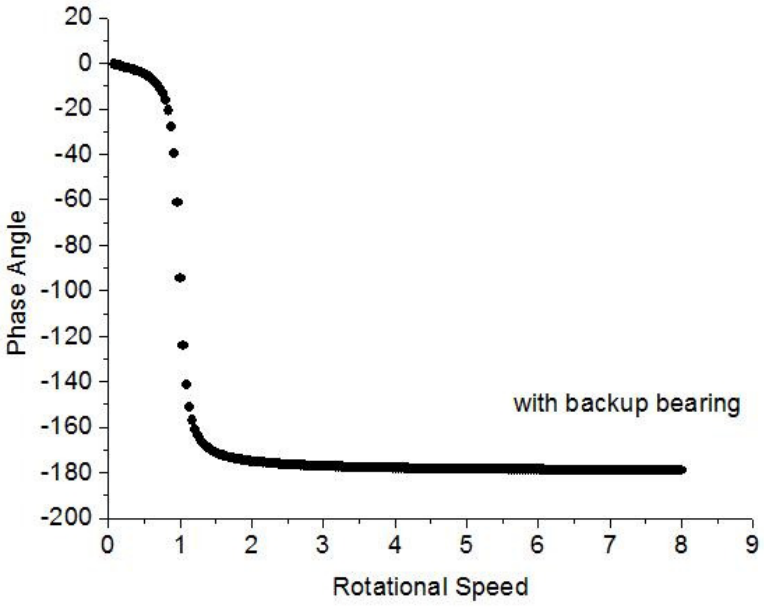

Fig. 6.13: Phase diagram $R = 0.5, a = 0.1, \mu = 0.0$

6.3.1.2 When R=0.5 and a=0.2

In this condition, the subtracted value 'R' and 'a' is 0.3. So the nearest gap between the shaft and inner surface of the lemon type backup bearing is 0.3 which was δ in the previous chapter's simulation for circular backup bearing. Fig. 6.14 enlightens this scenario. Here the clearance for the circular type guide is the nearest gap between the shaft and the inner surface of the guide for lemon type guide. Fig. 6.15 depicts that when the rotating speed is higher the contact between the rotor and guide drops down. Here the system reaches to the lower valued amplitude line. The resonance curve is similar with the graph where no backup bearing is implemented. And this scenario is completely opposite from the circular type backup bearing result where $\delta = 0.3$ and $\mu = 0.0$ which is enlightened in Fig. 6.16. From Fig. 6.16, it is certain that when the rotating speed is higher the contact between rotor and guide drops down and there is no rubbing in case of lemon type backup bearing whereas in case of circular backup bearing there is continuous rubbing between rotor and guide even in the lower rotational speed range. So, the amplitude of vibration is less in case of lemon type bearing. And the same phenomenon as before which is increasing the friction coefficient will not increase the probability of contact between the rotor and guide. There is no rubbing between the rotor and guide after the resonance. The whirling speed and phase diagrams for this condition are similar with the diagrams which are showed earlier in Fig. 6.12 and 6.13.

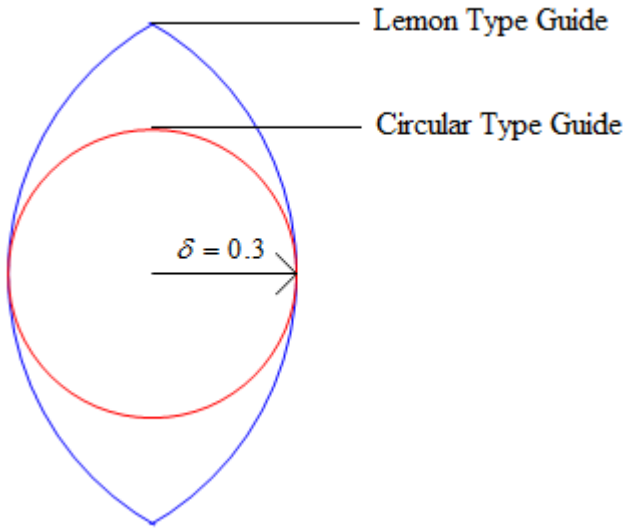

Fig. 6.14: Comparison between lemon and circular type guide.

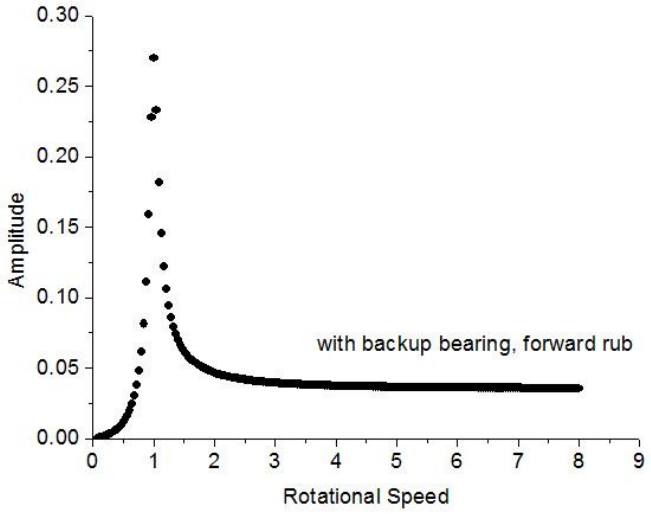

Fig. 6.15: Resonance Curve $R = 0.5, a = 0.2, \mu = 0.0$.

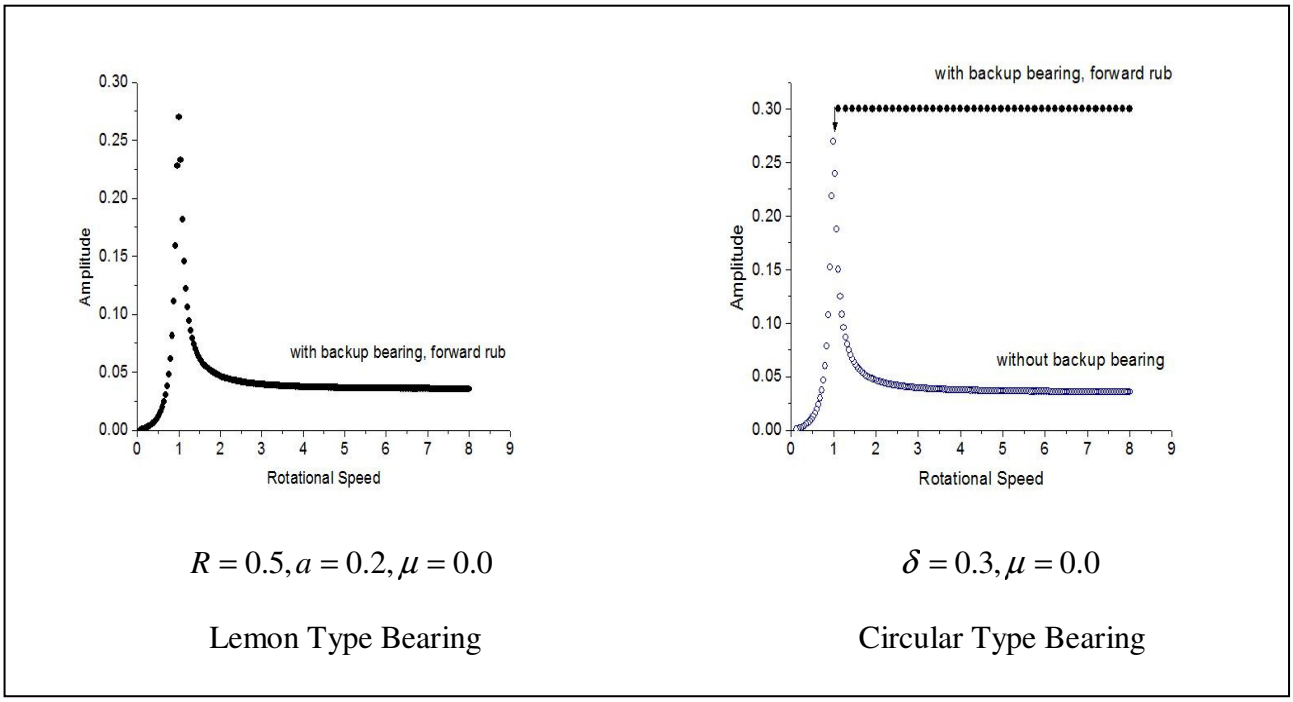

$R = 0.5, a = 0.2, \mu = 0.0$

Lemon Type Bearing

$\delta = 0.3, \mu = 0.0$

Circular Type Bearing

Fig. 6.16: Comparison between the simulation results of lemon and circular type bearing.

6.3.1.3 When R=0.5 and a=0.3

In this case, the subtracted value 'R' and 'a' is 0.2. So the nearest gap between the shaft and inner surface of the lemon type backup bearing is 0.2 which was δ in the previous simulation for circular backup bearing. Fig. 6.17 enlightens this scenario. Here the clearance for the circular type guide is the nearest gap between the shaft and the inner surface of the guide for lemon type guide. Fig. 6.18 depicts that when the rotating speed is higher the contact between the rotor and guide drops down. Here the system reaches to the lower valued amplitude line. The resonance curve is similar with the graph where no backup bearing is implemented. And this scenario is also completely opposite from the circular type backup bearing result where $\delta = 0.2$ and $\mu = 0.0$ which is enlightened in Fig. 6.19. From Fig. 6.19, it is certain that when the rotating speed is higher the contact between rotor and guide drops down and there is no rubbing in case of lemon type backup bearing whereas in case of circular backup bearing there is continuous rubbing between rotor and guide even in the lower rotational speed range. So, the amplitude of vibration is less in this case. And this shows the minimization of rubbing between rotor and stator contact. The whirling speed and phase diagrams for this condition are similar with the diagrams which are showed earlier in Fig. 6.12 and 6.13.

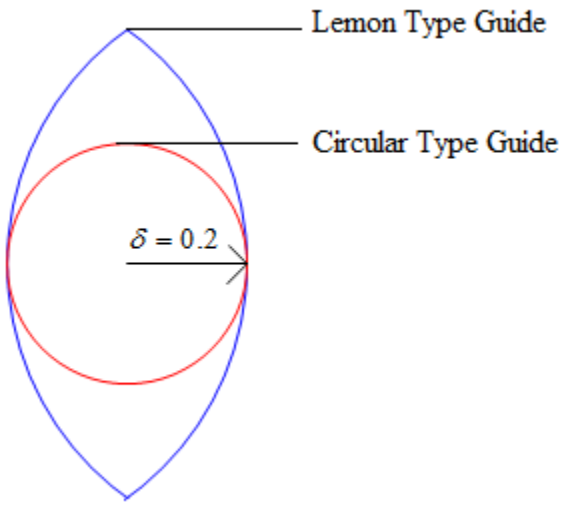

Fig. 6.17: Comparison between lemon and circular type guide.

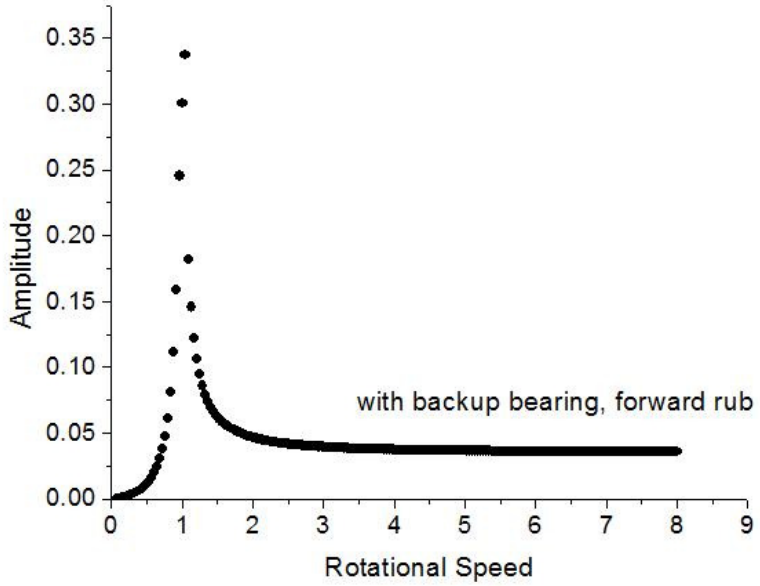

Fig. 6.18: Resonance Curve $R = 0.5, a = 0.3, \mu = 0.0$.

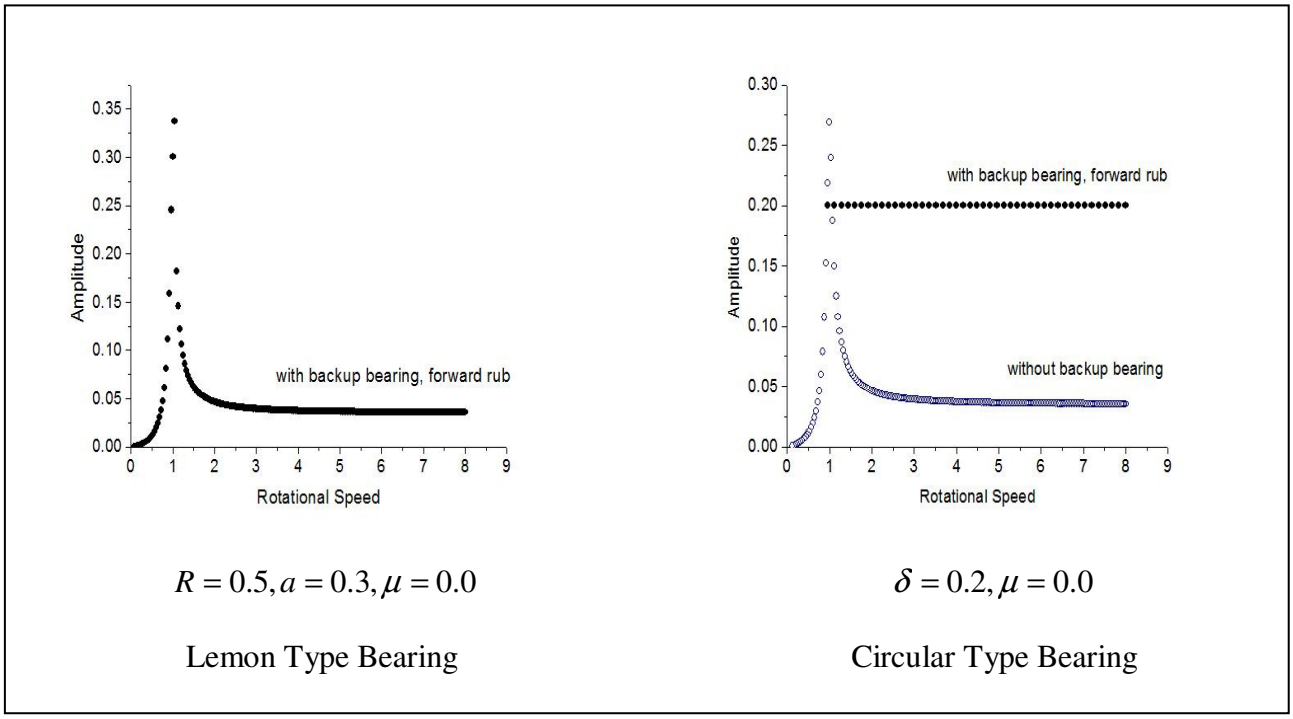

$R = 0.5, a = 0.3, \mu = 0.0$

Lemon Type Bearing

$\delta = 0.2, \mu = 0.0$

Circular Type Bearing

Fig. 6.19: Comparison between the simulation results of lemon and circular type bearing.

6.3.1.4 When R=0.5 and a=0.4

In this case, the subtracted value 'R' and 'a' is 0.1. So the nearest gap between the shaft and inner surface of the lemon type backup bearing is 0.1 which was δ in the previous simulation in the previous chapter for circular backup bearing. Fig. 6.20 enlightens this scenario. Here the clearance for the circular type guide is the nearest gap between the shaft and the inner surface of the guide for lemon type guide. Fig. 6.21 depicts that rubbing occurs up to rotational speed 4.38 and after this speed the contact between rotor and guide just drops down. It has been investigated carefully that when the nearest gap between the shaft and inner surface of the backup bearing is 0.1, then only rubbing phenomenon was observed after the resonance. But in all the other clearances described in previous sections there was no rubbing phenomenon. The scenario is also different from the circular type backup bearing result where $\delta = 0.1$ and $\mu = 0.0$ which is enlightened in Fig. 6.22. In Fig. 6.22, it is observed that the rubbing occurs almost up to rotational speed 0.84 in case of circular backup bearing where as in this certain condition for lemon type backup bearing the rubbing occurs up to rotational speed 4.38. So, the amplitude of vibration becomes less early in the higher rotating speed range in case of lemon type backup bearing. And this enlightens the minimization of rubbing between rotor and stator contact. Fig. 6.23 shows the whirling speed diagram where the whirling speed is almost half of the rotational speed up to rotating speed 4.38. After this rotating speed, the whirling speed and rotational speed becomes same. Furthermore, the direction of the speed is same in this case and this phenomenon is forward rubbing. Fig. 6.24 highlights the phase diagram. From this phase diagram, it is clear that up to rotating speed 4.38, the phase angles show random behavior. But after this speed, the phase angles just follow the same path as shown in Fig. 6.13. Therefore, all the information in this particular section enlightens that during rubbing in case of implementing lemon type backup bearing, the whirling and phase characteristics are different from that of circular backup bearing.

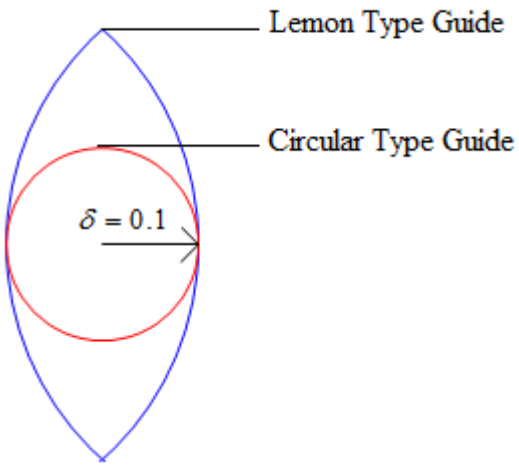

Fig. 6.20: Comparison between lemon and circular type guide.

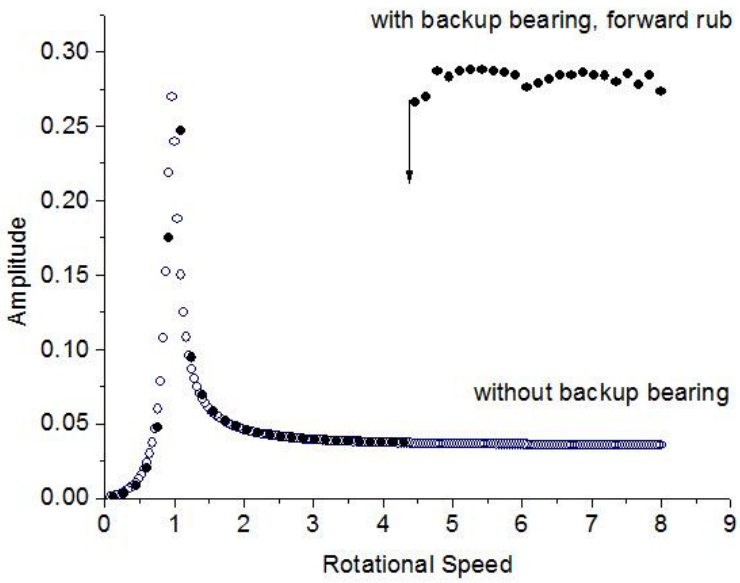

Fig. 6.21: Resonance Curve $R = 0.5, a = 0.4, \mu = 0.0$.

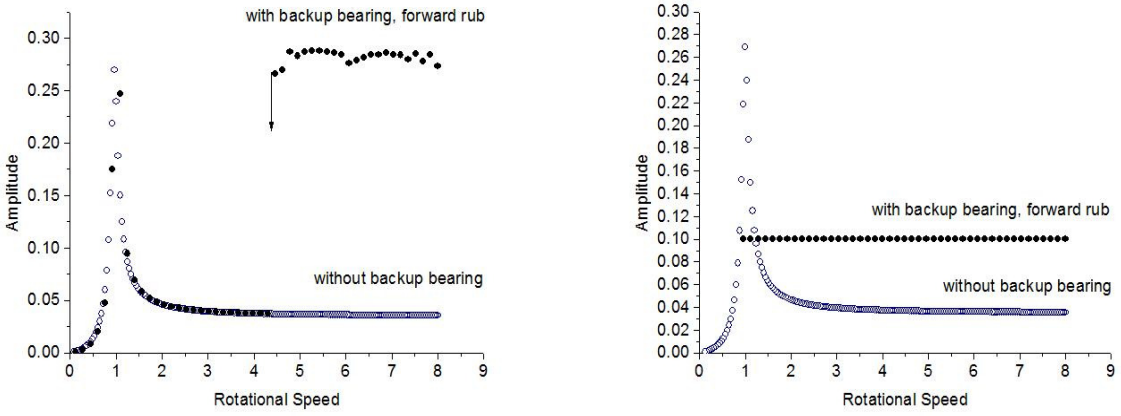

$R = 0.5, a = 0.4, \mu = 0.0$

Lemon Type Bearing

$\delta = 0.1, \mu = 0.0$

Circular Type Bearing

Fig. 6.22: Comparison between the simulation results of lemon and circular type bearing.

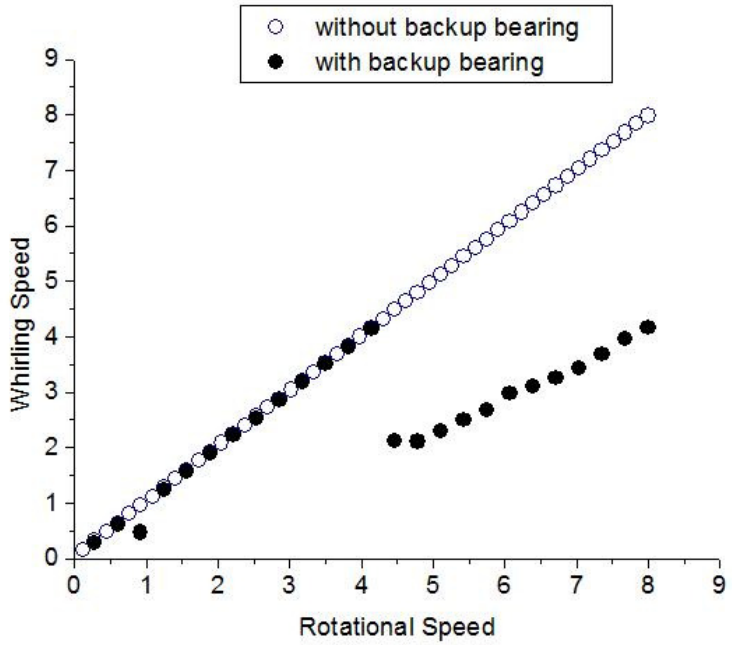

Fig. 6.23: Whirling speed diagram $R = 0.5, a = 0.4, \mu = 0.0$

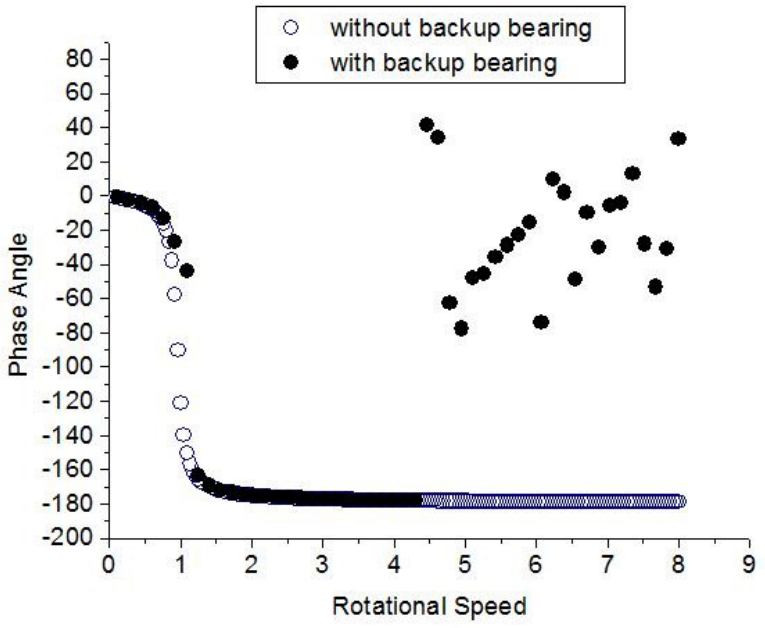

Fig. 6.24: Phase diagram $R = 0.5, a = 0.4, \mu = 0.0$

6.3.2 Rotor Orbits

This section describes the orbits of the rotor for three cases when the nearest gap between the rotor and inner surface of the lemon type bearing is 0.1, 0.2 and 0.3. All the orbits for different clearances are visualized when the rotating speed is 8.0 and friction coefficient is 0. From Fig. 6.25, a lemon shaped rotor orbit is obtained. In this case, the rubbing continues throughout the speed. In Fig. 6.26, the rotor trajectories are different from Fig. 6.25. Fig. 6.26 depicts that at the inception of simulation time, the rotor orbit is lemon shaped but with the increase in simulation time, the contact between the rotor and guide drops down and the trajectories concentrate into the center of the lemon type backup bearing. From this figure, it is also noticeable that there are some random impacts of the rotor with the guide. Fig. 6.27 shows the rotor orbit when the nearest gap between rotor and guide is 0.3. Due to the increase in clearance, the rotor does not follow the same trajectories all the time. In this case also, at the inception of simulation time, the rotor orbit is lemon shaped but with the increase in simulation time, the contact between the rotor and guide drops down earlier compared with Fig. 6.26 and the trajectories concentrate into the center of the lemon type backup bearing.

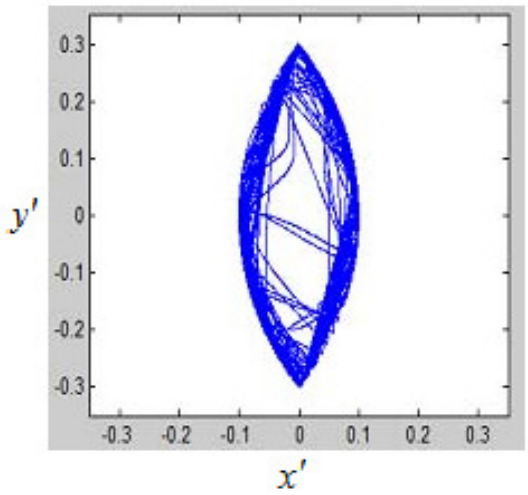

Fig. 6.25: Rotor orbit, $R = 0.5, a = 0.4, \mu = 0.0, \omega' = 8.0$

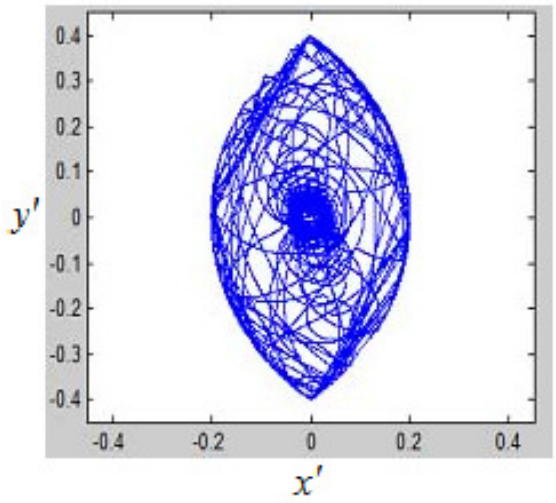

Fig. 6.26: Rotor orbit, $R = 0.5, a = 0.3, \mu = 0.0, \omega' = 8.0$

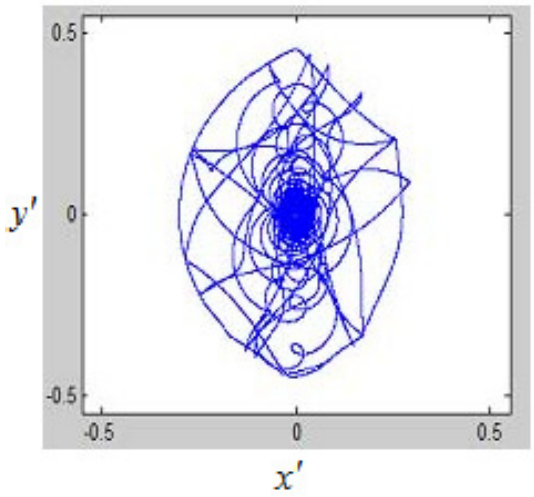

Fig. 6.27: Rotor orbit, $R = 0.5, a = 0.2, \mu = 0.0, \omega' = 8.0$

6.3.3 Comparison among the Results of Different Clearances of Lemon Type Guide

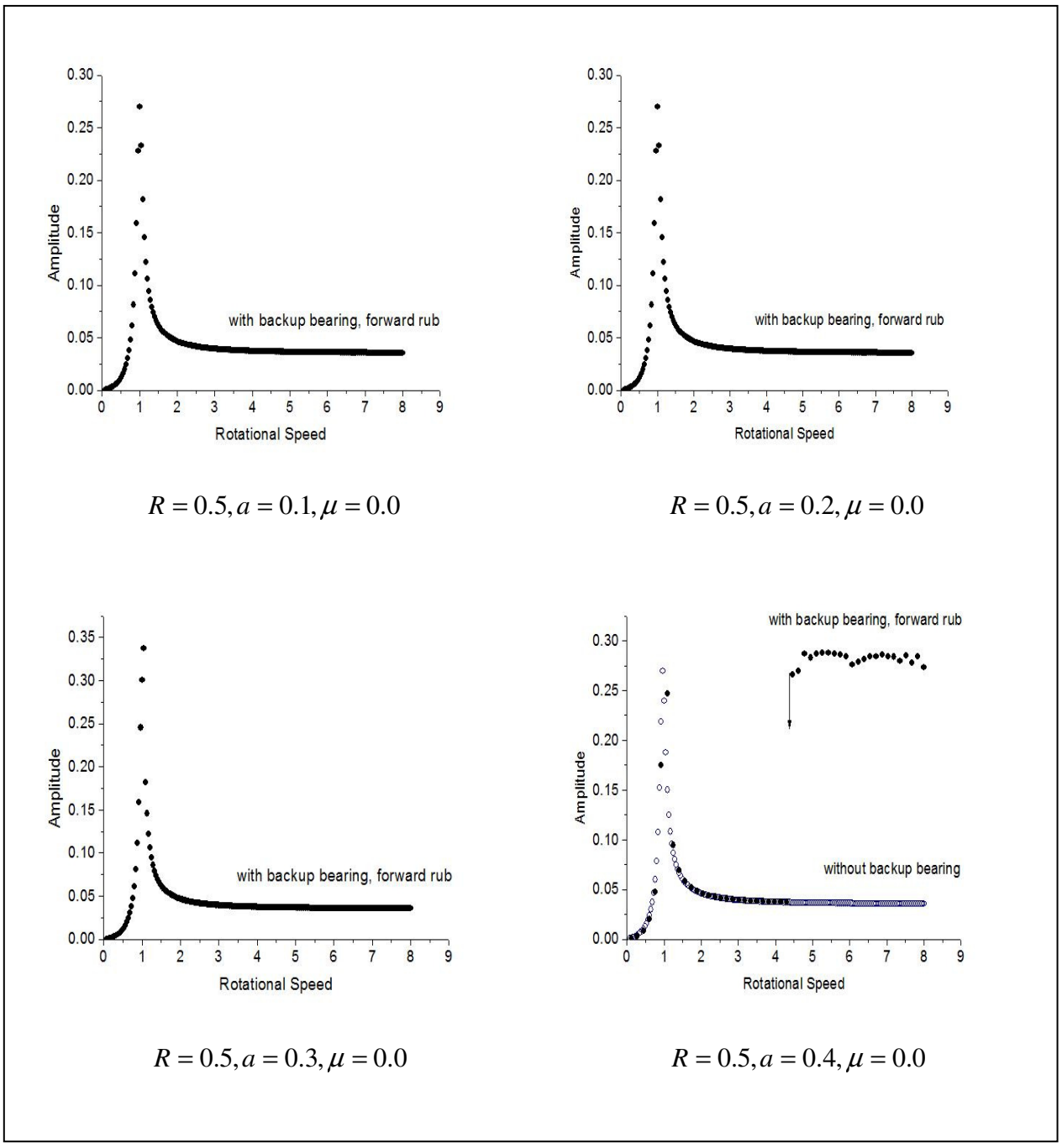

Fig. 6.28: Comparison among the results of different clearances when the nearest gap between rotor and guide $\delta = 0.4, \delta = 0.3, \delta = 0.2$ and $\delta = 0.1$

Fig. 6.28 shows the comparison among the different nearest gaps between rotor and guide for 0.4, 0.3, 0.2 and 0.1. From the Fig. 6.28, it is clear that when the nearest gap between rotor and guide is 0.4 or 0.3 or 0.2 the resonance curve is same except in case of clearance 0.2 when the rotational speed is 1.0 then the amplitude of vibration becomes 0.3. But the amplitude of vibration is 0.27 when the nearest gaps between rotor and guide are 0.4 and 0.3. For $\delta = 0.4, \delta = 0.3$ and $\delta = 0.2$, there is no rubbing between the rotor and guide. Therefore, the amplitude of vibration is very less in these clearances. On the other hand, when the nearest gap between the rotor and guide is 0.1, alternatively when $\delta = 0.1$, there is rubbing between rotor and guide upto rotational speed 4.38. And after this speed, the contact between rotor and guide falls down and the system reaches to the lower valued amplitude line. So, from the simulation results for lemon type guide, it is evident that when the nearest gap between rotor and guide is 0.1, then the rubbing between rotor and guide happens only whereas in all the other nearest gaps between rotor and guide which are $\delta = 0.4, \delta = 0.3$ and $\delta = 0.2$, there is no rubbing between rotor and guide. In conclusion, it can be added that the amplitude of vibration is decreased significantly by using the lemon type guide in rotating machineries.

6.4 Experimental Results of Lemon Type Backup Bearing

Lemon type bearing is not available in Bangladesh. So, in this experiment a lemon type guide was designed and manufactured from brass material in IUT machine shop. Fig. 6.29 is the lemon type guide which was used in the experiment. In this case, the nearest gap between the shaft and inner surface of the lemon type guide is kept 2 mm so that this result can be compared qualitatively with the previous results obtained from implementing circular backup bearing. And the longest distance from the shaft to the inner surface of the lemon type guide is 4 mm.

Fig. 6.29: Lemon type guide.

Fig. 6.30 depicts the lemon type guide which is implemented in experiment as backup bearing.

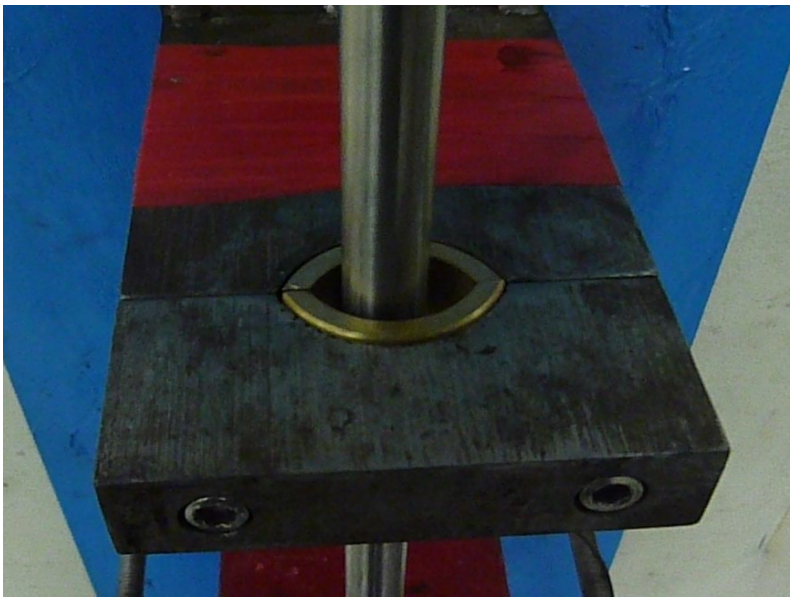

Fig. 6.30: Implementation of lemon type guide in the experiment.

The experimental results are obtained using the disk of 5 mm and 10mm thickness. Fig. 6.31 shows the experimental result of 5 mm disk thickness. From this figure, with the increase of the motor speed, the amplitude of vibration increases up to 2160 rpm. And from 2160 to 2520 rpm there is rubbing between rotor and guide. After 2520 rpm, the contact between rotor and guide suddenly drops down and the amplitude of vibration decreases significantly. Therefore, the rubbing between rotor and guide is minimized. Fig. 6.32 depicts the result when the disk thickness is 15 mm. In this case, the amplitude of vibration increases up to 1440 rpm. After that there is rubbing between rotor and guide from 1440 to 1980 rpm. And after this speed, the contact between rotor and guide suddenly drops down and the amplitude of vibration is minimized. So, from these experimental results it is evident that after the range of critical speed, the amplitude of vibration is decreased significantly which validates the previous simulation results in Fig. 6.9, 6.15 and 6.18 qualitatively.

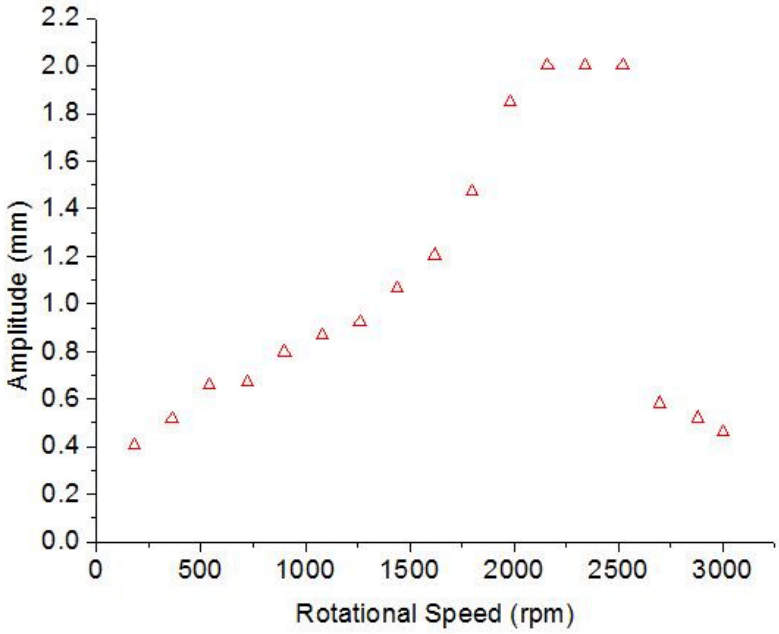

Fig. 6.31: Resonance Curve, disk thickness 5 mm.

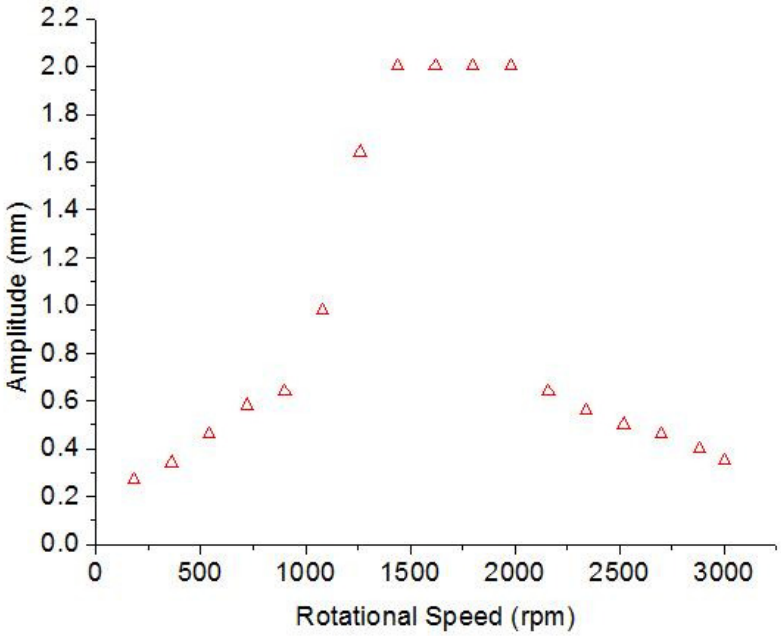

Fig. 6.32: Resonance Curve, disk thickness 15 mm.

Chapter 7

Conclusions and Future Works

7.1 Conclusions

The following concluding remarks can be obtained for the rotor-shaft-backup bearing system:

1. Increase in friction coefficient up to certain level will drop the contact between rotor and guide earlier in the higher rotating speed range. It has been enlightened for the clearances $\delta = 0.4$ and 0.3 for circular backup bearing between rotors and guides that increasing the friction coefficient before 0.1, the contact between rotor and guide dropped down earlier in the rotational speed range. It has also been observed that in case of $\delta = 0.4$, the contact between rotor and guide drops down earlier than in case of $\delta = 0.3$. Therefore, it can be concluded that if the clearance is higher and the friction coefficient is increased up to certain level, then the rubbing between rotor and guide will certainly be minimized.

2. Decrease in the clearance between rotor and guide increase the rubbing between rotor and guide. Although in this scenario, the excessive vibration is minimized, but the rubbing is not good for rotor-guide system. It has been confirmed that when clearance δ is 0.1 the rubbing between rotor and stator is more than when δ is 0.2. And in these cases, increase in the friction coefficient up to certain level will not drop down the contact between rotor and guide earlier. So, it can be decided to minimize excessive rubbing between rotor and guide, lower clearances between rotor and guide has to be avoided.

3. If the friction force becomes larger, the backward whirling motion becomes easier to occur. This has been observed that for all clearances, when the friction coefficient is 0.1 and above the rubbing is backward. Backward rubbing is very dangerous for the rotating machineries. So, to avoid backward rubbing, the friction coefficient must be lower.

4. As the friction increases, contact region for the forward whirling motion becomes narrower.

5. As the gap between the backup bearing and the shaft is decreasing, the forward whirling motion becomes easier to occur.

6. In forward rub, the whirling speed and rotational speed are same. Also the direction of both the speed is same. But in backward rub, the whirling and rotational speed is different and the direction of both the speed is opposite.

7. For the minimization of rubbing, lemon type backup bearing works certainly better than circular backup bearing. Simulation as well as experimental results showed that in case of implementing lemon shaped guide; the rotor reaches to the lower valued stable amplitude line after the resonance frequency. Therefore, these results confirm the possibility of the minimization of rubbing between rotor and guide.

8. Finally, it is possible to reduce the excessive vibration and rubbing by regulating the clearance and type of backup bearing.

7.2 Future Works

Future works of this research work involves:

1. A mathematical analysis will be done for the whirling speed in case of lemon type backup bearing particularly when the nearest gap between the rotor and guide is 0.1.

2. The simulation results will be compared with the experimental results quantitatively.

REFERENCES

1. LI Y., Modeling and Performance Investigation of a Rotor with Dissimilar Bearing Support System, M.Sc Thesis, Cleveland State University, April 2011.
2. Ishida Y., Hossain M. Z., Inoue T., Yasuda S., "Forward and Backward Whirling due to Contact and Its Prevention" Japan Society of mechanical engineering Dynamics and Design Conference 2003, CD-ROM, 640.
3. Choi Y.S., Investigation on the Whirling Motion of full Annular Rotor Rub, Journal of Sound and Vibration (2002) 258 (1), 191-198.
4. Stodora A. (1924), Dampf-und Gas-Turbinen, Verlag von Julius Springer, Berlin; English translation (1927), Steam and Gas Turbines, McGraw-Hill, New York.
5. Dunkerley, S. (1894), On the whirling and vibration of shaft, Philos. Trans. R. Soc. London, Ser. A, Vol. 185, pp.279-359.
6. Holtzer, H. (1921), Die Berechnung der Drehschwingungen, Springer-Verlag, Berlin.
7. Newkirk, B.L. (1924), Shaft Whipping, Gen. Electr. Rev., Vol.27, No.3, pp.169-178.
8. Kimball, A.L. (1924), Internal friction theory of shaft whirling, Gen. Electr. Rev., Vol.27, No. 4, pp.244-251.
9. Newkirk, B.L., and Taylor, H.D. (1925), Shaft whirling due to oil action in journal bearings, Gen. Electr. Rev., Vol. 28, No. 7, pp.559-568.
10. Bishop, R.E.D. (1959), Vibration of rotating shafts, J. Mech. Eng. Sci., Vol. 1, No. 1, pp.50-65.
11. Bishop, R.E.D., and Gladwell, G.M.L. (1959), The vibration and balancing of an unbalanced flexible rotor, J. Mech. Eng. Sci., Vol. 1, No. 1, pp.66-77.
12. Bishop, R.E.D., and Parkinson, A. G. (1965), Second order vibration of flexible shafts, Philos. Trans. R. Soc. London, Ser. A, Vol. 259, No. 1095, pp.1-31.
13. Eshleman, R.L., and Eubanks, R. A. (1969), On the critical speeds of a continuous rotor, Trans. ASME, J. Eng. Ind., Vol. 91, No. 4, pp.1180-1188.
14. Miwa, S., and Shimomura, G. (1976), Balancing of rotating machinery, Corona Publishing Co., Tokyo (in Japanese).
15. Yamamoto, T. (1955), On the critical speed of a shaft of sub-harmonic oscillation, Trans. JSME, Vol. 21, No. 111, pp.853-858 (in Japanese).

16. Yamamoto, T. (1957), On the vibrations of a rotating shaft, Chap. II: Non-linear and non-symmetrical spring characteristics of the shaft supported by single-row radial ball bearings; Chap. III: On the critical speed of a shaft of sub-harmonic oscillation and on sub-harmonic oscillation on rectilinear vibrations, Mem. Fac. Eng. Nagoya Univ., Vol. 9, No.1, pp.25-40.
17. Gasch, R. (1976), Dynamic behavior of a simple rotor with a cross-sectional crack, Proceedings of the International Conference on Vibrations in Rotating Machinery, Institute of Mechanical Engineers, New York, pp.123-128.
18. Henry, T.A., and Okah-Avae, B.E. (1976), Vibrations in cracked shaft, Proceedings of the International Conference on Vibrations in Rotation Machinery, Institute of Mechanical Engineers, New York, pp.15-17.
19. Black H.F., 1968 Journal of Mechanical Engineering Science 10, 1-12. Interaction of a whirling rotor with a vibrating stator across a clearance annulus.
20. Ehrich, F.F., Stator whirl with rotors in bearing clearance ASME, (1966) 66, WA/MD-8.
21. Muszynska A. 1984 ImechE C 281/84, 327-335. Partial lateral rotor to stator rubs.
22. Ishida Y., Inagaki M., Ejima R., Hayashi A., Nonlinear resonances and self-excited oscillations of a rotor caused by radial clearance and collision. Nonlinear Dyn (2009) 57: 593–605, DOI 10.1007/s11071-009-9482-3.
23. Pennacchi P., Bachschmid N., Tanzi E., Light and short arc rubs in rotating machines: Experimental tests and modeling, Mechanical Systems and Signal Processing, Volume 23, Issue 7, October 2009, Pages 2205-2227.
24. Chu F., Lu W., Experimental observation of nonlinear vibrations in a rub-impact rotor system, Journal of Sound and Vibration, 283 (2005), 621–643.
25. Muszynska A., Goldman P., Chaotic Responses of Unbalanced Rotor/Bearing/Stator Systems with Looseness or Rubs, Chaos, Solitons & Fractals, Vol. 5, No. 9, pp. 1683-1704, 1995.
26. Feng Z. C., Zhang X. Z., Rubbing phenomena in rotor–stator contact, Chaos, Solitons and Fractals 14 (2002) 257–267.
27. Chu F., Zhang Z., Periodic, Quasi-Periodic and Chaotic Vibrations of a Rub-Impact Rotor System Supported on Oil Film Bearings, Int. J. Engng Sci, Vol. 35, No. 10/It, pp. 963-973, 1997.
28. Wenhui X., Yougang T., Yushu C., Analysis of motion stability of the flexible rotor-bearing system with two unbalanced disks, Journal of Sound and Vibration 310 (2008) 381–393.

29. Lu Q.-S., Li Q.-H., Twizell E.H., The existence of periodic motions in rub-impact rotor systems, Journal of Sound and Vibration, 264 (2003), 1127–1137.
30. Al-Wedyan H. M., Tahat M. S., Mutasher S.A., The Behaviour of the Jeffcott Rotor Under a Vibrating Base of Fluid Film Bearing, Suranaree J. Sci. Technol. 15(3):167-176, 2008.
31. Li G.X., Paidoussis M.P., Impact Phenomena of Rotor-Casing Dynamical Systems. Nonlinear Dynamics 5 (1994), 53-70.
32. Patel T. H., Darpe A.K., Experimental Investigations on Vibration Response of Misaligned Rotors. Mechanical Systems and Signal Processing 23 (2009), 2236-2252.
33. Bachschmid N., Pennacchi P., Vania A., Thermally induced vibrations due to rub in real rotors. Journal of Sound and Vibration, 299 (2007), 683-719.
34. Curami A., Pizzigoni B., Vania A., On the rubbing phenomena in turbo machinery, in: Proceedings of the IFToMM International Conference on Rotor dynamics, Tokyo, September 14–17, 1986, pp. 481–486.
35. Stegemann D., Reimche W., Beermann H., Sudmersen U., Analysis of short-duration rubbing process in steam turbines, VGB Kraftwerkstechnik 73 (10) (1993)739–745.
36. Nagaya K., Takeda S., Tsukui Y., and Kumaido T., Active control method for passing through critical speeds of rotating shafts by changing stiffness of the supports with use of memory metals, Journal of Sound and Vibration 113 (1983), 307-315.
37. Suherman S., and Plaut R.H., Use of a flexible internal support to suppress vibration of a rotating shaft passing through a critical speed, Journal of Vibration and Control 3 (1997), 213-233.
38. Yao G.Z. and Meng G., Vibration control of a rotor system by disk type electrorheological damper, Journal of Sound and Vibration 219, 1999, 175-188.
39. Wang J.X. and Meng G., Application of magnetorheological fluid damper in rotor vibration control, Chinese Journal of Chemical Physics 14, 2001, 548-554.
40. Ding Q., Backward Whirl and Its Suppression of a Squeeze Film Damper Mounted Rotor/Casing System in Passage through Critical Speed with Rubs, Journal of Vibration and Control, 10: 561-573,2004.
41. Jiang J., Ulbrich H., Chavez A., Improvement of rotor performance under rubbing conditions through active auxiliary bearings. International Journal of Non Linear Mechanics, 41 (2006), 949-957.

42. Inoue T., Ishida Y., Fei G., Hossain M. Z., Suppression of the Forward Rub in Rotating Machinery by an Asymmetrically Supported Guide. J. Vib. Acoust. 133, 021005 (2011).
43. Yamamoto T., Ishida Y., Linear and Non Linear Rotor Dynamics. Wiley Series in Non Linear Science. ISBN 0-471-18175-7.
44. Goldman and Muszynska, Chaotic Behavior of Rotor/Stator Systems with Rubs, ASME Turbo Expo Conference (1993), 1-8.
45. Momono T., Rolling Bearing Stiffness, NSK Technical Journal, NO.669, (2000), pp.32-41.

APPENDIX

Stability Analysis

Forward Whirling Analysis [2]

Black has shown the response curve of forward rub and stability theoretically for the 4 degree-of-freedom rotor-stator with the flexible support. But in this thesis, a simple theoretical explanation and response curve are introduced for the rotor-to-rigid guide, 2 degree-of-freedom [2]. Equation 4.44 and 4.45 transforms to polar coordinate (r,β) by the expressions $x = r\cos\phi = r\cos(\omega t + \beta)$ and $y = r\sin\phi = r\sin(\omega t + \beta)$. Let us assume that r and β change slowly with time. So, the orders of the terms are defined as $\dot{r} = O(\varepsilon)$, $\dot{\beta} = O(\varepsilon)$ and $\ddot{r} = O(\varepsilon^2)$ where ε represents a small parameter and $O(\varepsilon)$ represents the same order of ε. Again, damping coefficient c is considered small with the order $O(\varepsilon)$. Now putting the above x and y expressions in equation 4.44 and 4.45 and equating the both sides by the $\cos\phi$ and $\sin\phi$, one can obtain the equations taking the terms up to the order $O(\varepsilon)$:

$$\left.\begin{aligned} -r(\omega^2 + 2\omega\dot{\beta}) + r &= e\omega^2\cos\beta - k_e(r-\delta) - c_e\dot{r} \\ -2\dot{r}\omega - cr\omega &= e\omega^2\sin\beta \end{aligned}\right\} \quad (1)$$

For simplification, the damping coefficient c is taken zero. For the steady state solution, putting $r = R_0$ and $\beta = \beta_0$ in equation 1, the equation becomes

$$\left.\begin{aligned} -R_0\omega^2 + R_0 &= e\omega^2\cos\beta_0 - k_e(R_0 - \delta) \\ 0 &= e\omega^2\sin\beta_0 \end{aligned}\right\} \quad (2)$$

From equation 2, one can find the following two conditions:

$$\left.\beta_0 = 0, \quad R_0 = \frac{e\omega^2 + k_e\delta}{1 + k_e - \omega^2}\right\}$$

$$\left.\beta_0 = -\pi, \quad R_0 = \frac{-e\omega^2 + k_e\delta}{1 + k_e - \omega^2}\right\} \quad (3)$$

For stability checking, some disturbances are considered which change $r = R_0 + \xi$ and $\beta = \beta_0 + \eta$. Order of ξ and η are considered as $O(\varepsilon)$ and, $\dot{\xi}$ and $\dot{\eta}$ are $O(\varepsilon^2)$. Putting these

values in equation 1 and taking the terms from the both sides up to the order $O(\varepsilon^2)$, and after eliminating the terms of steady state by equation 2 , the equations are as follows:

$$\left.\begin{aligned} -(2R_0\omega\dot{\eta}+\xi\omega^2)+\xi &= e\omega^2\eta\sin\beta_0 - k_e\xi - c_e\dot{\zeta} \\ -2\dot{\xi}\omega &= e\omega^2\eta\cos\beta_0 \end{aligned}\right\} \quad (4)$$

Putting the value $\xi = Ae^{st}$, $\eta = Be^{st}$ in equation 4, the characteristic equation becomes

$$4R_0s^2 + (c_e\cos\beta_0 - 2\omega\sin\beta_0)es + \{(1-\omega^2)+k_e\}e\cos\beta_0 = 0 \quad (5)$$

From now, the stability and the resonance phenomena are discussed by the two states of equation 3.

Whirling with pattern O-M-G

In the first state of equation 3 where $\beta_0 = 0$ demonstrates that the origin O, geometrical center M and center of gravity G are in line, and G is outside of M.

(a) No contact forward whirling motion:

When the amplitude is less than δ, the rotor does not contact with the guide. Putting $k_e = 0$, equation 3 can be written as:

$$\beta_0 = 0, \quad R_0 = \frac{e\omega^2}{1-\omega^2} \quad (6)$$

This solution exists in the rotational speed range less than ω_B which can be found by putting δ in replacement of R_0 in equation 6 in the sub critical speed range where $\omega < 1$.Then the characteristic equation 5 can be written as:

$$4R_0s^2 + (1-\omega^2)e = 0 \quad (7)$$

In the sub critical speed range $\omega < 1$, the characteristic roots are purely imaginary which indicates that the solution is stable if some inevitable damping exists in the system. This stable solution is depicted by the solid line AB in the Fig. 1.

(b) Forward rub:

$$\beta_0 = 0, \quad R_0 = \frac{e\omega^2 + k_e\delta}{1+k_e-\omega^2} \quad (8)$$

Equation 3 holds in this case as the stiffness k_e comes in action during contact with the guide. When $R_0 = \delta$, equation 8 coincides with equation 6. This means $R_0 = \delta$ at $\omega = \omega_B$. And, equation 8 also demonstrates that R_0 increases with the increasing of ω. So, as k_e possesses a very high stiffness compared with the shaft stiffness, the amplitude is always larger than the gap δ for the rotational speed above ω_B, i.e., the forward rub occurs in the wide range above the critical speed. In this condition, the characteristic equation 5 becomes as:

$$4R_0 s^2 + c_e e s + (1 - \omega^2 + k_e)e = 0 \tag{9}$$

From Routh-Hurwitz criteria, the solution becomes stable if

$$1 - \omega^2 + k_e > 0 \tag{10}$$

Since the stiffness of k_e is very high, the above condition holds. This stable solution is depicted by the solid line BE in Fig. 1.

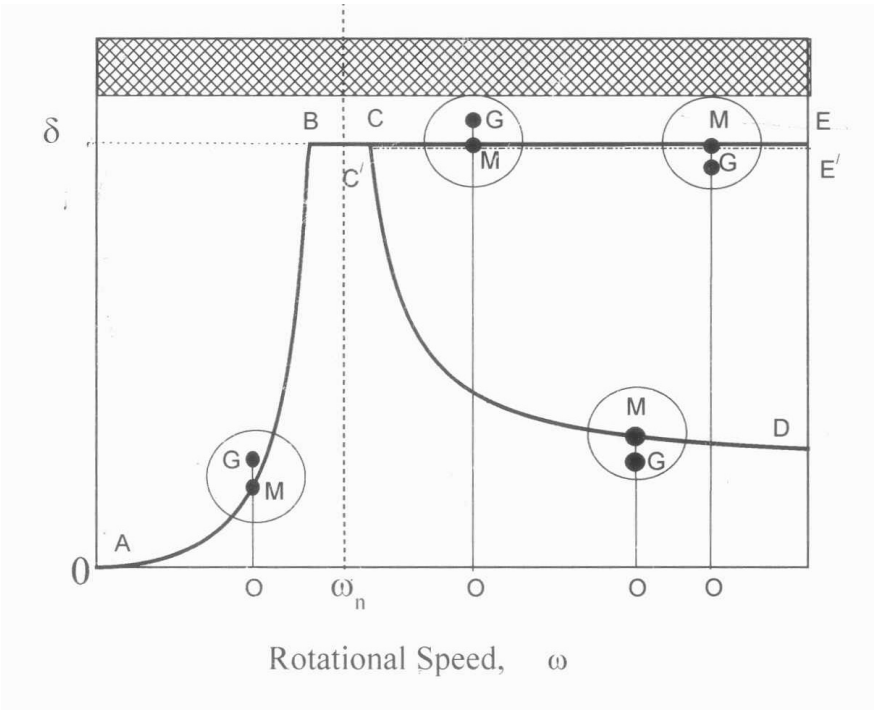

Fig. 1: Stability analysis of forward rubs [2].

Whirling with pattern O-G-M

In the 2nd state of equation 3 where $\beta_0 = -\pi$ demonstrates that the origin O, the center of gravity G and the geometrical center M are in line, and G is inside of M.

(a) No contact motion of equation 3 can be written as:

$$\beta_0 = -\pi, \quad R_0 = -\frac{e\omega^2}{1-\omega^2} \tag{11}$$

Here, ω represents ω_c at $R_0 = \delta$. The similar condition is appeared which is discussed in the previous section where the stable solution is found, and the solution is depicted by the solid line CD in Fig. 1.

(b) Contact motion:

Equation 3 becomes as:

$$\beta_0 = -\pi, \quad R_0 = \frac{-e\omega^2 + k_e\delta}{1 + k_e - \omega^2} \tag{12}$$

And, the characteristic equation 5 becomes as:

$$4R_0 s^2 - c_e e s - (1 - \omega^2 + k_e)e = 0 \tag{13}$$

Since the coefficient for the 2nd term is negative, this steady state solution is always unstable depicted by the broken line C′E′ in Fig. 1.

With friction

If the friction force works, using the equations 4.23, 4.44 and 4.45, the polar form equations of motion become as:

$$\left.\begin{aligned} -r(\omega^2 + 2\omega\dot{\beta}) + r &= e\omega^2\cos\beta - k_e(r-\delta) - c_e\dot{r} \\ -2\dot{r}(\omega + \dot{\beta}) - cr\omega &= e\omega^2\sin\beta + \mu\{k_e(r-\delta) + c_e\dot{r}\} \end{aligned}\right\} \tag{14}$$

Backward whirling analysis [2]

Let us consider the backward contact whirling motion with a negative angular velocity ($\Omega < 0$), where the rotational speed ω is positive. Now, from the equation 4.23, it is observed that the friction force can change its direction depending on the direction of the velocity of the contact point. For backward rub, the $\pm$ sign can be explained as the relationship between the whirling speed Ω and the rotational speed ω. Fig. 2 shows the direction of friction force F_f, and threshold value of backward whirling is Ω_0. If ω, Ω, R_s and δ are the shaft rotational speed, whirling

speed, radius of the inner ring and the gap between the shaft and the inner ring of the bearing respectively, the whirling speed becomes as:

$$\Omega = -\frac{R_s \omega}{\delta}$$

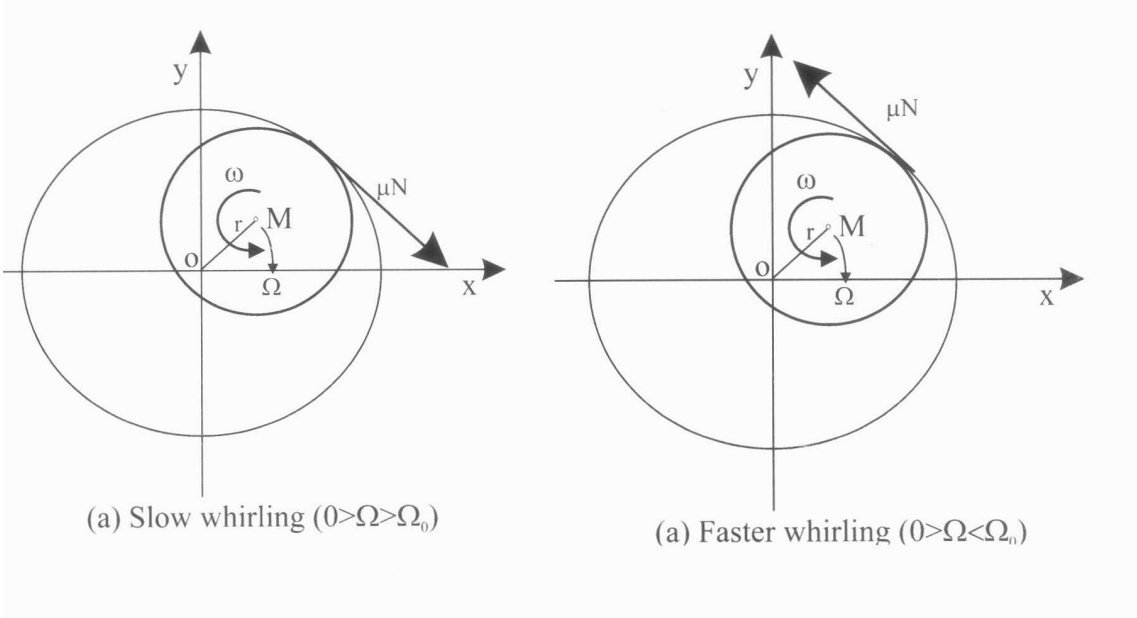

Fig. 2: Direction of friction and backward whirling speed due to change of friction force [2].

Now, if the backward whirling Ω is slower than the threshold value Ω_0, $0 > \Omega > \Omega_0$, the friction works at the direction shown in Fig. 2(a), and the upper sign of the equation 4.23 is adopted. On the contrary, while Ω is faster than Ω_0, $0 > \Omega_0 > \Omega$, the lower sign of equation 4.23 is adopted. Now in the polar form of equation 4.44 and 4.45 become as:

$$\begin{aligned} &\ddot{r} - r\dot{\phi}^2 + c\dot{r} + r + k_e(r-\delta) + c_e\dot{r} = e\omega^2 \cos(\phi - \omega t) \\ &-(2\dot{r}\dot{\phi} + r\ddot{\phi}) - cr\dot{\phi} \mp \mu(k_e(r-\delta) + c_e\dot{r}) = e\omega^2 \sin(\phi - \omega t) \end{aligned} \tag{15}$$

The second equation of equation 15 can be rewritten as below for threshold value:

$$r\ddot{\phi} = -2\dot{r}\dot{\phi} - cr\dot{\phi} - \mu(k_e(r-\delta) + c_e\dot{r}) - \hat{e}\omega^2 \sin(\phi - \omega t) \tag{16}$$

And for the above threshold value:

$$r\ddot{\phi} = -2\dot{r}\dot{\phi} - cr\dot{\phi} + \mu(k_e(r-\delta) + c_e\dot{r}) - e\omega^2 \sin(\phi - \omega t) \tag{17}$$